



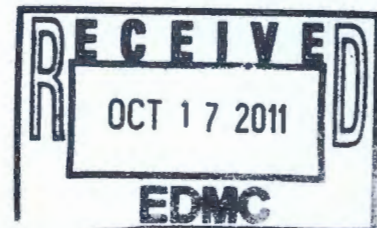
U.S. DEPARTMENT OF  
**ENERGY**

PNNL-17818

Prepared for the U.S. Department of Energy  
under Contract DE-AC05-76RL01830

# 300 Area Treatability Test: Laboratory Development of Polyphosphate Remediation Technology for In Situ Treatment of Uranium Contamination in the Vadose Zone and Capillary Fringe

DM Wellman	EA Cordova
EM Pierce	ET Clayton
DH Bacon	KE Parker
M Oostrom	RM Ermi
KM Gunderson	SR Baum
SM Webb	VR Vermeul
CC Bovaird	JS Fruchter



September 2008



**Pacific Northwest**  
NATIONAL LABORATORY

attached to: 0099752

**DISCLAIMER**

This report was prepared as an account of work sponsored by an agency of the United States Government. Neither the United States Government nor any agency thereof, nor Battelle Memorial Institute, nor any of their employees, makes any warranty, express or implied, or assumes any legal liability or responsibility for the accuracy, completeness, or usefulness of any information, apparatus, product, or process disclosed, or represents that its use would not infringe privately owned rights. Reference herein to any specific commercial product, process, or service by trade name, trademark, manufacturer, or otherwise does not necessarily constitute or imply its endorsement, recommendation, or favoring by the United States Government or any agency thereof, or Battelle Memorial Institute. The views and opinions of authors expressed herein do not necessarily state or reflect those of the United States Government or any agency thereof.

**PACIFIC NORTHWEST NATIONAL LABORATORY**

*operated by*

**BATTELLE**

*for the*

**UNITED STATES DEPARTMENT OF ENERGY**

*under Contract DE-AC05-76RL01830*



**Printed in the United States of America**

**Available to DOE and DOE contractors from the  
Office of Scientific and Technical Information,  
P.O. Box 62, Oak Ridge, TN 37831-0062;  
ph: (865) 576-8401  
fax: (865) 576-5728  
email: reports@adonls.osti.gov**

**Available to the public from the National Technical Information Service,  
U.S. Department of Commerce, 5285 Port Royal Rd., Springfield, VA 22161  
ph: (800) 553-6847  
fax: (703) 605-6900  
email: orders@ntis.fedworld.gov  
online ordering: <http://www.ntis.gov/ordering.htm>**



This document was printed on recycled paper.

(9/2003)

# **300 Area Treatability Test: Laboratory Development of Polyphosphate Remediation Technology for In Situ Treatment of Uranium Contamination in the Vadose Zone and Capillary Fringe**

DM Wellman	EA Cordova
EM Pierce	ET Clayton
DH Bacon	KE Parker
M Oostrom	RM Ermi
KM Gunderson	SR Baum
SM Webb	VR Vermeul
CC Bovaird	JS Fruchter

September 2008

Prepared for  
the U.S. Department of Energy  
under Contract DE-AC05-76RL01830

Pacific Northwest National Laboratory  
Richland, Washington 99352

## Summary

The Hanford Site is a former nuclear defense production facility. A groundwater plume containing uranium, originating from a combination of purposeful discharges of wastewater to cribs, trenches, and ponds, along with some accidental leaks and spills related to nuclear fuel fabrication activities, has persisted beneath the Hanford Site 300 Area for many years. Despite the cessation of uranium releases and the removal of shallow vadose zone source materials, the remedial action objective to lower the concentration of groundwater uranium to the U. S. Environmental Protection Agency maximum contaminant level concentration of 30  $\mu\text{g/L}$  has not been achieved within the anticipated 10-year time period. Some unknown amount of contamination remains in the vadose zone beneath the lower extent of the excavation activities. Additional contamination also may remain beneath buildings and facilities in the southern portion of the 300 Area, which has not been decontaminated and decommissioned. The use of polyphosphate technology for source treatment in the vadose zone and capillary fringe is expected to accelerate the natural attenuation of uranium to thermodynamically stable uranium-phosphate minerals. This effort will complement the current 300 Area treatability test being conducted within the saturated zone (e.g., 300 Area aquifer) for in situ treatment of uranium-contaminated groundwater.

Polyphosphate technology has been demonstrated for in situ precipitation of phosphate phases to control the long-term fate of uranium. A critical component of the development and testing is detailed evaluation to determine if polyphosphate technology could be modified for infiltration from ground surface or some depth of excavation to stabilize source uranium phases. This report presents results from bench-scale treatability studies conducted under site-specific conditions to optimize the polyphosphate amendment for implementation of a field-scale technology demonstration to stabilize uranium within the 300 Area vadose zone and capillary fringe of the Hanford Site. Documented in this report are data related to 1) the retardation of polyphosphate as a function of water content and pore water velocity, 2) the reaction between uranium-bearing solid phases and aqueous polyphosphate remediation technology as a function of polyphosphate composition and concentration, 3) the mechanism of autunite formation via the reaction of solid-phase calcite-bound uranium and aqueous polyphosphate remediation technology, 4) the transformation mechanism and reaction kinetics between uranyl-carbonate and -silicate minerals with the polyphosphate remedy under advective conditions, and 5) the extent and rate of uranium released and immobilized as a function of polyphosphate composition and the infiltration rate of the polyphosphate remedy. Kinetic rate law parameters were determined from single-pass flow-through experiments. Pressurized unsaturated flow tests were used to determine the effect of polyphosphate composition, concentration, and infiltration rate on the unsaturated transformation of uranium minerals in the presence of polyphosphate technology. The mobility of polyphosphate under unsaturated conditions was determined using the unsaturated flow apparatus. Key laboratory results indicate:

- Controlled infiltration of polyphosphate will does not increase aqueous uranium concentrations.
- Orthophosphate affords the greatest control over the aqueous concentration of uranium under the pH range of 6 to 8, maintaining aqueous uranium concentrations less than 30  $\mu\text{g/L}$  at a  $\text{g} [\text{PO}_4^{3-}]_{\text{aq}}/\text{g}$ .
- A polyphosphate formulation consisting of 90% orthophosphate ( $4.74 \times 10^{-2} \text{ M}$ ) and 10% tripolyphosphate ( $1.75 \times 10^{-3} \text{ M}$ ) will provide the rapid stabilization of uranium-solid phases through transformation to uranium-phosphate phases, and mitigate the flux of uranium from the vadose zone and capillary fringe during infiltration.

- Stabilization of soluble uranium-bearing minerals occurs by the formation of a uranium-phosphate “rind” on the surface of uranium-rich calcite and uranyl-silicate minerals.

The geochemical and thermodynamic data obtained from bench-scale testing was used to update the database for EQ3/6, version 8.0, to allow reactive transport simulation of polyphosphate infiltration at the intermediate- and field-scale using STOMP (Subsurface Transport Over Multiple Phases computer model).

Results of reactive transport simulations suggest that drip infiltration at an application rate of 0.05 L/hr over a scale 102 cm wide x 80 cm high x 5.5 cm deep controls the saturation beneath a drip infiltration source; the vertical average linear velocity 20 cm beneath the point source is 10.4 cm/hr. This results in a travel time of 5.79 hours vertically through the 60-cm-deep vadose zone. Assuming a  $K_d$  of 0.0037 for phosphate, simulations indicate that a low water application rate will increase contact time of dissolved phosphate with U-bearing minerals in the sediment and minimize flushing. The presence of heterogeneities and the uncertainty regarding the true reactive surface area of the fine-grained materials at the field scale may have a significant effect on the efficacy and emplacement of the remedial action. Currently, additional intermediate-scale tests are being conducted to evaluate the effect of heterogeneities on the remediation of uranium minerals under conditions relevant to the vadose zone and capillary fringe. These results will be used to test and verify a site-specific, variable-saturation, reactive-transport model and to aid in the design of a pilot-scale field test of this technology. In particular, the infiltration approach and monitoring strategy of the pilot test will be based primarily on results from intermediate-scale testing. The results of this investigation provide valuable information for designing a full-scale remediation of uranium in the 300 Area vadose zone and capillary fringe. Data obtained from this study will be used to develop implementation cost estimates, identify implementation challenges, and investigate the capability of the technology to meet remedial objectives. This information will be used to establish the viability of the method and determine how best to implement the technology in the field.

## Acknowledgments

Funding for this project was provided by the U.S. Department of Energy (DOE), Office of Environmental Management, EM-20 Environmental Cleanup and Acceleration (Mark Gilbertson); and by Fluor Hanford, Inc. (Jane Borghese).

The authors gratefully acknowledge Theresa Queen, Matthew Covert and Tom Wiestma for their support of intermediate-scale testing conducted in part at the William R. Wiley Environmental Molecular Sciences Laboratory (EMSL), a DOE Office of Science User Facility, under proposal number 24812.

Portions of this research were carried out at the Stanford Synchrotron Radiation Laboratory, a national user facility operated by Stanford University on behalf of the U.S. Department of Energy, Office of Basic Energy Sciences, at beam line 11-2 under proposals 2E10 and 2E19. The authors gratefully acknowledge the assistance and support of John Bargar and the assistance of Jeff Catalano in conducting XANES and EXAFS analyses.

The authors wish to gratefully acknowledge and thank the following individuals for their support in various aspects of this investigation: Keith Geiszler and Mike Lindberg for their planning and support of analytical work; Igor Kutnyakov for conducting select x-ray diffraction and carbon analyses; Kim Griswold and Kenton Rod for assistance with pressurized unsaturated flow testing; Emily Richards for organizing and assisting with single-pass flow-through testing; and Laken Top, Katherine Harris, Sara Rither, Sarah Sederberg, De'Chauna Skinner, and Dianna Delegado for various portions of this work.

## Acronyms and Abbreviations

ASTM	American Society of Testing Materials
BET	Brunauer-Emmett-Teller
BTC	breakthrough curve
DCP	dicalcium phosphate
DDI	distilled, deionized water
DOE	U. S. Department of Energy
EDS	energy dispersive spectroscopy
Eh	oxidation potential
EMSL	Environmental Molecular Science Laboratory
EPA	U. S. Environmental Protection Agency
EXAFS	extended x-ray absorption fine structure spectroscopy
FY	fiscal year
GEA	gamma energy analysis
HDPE	high-density polyethylene
HGW	Hanford groundwater
HPLC	high pressure liquid chromatography
HPA	Hydraulic Properties Apparatus
ICDD	International Center for Diffraction Data
ICP-OES	inductively coupled plasma-optical emission spectrometry
ICP-MS	inductively coupled plasma-mass spectrometry
IHCA	Integrated Hydraulic Conductivity Apparatus
IFEFFIT	Interactive XAFS Analysis and FEFF Fitting
LFI	Limited-field investigation
MCL	maximum concentration limit [in groundwater reports, MCL = maximum contaminant level]
NPP	North Process Pond
OCP	octacalcium phosphate
PFA	perfluoroalkoxide
PFBA	pentafluorobenzoic acid
PNNL	Pacific Northwest National Laboratory
<sup>31</sup> P NMR	phosphorus-31 nuclear magnetic resonance
PUF	pressurized unsaturated flow
ROD	record of decision
SEM	scanning electron microscopy
SEM-EDS	scanning electron microscopy-energy dispersive spectroscopy
SFTL	Subsurface Flow and Transport Laboratory

SPFT	single-pass flow-through
SSRL	Stanford Synchrotron Radiation Laboratory
STOMP	Subsurface Transport Over Multiple Phases
THAM	<i>tris</i> hydroxymethyl aminomethane
$\mu$ -XRD	micro-x-ray diffraction
$\mu$ -XRF	micro x-ray fluorescence
UFA	unsaturated flow apparatus
XANES	x-ray absorption near edge spectroscopy
XAFS	x-ray absorption fine structure
XRD	x-ray diffraction

# Contents

Summary .....	iii
Acknowledgments.....	v
Acronyms and Abbreviations .....	vii
1.0 Introduction .....	1.1
1.1 Purpose and Scope .....	1.1
1.2 Report Contents and Organization .....	1.2
2.0 Background.....	2.1
2.1 300 Area Uranium Contamination.....	2.1
2.2 300 Area Uranium Plume.....	2.3
2.3 Uranium (VI) Solid Phase Speciation .....	2.6
2.4 Polyphosphate Remediation Technology .....	2.8
3.0 Laboratory-Scale Testing – Materials and Methods.....	3.1
3.1 Behavior of Polyphosphate Amendment Under Unsaturated Conditions .....	3.1
3.2 Sequestration of Uranium with Calcite .....	3.3
3.2.1 Calcite Pre-Equilibration.....	3.3
3.2.2 Kinetic Experiments.....	3.4
3.2.3 Loading Experiments .....	3.4
3.2.4 Equilibrium Partition Coefficient, $K_d$ , Experiments .....	3.5
3.3 Synthesis of Uranium Minerals.....	3.5
3.3.1 Synthesis of Uranium-Bearing Calcite.....	3.6
3.3.2 Synthesis of Uranophane.....	3.6
3.4 Characterization of Pristine and Reacted Uranium Minerals – Uranium-Rich Calcite, Uranophane, and Meta-Torbernite .....	3.6
3.4.1 X-Ray Diffraction .....	3.7
3.4.2 Scanning Electron Microscopy – Energy Dispersive Spectrometry .....	3.7
3.4.3 N <sub>2</sub> -Adsorption BET Surface Area.....	3.7
3.4.4 Extended X-Ray Absorption Fine Structure Spectroscopy .....	3.8
3.5 Stability of Uranium Minerals – Uranium-Rich Calcite, Uranophane, and Meta- Torbernite.....	3.8
3.5.1 Single-Pass Flow-Through Test Methods .....	3.8
3.5.2 Rate Calculations and Uncertainty .....	3.10
3.6 Interaction of Polyphosphates with Uranium Minerals – Uranium-Rich Calcite, Uranophane, and Meta-Torbernite .....	3.12
3.6.1 Kinetic Experiments.....	3.12
3.6.2 Loading Experiments .....	3.12
3.6.3 Unsaturated Weathering of Uranium Minerals During Polyphosphate Remediation .....	3.13

4.0	Results and Discussion .....	4.1
4.1	Transport of Polyphosphate Under Unsaturated Conditions.....	4.1
4.1.1	Ortho-, Pyro-, and Tripolyphosphate Transport Under Unsaturated Conditions .....	4.2
4.2	Interaction of Polyphosphate with Calcite-Bound Uranium .....	4.7
4.2.1	Sequestration of Uranium with Calcite .....	4.7
4.2.2	Dissolution Kinetics of Uranium-Rich Calcite.....	4.10
4.2.3	Effect of Aqueous Phosphate on Uranium-Rich Calcite.....	4.13
4.2.4	Stabilization of Uranium-Bearing Calcite with Polyphosphates.....	4.16
4.3	Effect of Polyphosphate on Uranium Mineralogy .....	4.17
4.3.1	Dissolution Kinetics of Uranophane .....	4.18
4.3.2	Dissolution Kinetics of Meta-Torbernite, $\text{Cu}(\text{UO}_2)_2(\text{PO}_4)_2 \cdot x\text{H}_2\text{O}$ .....	4.21
4.3.3	Unsaturated Weathering of Uranium Minerals During Polyphosphate Remediation .....	4.24
4.4	Hydraulic Properties of Sediment Mixtures.....	4.36
4.5	Simulations of Intermediate-Scale Infiltration Experiments.....	4.37
5.0	Conclusions .....	5.1
6.0	References .....	1

## Figures

2.1	Map of the Hanford Site.....	2.2
2.2	300 Area Detail Map Showing Uranium Plume in December 2005.....	2.4
2.3	300 Area Detail Map Showing Uranium Plume in June 2006.....	2.5
2.4	Conceptual Model of Uranium Remobilization During High River Stage.....	2.6
2.5	Schematic Depicting the Step-Wise Hydrolysis of Sodium Tripolyphosphate.....	2.9
2.6	Hydrolysis Rate of Polyphosphate Molecules as a Function of pH.....	2.9
2.7	Schematic Depicting a Proposed Treatability Test of Polyphosphate to Stabilize Uranium in the Vadose Zone and Capillary Fringe.....	2.10
3.1	Schematic of UFA Constant Flow Rotor and Rotating Seal Assembly.....	3.2
3.2	Schematic of the Single-Pass Flow-Through Dissolution Test System.....	3.9
3.3	Photo of PUF Column Assembly.....	3.13
4.1	Observed Phosphate Transport at ~22% an Average $v$ of 20 cm hr <sup>-1</sup> .....	4.4
4.2	Observed Phosphate Transport at ~22% and 15% Water Saturation for Orthophosphate, Pyrophosphate, Tripolyphosphate, and Phosphate Formulation at an Average $v$ of 20 cm hr <sup>-1</sup> ..	4.4
4.3	Observed Phosphate Transport at an Average $v$ of 20 and 2 cm hr <sup>-1</sup> for Orthophosphate, Pyrophosphate, Tripolyphosphate, and Phosphate Formulation at an Average Water Saturation of ~15%.....	4.6
4.4	Uranium Loading on Calcite over the pH Range of 6.5 to 8 in Calcite-Equilibrated Groundwater.....	4.8
4.5	Percent Distribution of U(VI) Species Calculated with MINTEQA2 at 25°C, Ionic Strength = 0.1 M, and pCO <sub>2</sub> = 10 <sup>-3.5</sup> Bar for a Total U(VI) = 1 × 10 <sup>-6</sup> M in Hanford Groundwater Well-699-S3-25.....	4.9
4.6	Speciation of Dominant Calcite Surface Sites at 25°C, I = 0.01 M, [Ca <sup>2+</sup> ] <sub>tot</sub> = 10 <sup>-3</sup> M, and pCO <sub>2</sub> = 10 <sup>-3.5</sup> atm.....	4.9
4.7	EXAFS and Fourier Transform Spectra of Calcite Reacted with 60 ppm Uranium.....	4.10
4.8	Scanning Electron Microscopy Image of Uranium-Rich Calcite.....	4.10
4.9	Log <sub>10</sub> Uranium Release Rate as a Function of Temperature-Corrected pH for Uranium-Rich Calcite in 0.01 M TRIS Solution.....	4.12
4.10	Scanning-Electron Microscopy Image of Uranium-Rich Calcite After Single-Pass Flow-Through Dissolution Tests.....	4.12
4.11	Log <sub>10</sub> Rate of Uranium Release from Uranium-Rich Calcite as a Function of [PO <sub>4</sub> <sup>3-</sup> ] <sub>(aq)</sub> at pH = 7.5, 23°C.....	4.13
4.12	EXAFS of Autunite-Group Mineral, X <sub>3-n</sub> <sup>(n)+</sup> [(UO <sub>2</sub> )(PO <sub>4</sub> ) <sub>2</sub> · xH <sub>2</sub> O, U-Calcite, and Calcite Reacted with 60 ppm Uranium in the Presence of 340 ppb Phosphate at pH 7, pH 7.5, and pH 8.....	4.15
4.13	Activity/Activity Diagram Showing the Stability of Ca-Meta-Autunite Calculated with Geochemist's Workbench®.....	4.15
4.14	Concentration of Aqueous Uranium Released Through the Reaction of Ortho-, Pyro-, and Tripolyphosphate with Uranium-Rich Calcite as a Function of pH and the Ratio of g [PO <sub>4</sub> <sup>3-</sup> ] <sub>aq</sub> /g Uranium-Calcite.....	4.17

4.15	Log <sub>10</sub> Uranium Release Rate as a Function of pH for Uranophane in 0.05 M TRIS Solution....	4.20
4.16	Log <sub>10</sub> Rate of Uranium from Uranophane Release as a Function of [PO <sub>4</sub> <sup>3-</sup> <sub>(aq)</sub> ] at pH = 7.5, 23°C .....	4.20
4.17	The Structure of Autunite, Determined by Single-Crystal X-Ray Diffraction .....	4.21
4.18	Log <sub>10</sub> Uranium Release Rate as a Function of Temperature-Corrected pH for Meta-Torbernite in 0.05 M TRIS Solution .....	4.22
4.19	Log <sub>10</sub> Uranium Release Rate as a Function of Temperature Corrected pH for Ca-Meta-Autunite in 0.05 M TRIS Solution.....	4.23
4.20	Log <sub>10</sub> Rate of Uranium Release from Meta-Torbernite as a Function of [PO <sub>4</sub> <sup>3-</sup> <sub>(aq)</sub> ] at pH = 7.5, 23°C .....	4.24
4.21	The XANES Spectrum of Sample B11494, Indicating the Presence of Only U(VI).....	4.26
4.22	Log <sub>10</sub> Concentration of Elements, in µg/L, Released from the Tripolyphosphate -Treated Column Measured in the Effluent Solutions as a Function of Time, in Days.....	4.27
4.23	Log <sub>10</sub> Concentration of Elements, in µg/L, Released from the Control Column Measured in the Effluent Solutions as a Function of Time, in Days .....	4.27
4.24	Geochemical Thermodynamic Modeling Results Depicting the Predicted Saturation Indices for Uranium Solid Phases and Calcite Based on Effluent Solution Compositions .....	4.28
4.25	EXAFS of Autunite-Group Mineral, X <sub>3-n</sub> <sup>(n)</sup> [(UO <sub>2</sub> )(PO <sub>4</sub> ) <sub>2</sub> · xH <sub>2</sub> O, U-Calcite, and 300 Area Sediment PUF Column Containing ~540 mg/kg Uranium as Uranium Coprecipitated with Calcite Leached with 1000 ppm Tripolyphosphate and Hanford Groundwater.....	4.29
4.26	Concentration of Uranium, µg/L, Released from 25% Ortho-, 65% Pyro-, 10% Tripolyphosphate-Treated Column Measured in the Effluent Solutions as a Function of Time and Pore Volume .....	4.31
4.27	Concentration of Uranium, µg/L, Released from the 70% Ortho-, 20% Pyro-, 10% Tripolyphosphate-Treated Column Measured in the Effluent Solutions as a Function of Time and Pore Volume .....	4.31
4.28	Concentration of Uranium, µg/L, Released from 90% Ortho- and 10% Tripolyphosphate-Treated Column Measured in the Effluent Solutions as a Function of Time and Pore Volume.....	4.32
4.29	EXAFS of Uranium-Rich Calcite Reacted with 90% Ortho-/10% Tripolyphosphate, 70% Ortho-/20% Pyro-, and 10% Tripolyphosphate, and 25% Ortho-/65% Pyro-, and 10% Tripolyphosphate.....	4.33
4.30	Concentration of Uranium, µg/L, in the Effluent Solutions as a Function of Time and Pore Volume Released from Uranium-Calcite-Bearing Column Treated with 90% Ortho- and 10% Tripolyphosphate .....	4.34
4.31	Concentration of Uranium, µg/L, in the Effluent Solutions as a Function of Time and Pore Volume Released from the Uranophane-Bearing Column Treated with 90% Ortho- and 10% Tripolyphosphate .....	4.35
4.32	Concentration of Uranium, µg/L, in the Effluent Solutions as a Function of Time and Pore Volume Released from the Meta-Torbernite-Bearing Column Treated with 90% Ortho- and 10% Tripolyphosphate .....	4.36
4.33	Initial Water Saturation for Simulations of Box Infiltration Experiment.....	4.38

4.34	Simulated Water Saturations After 1 Day of 1-L/hr Drip Infiltration Applied at $x = 34$ cm, $z = 80$ cm.....	4.39
4.35	Simulated Tracer Aqueous Concentrations After 1 Hour of 1-L/hr Drip Infiltration Applied at $x = 34$ cm, $z = 80$ cm.....	4.40
4.36	Simulated Tracer Aqueous Concentrations After 1 Day of 1-L/hr Drip Infiltration Applied at $x = 34$ cm, $z = 80$ cm.....	4.40
4.37	Simulated Water Saturations After 1 Day of 0.05-L/hr Drip Infiltration Applied at $x = 34$ cm, $z = 80$ cm.....	4.41
4.38	Simulated $K_d = 0.037$ Phosphate Aqueous Concentrations After 1 Hour of 0.05-L/hr Drip Infiltration .....	4.42
4.39	Simulated $K_d = 0.037$ Phosphate Aqueous Concentrations After 1 Day of 0.05-L/hr Drip Infiltration .....	4.42

## Tables

3.1	Experimental Conditions for the Quantification of Polyphosphate Mobility as a Function of Water Content and Pore Water Velocity .....	3.3
3.2	Composition of Solutions Used in Single-Pass Flow-Through Experiments .....	3.10
3.3	Surface Area of Uranium Minerals as Measured by BET $N_2$ -Adsorption .....	3.10
3.4	Conditions for Quantification of the Kinetic Interaction of Polyphosphate with Uranium-Bearing Calcite.....	3.12
3.5	Experimental Conditions for Quantifying the Loading of Polyphosphate on Uranium-Bearing Calcite.....	3.13
3.6	Sediment and Uranium Mineral Composition of Columns Used in the Evaluation of Polyphosphate Remediation Under Vadose Zone Conditions .....	3.14
4.1	Polyphosphate Transport Parameters in $<2$ -mm Fraction from Hanford 300 Area Vadose Sediments Determined by Direct Measurement or Analysis of Breakthrough Curves.....	4.3
4.2	Field Transport Parameters Calculated from Laboratory-Derived Transport Parameters .....	4.6
4.3	Standard Fits as Measured from $k = 3-12$ , $k^3$ Weighted .....	4.15
4.4	Table of Calculated or Measured $\log K_{sp}$ Values of Uranyl Phosphate Solids .....	4.23
4.5	Polyphosphate Formulations for Uranium Stabilization via Infiltration Under Unsaturated Conditions .....	4.30
4.6	Percentages of Coarse Gravel, Gravel, Sand, and Fines in Sediment Mixtures A, B, and C.....	4.36
4.7	Saturated Hydraulic Conductivity of the Three Sediment Mixtures .....	4.37
4.8	Parameters and Statistics for the van Genuchten Function Fitted to Data from the Multistep Method Using SFOPT .....	4.37
4.9	Hydraulic and Solute Transport Properties Used for Hanford Sediment in Intermediate-Scale Simulations .....	4.38
4.10	Vertical Velocities and Saturations 20 cm Below Drip Source .....	4.41

## 1.0 Introduction

The U.S. Congress authorized \$10 million to the U.S. Department of Energy Office (DOE) of Environmental Management (specifically, EM-20 Environmental Cleanup and Acceleration) for fiscal year (FY) 2006 to analyze contaminant migration in southeastern Washington State from the Hanford Site to the Columbia River and to introduce new technology approaches to solving contamination migration issues. Nine projects were selected to meet the objectives of the appropriation, including Pacific Northwest National Laboratory's (PNNL's) performance of bench-scale and field-scale treatability tests to determine the efficacy of using polyphosphate injection into the saturated zone to treat groundwater uranium contamination at the Hanford 300 Area. In FY 2007, EM-20 made an additional \$2 million available to pursue follow-on projects, which included bench-scale treatability testing by PNNL that was designed to evaluate whether polyphosphate technology could be modified for infiltration from either ground surface or some depth of excavation to stabilize uranium, *in situ*, within sediments in the deep vadose zone and capillary fringe above the 300 Area aquifer.

An ongoing treatability test to evaluate the efficacy of using polyphosphate injections to treat uranium-contaminated groundwater *in situ* is expected to decrease the current aqueous uranium concentration and mitigate the flow of contaminated groundwater to the river. However, remediation of the aquifer does not address a potential recalcitrant source of uranium located in the vadose zone and capillary fringe. Therefore, a series of bench-scale and intermediate-scale laboratory experiments was needed to evaluate the efficacy of using polyphosphate to stabilize soluble uranium phases contained within the vadose and capillary fringe as stable uranium phosphate minerals.

### 1.1 Purpose and Scope

A laboratory testing program was performed at PNNL to evaluate and optimize polyphosphate remediation technology for infiltration, either from ground surface or some depth of excavation, to provide direct stabilization of uranium within the deep vadose and capillary fringe above the 300 Area aquifer. As reported in this document, the focus was to conduct bench-scale treatability studies under site-specific conditions to optimize the polyphosphate amendment for implementation of a field-scale technology demonstration to stabilize uranium within the 300 Area vadose zone and capillary fringe of the Hanford Site. Source treatment is expected to attenuate uranium and accelerate the formation of thermodynamically stable uranium-phosphate minerals, thereby enhancing the performance of the proposed polyphosphate remediation within the 300 Area aquifer.

The general treatability testing approach consisted of conducting laboratory studies with site sediment and groundwater and under site conditions to develop an effective chemical formulation and infiltration approach for implementation of polyphosphate technology. Laboratory-scale tests were used to accomplish the following:

- Quantify the mobility of polyphosphate under water content and porewater velocities relative to the vadose zone and capillary fringe.
- Evaluate uranium-phosphate formation via the reaction between uranium-bearing solid phases and aqueous polyphosphate remediation technology as a function of polyphosphate composition and concentration.

- Develop an understanding of the mechanism of autunite formation via the reaction of solid-phase calcite-bound uranium and aqueous polyphosphate remediation technology.
- Develop an understanding of the transformation mechanism and reaction kinetics between uranyl-carbonate and -silicate minerals with the polyphosphate remedy under advective conditions.
- Quantify the stability of uranyl-carbonate, -silicate, and -phosphate phases controlling uranium in the vadose zone and capillary fringe under site specific conditions and during polyphosphate remedial actions.
- Quantify the extent and rate of uranium released and immobilized as a function of polyphosphate composition, concentration, and based on the infiltration rate of the polyphosphate remedy.
- Incorporate fundamental geochemical and thermodynamic data associated with polyphosphate technology and remediation into reactive transport codes to allow predictive simulations of polyphosphate remedial actions.

The results of predictive modeling simulations and intermediate scale testing quantify the transport of polyphosphate and the reaction of polyphosphate with uranium minerals under conditions relevant to the vadose zone and capillary fringe at a scale that bridges the gap between the small-scale unsaturated flow apparatus studies and the field scale. These results are being used to test and verify a site-specific, variable-saturation, reactive transport model and to aid in the design of a pilot-scale field test of this technology. In particular, the infiltration approach and monitoring strategy of the pilot test will be based primarily on results from intermediate-scale testing. Data obtained from this study will be used to develop implementation cost estimates, identify implementation challenges, and investigate the capability of the technology to meet remedial objectives. This information will be used to establish the viability of the method and determine how best to implement the technology in the field.

## **1.2 Report Contents and Organization**

The ensuing sections of this report begin by providing background information on uranium contamination in the 300 Area and the selection of polyphosphate remediation technology for further site-specific evaluation and treatability testing (Section 2.0). Section 3.0 describes the laboratory-scale testing materials and methods. Section 4.0 presents study results and discusses the transport of polyphosphates under unsaturated conditions, the stability of uranium source minerals, the interaction of polyphosphate with solid phase uranium source minerals, the effect of polyphosphate on uranium mineralogy, quantification of hydrodynamic properties for 300 Area sediments at the intermediate-scale, and predictive simulations of polyphosphate infiltration at an intermediate-scale. Finally, Section 5.0 presents concluding remarks.

## 2.0 Background

This section provides background information on uranium contamination in the 300 Area and the selection of polyphosphate remediation technology for further site-specific evaluation and treatability testing. In 1996, a record of decision (EPA 1996) identified the following interim actions for remediation of the uranium contaminant plume beneath the 300 Area:

- continued groundwater monitoring to determine how contaminant conditions may change with time
- institutional controls to limit the use of groundwater.

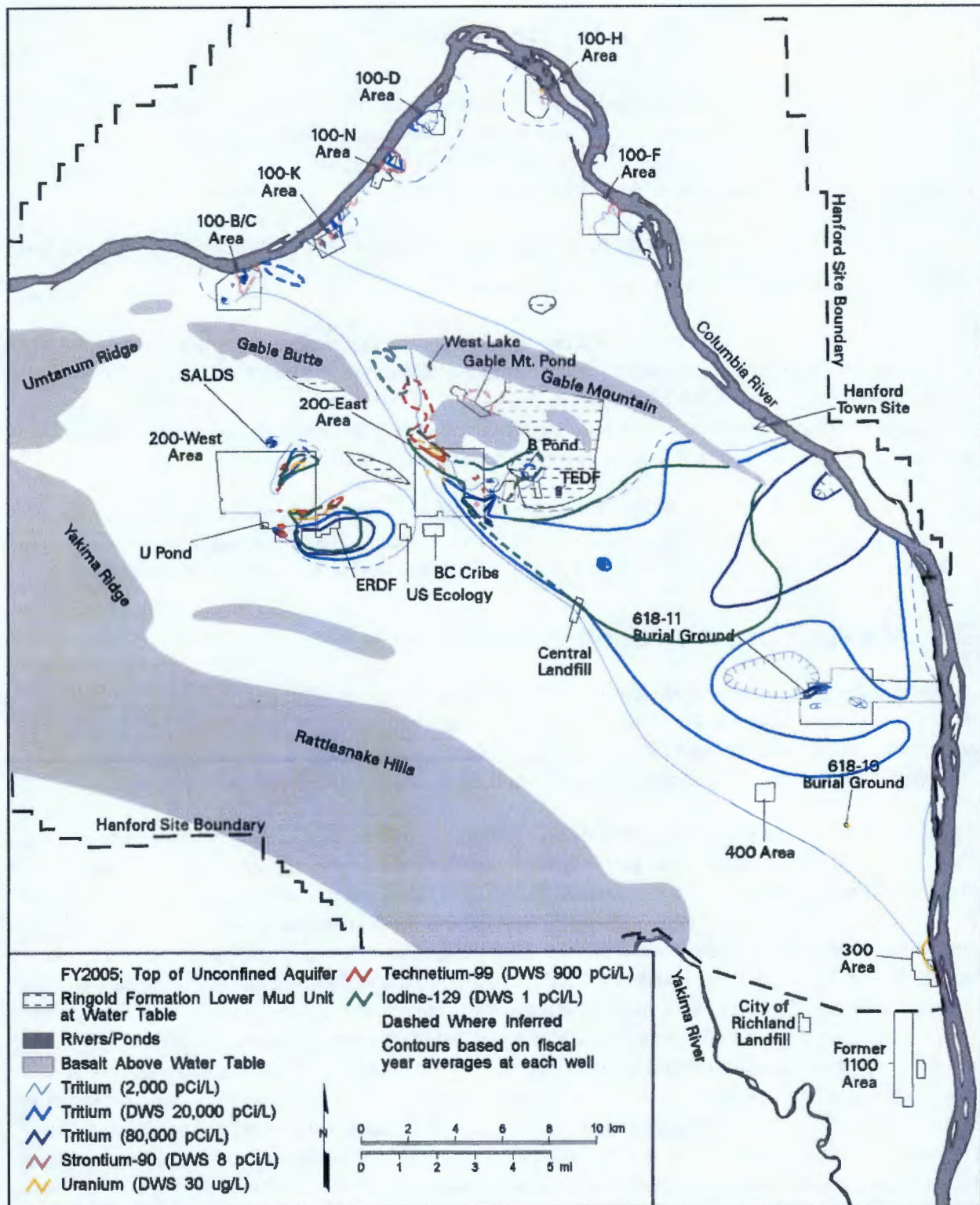
Interim-action results have determined that uranium concentrations in the groundwater plume have been generally declining, but still persist at concentrations above the drinking water standard (remediation goal). Therefore, it is necessary to re-evaluate the remedy for uranium contamination because the rate of decrease in uranium concentrations is significantly different than the rate of decrease expected and used as a basis for the remedy selection in the current record of decision (ROD).

During the 300-FF-5 Phase III Feasibility Study technology screening process, the polyphosphate treatment was judged to be the most promising among five other active remedial technologies for uranium at this site for reducing the concentration of dissolved uranium, and it was selected for further testing.

### 2.1 300 Area Uranium Contamination

During the period spanning the startup of Hanford reactors in 1944 through the late 1980s, facilities in the 300 Area of the Hanford Site were primarily involved with fabricating nuclear fuel for plutonium production (Young and Fruchter 1991). The range of activities produced a wide variety of waste streams that contained chemical and radiological constituents (Gerber 1992; DeFord et al. 1994).

The 300-FF-5 Operable Unit, a groundwater operable unit, is located in the southeast portion of the Hanford Site and includes the water and solids that constitute the aquifer (Figure 2.1). The contaminated groundwater contained in this operable unit consists of contaminants at concentration levels that exceed the U.S. Environmental Protection Agency (EPA) standards for drinking water supplies. These contaminants were released from waste sites in three geographic sub-regions of the operable unit: the 300 Area, 618-11 burial ground, and 316-4 cribs/618-10 burial ground (Figure 2.1), during past-practice disposal activities. Uranium is the most prominent waste constituent remaining in the environment, and it has persisted in waste sites and groundwater during the years after the shutdown of most fuel-fabrication activities and the cessation of liquid-effluent disposal to the ground. Uranium in soluble form is of concern because of its chemical toxicity and potential radiological exposure, although the concentrations in groundwater for chemical toxicity are lower than those associated with exceeding radiological dose standards. Specific criteria on the toxicity to freshwater aquatic organisms are not currently established, so by default, the criteria for the protection of aquatic organisms are the same as those applied for the protection of human health.



can\_gwf05\_005 February 21, 2006 11:24 AM

Figure 2.1. Map of the Hanford Site

## 2.2 300 Area Uranium Plume

A groundwater plume containing uranium from past-practice discharges of liquid waste associated with nuclear fuel fabrication activities has persisted beneath the Hanford Site 300 Area for many years. The uranium plume is just upstream of the City of Richland municipal water supply intake on the Columbia River. Elevated uranium concentrations enter the river along the shoreline and enter the riparian and river biota through seeps. The 1996 ROD for the 300-FF-5 Operable Unit (EPA 1996) stipulated an interim action program of a natural attenuation process accompanied by increased groundwater monitoring. The remedial action objective of the ROD is reduction of groundwater uranium to the EPA maximum contaminant level (MCL). The EPA's MCL in groundwater for drinking water supplies is currently 30 µg/L uranium, measured as total uranium in the water sample. During the remedial investigation in the early 1990s and the development of the initial ROD, the proposed standard for uranium was 20 µg/L.

The persistence of this plume is enigmatic for several reasons, including 1) discharges containing uranium-bearing effluent to ground-disposal sites ended in the mid-1980s; 2) contaminated soil associated with these waste sites was removed during the 1990s and backfilling was complete by early 2004; and 3) the aquifer is composed of highly transmissive fluvial sediment, suggesting rapid movement of groundwater. Also, a water-supply well located within the plume has been in operation since 1980 with no observable effect on the plume. Despite the cessation of uranium releases and the removal of shallow vadose zone source materials, the concentration of the uranium plume has not decreased as predicted. Figure 2.2 and Figure 2.3 display concentration contour maps outlining the uranium plume in December 2005 and June 2006. Comparison of these two figures suggests that during high river stage conditions, such as in June 2006 (Figure 2.3), uranium concentrations were elevated in localized areas farther inland than indicated during December 2005 (Figure 2.2).

Since the early 1990s, liquid-waste disposal sites and solid-waste burial grounds have been extensively remediated. As of March 2004, most liquid-waste disposal sites, which are located in the northern half of the 300 Area, have been excavated and backfilled, and the ground surface has been restored. However, some unknown amount of contamination remains in the vadose zone beneath the lower extent of the excavation activities. Additional contamination also may remain under buildings and facilities in the southern portion of the 300 Area, which has not been decontaminated and decommissioned. The current conceptual site model assumes that re-supply of the plume is occurring, with continuing release from the vadose zone beneath waste sites, the capillary fringe, and possibly from aquifer solids, as source candidates (Figure 2.4).



Figure 2.2. 300 Area Detail Map Showing Uranium Plume in December 2005

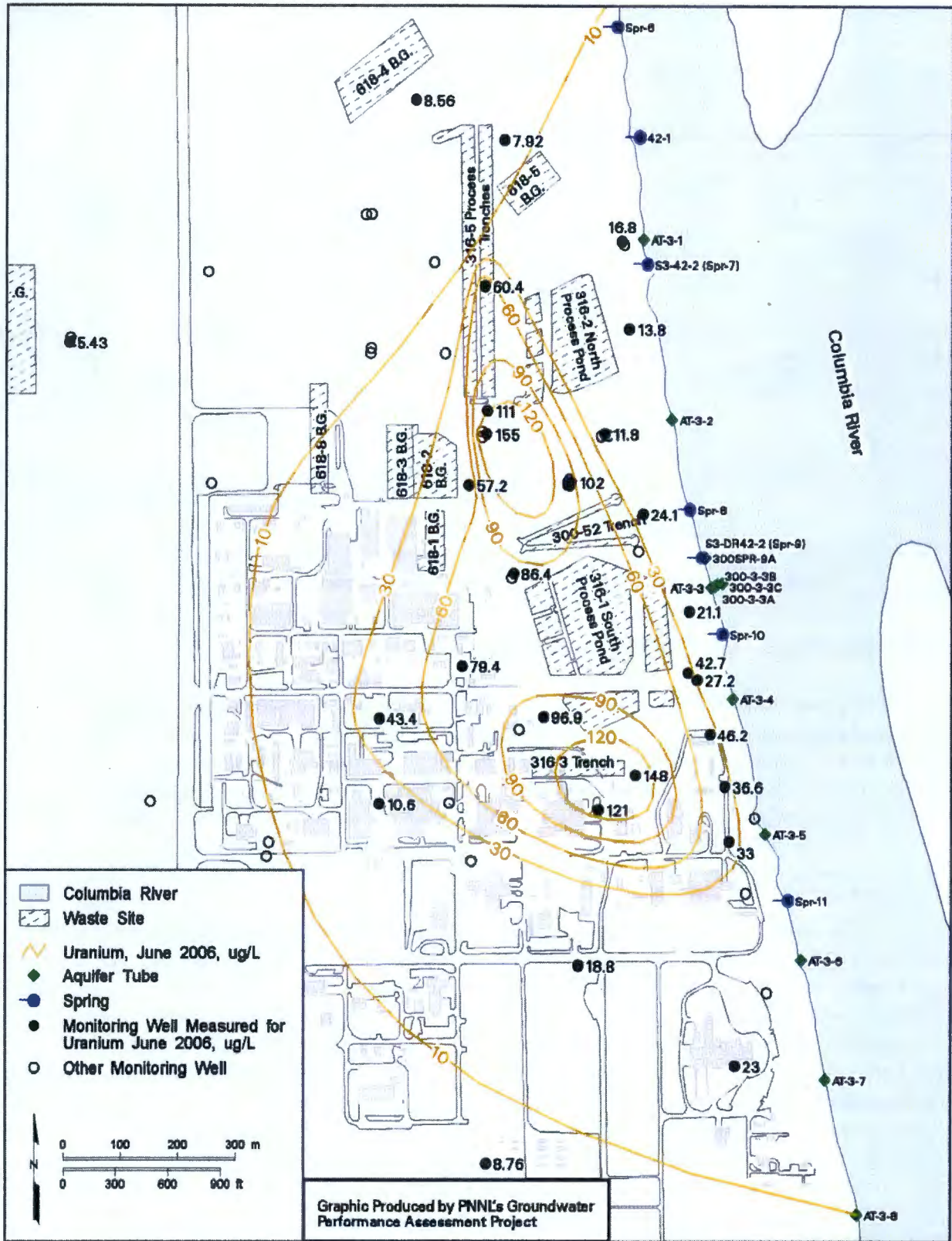


Figure 2.3. 300 Area Detail Map Showing Uranium Plume in June 2006

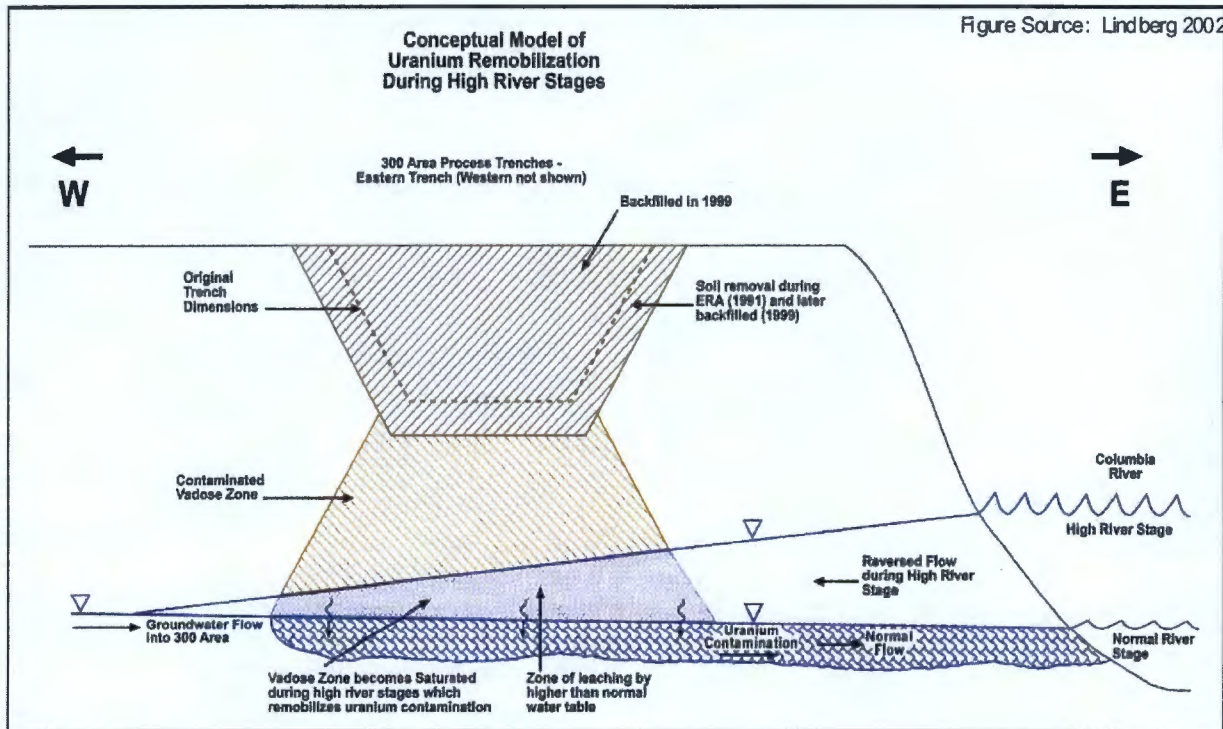


Figure 2.4. Conceptual Model of Uranium Remobilization During High River Stage

### 2.3 Uranium (VI) Solid Phase Speciation

The most abundant actinide element in the natural environment is uranium, with an average composition of ~1.2 to 1.3  $\mu\text{g/g}$  in sedimentary rocks, ~2.2 to 15  $\mu\text{g/g}$  in granites, and ~20 to 120  $\mu\text{g/g}$  in phosphate rocks (Langmuir 1997). In addition to its natural occurrence, operations related to nuclear energy and weapons production have resulted in widespread uranium contamination of geologic media in surface and subsurface environments (Abdelouas et al. 1999). In the United States, uranium has been recognized as one of the most frequently occurring radionuclides in groundwater and in soils/sediments at DOE facilities (Riley et al. 1992).

Speciation and aqueous chemistry of uranium is highly variable based on the environment within which it is found. The main variables affecting uranium geochemistry are the oxidation potential (Eh), pH, temperature, and chemical composition of the aqueous matrix. These four variables govern the thermodynamic and kinetic processes occurring within the system, including aqueous complexation, sorption, precipitation, and dissolution. Uranium has four known oxidation states: U(III), U(IV), U(V), and U(VI); however, only two dominate in natural systems. These valence states have a significant effect on the mobility of uranium in subsurface environments. The uranous ion [U(IV)] dominates under reducing conditions, whereas the uranyl ion ( $\text{UO}_2^{2+}$ ) dominates under oxidizing conditions. Under most redox conditions, dissolved U(III) oxidizes to U(IV), and dissolved U(V) as aqueous species ( $\text{UO}_2^+$ ) disproportionates to U(IV) and U(VI), aqueous species  $\text{UO}_2^{2+}$ . Accordingly, uranium minerals are broadly divided into two classes based on the dominant oxidation states of uranium present under environmental conditions. The reduced, uranous minerals contain U(IV) and the oxidized uranyl, minerals contain U(VI). Because many natural environments are under oxidizing conditions, most uranium-bearing minerals are uranyl minerals.

Depending on environmental conditions, U(VI) minerals may form via 1) direct precipitation under saturated conditions, 2) sorption leading to the precipitation of uranyl minerals, or 3) weathering products of primary uranium ore minerals such as uranium dioxide or uraninite,  $UO_2$  (Finch and Ewing 1992; Frondel 1956; Smith 1984). Precipitation of uranyl minerals follows the thermodynamic progression of first precipitating those that have the lowest solubilities, for which precipitation kinetics do not present significant barriers to nucleation, followed by precipitation of the advanced uranium minerals that occurs over a considerable time frame (Smith 1984; Finch et al. 1999). The general sequence begins with the formation of uranyl-hydroxides, followed by uranyl-carbonates, uranyl-silicates, and finally, the highly stable uranyl-phosphates. Many arid and semiarid environments, frequently proposed as disposal sites, have exhibited accelerated corrosion of uranium phases in spent nuclear fuel because of cycling between dry and wet periods (Finch et al. 1992; Finch and Ewing 1992). Wet-dry cycling increases swelling and cracking of the minerals resulting in an increase in the amount of surface area exposed to groundwater. This accelerates weathering of initial uranium minerals and favors formation of advanced uranium minerals, such as uranyl-phosphates (Sowder et al. 1999).

Worldwide, natural ore deposits demonstrate the significance of secondary mineralization in the fixation of uranium. Such ore deposits include the Koongarra deposit in Australia (Murakami et al. 1997) the Oklo deposit in Gabon, Africa (Jensen and Ewing 2001), and the Shinkolobwe deposit in the Zaire, Africa (Finch and Ewing 1991). The Shinkolobwe and Oklo deposits exhibit uranyl-silicate minerals maintaining control of long-term uranium migration as the primary minerals persisting in the far-field environment. At the Koongarra deposit, the prevalence of iron oxides in the region served as a precursory sorbent for heterogeneous precipitation of uranyl-phosphate minerals (Murakami et al. 1997; Payne et al. 1996). Extensive formation of advanced uranyl-phosphate minerals occurred in contradiction to solubility predictions and maintained long-term control of uranium concentrations (Murakami et al. 1997).

Uranyl minerals also have been found to be significant in anthropogenically contaminated areas. Autunite has been identified as a major phase controlling uranium migration at the Fernald site in Ohio (Buck et al. 1996; Morris et al. 1996) and at Oak Ridge, Tennessee (Roh et al. 2000). Within the 300 Area of the Hanford Site, uranium entered the subsurface environment through purposeful discharges of basic sodium aluminate and acidic uranyl-copper waste streams from the dissolution of nuclear fuel and fuel rod cladding. The North and South Process Ponds (NPP and SPP, respectively) received approximately 58,000 kg of uranium, 238,000 kg of copper, 1,156,000 kg of fluoride, 243,000 kg of nitrate, and large amounts of aluminum hydroxide (McKinley et al. 2007). Additionally, the addition of sodium hydroxide to neutralize the acidic waste stream resulted in a temporal variation in pH ranging from 1.8 to 11.4 (over-neutralization). Detailed x-ray absorption near edge spectroscopy (XANES) and extended x-ray absorption fine structure spectroscopy (EXAFS), electron and x-ray microprobe, scanning electron microscopy-energy dispersive spectroscopy (SEM-EDS), synchrotron-based micro-x-ray diffraction ( $\mu$ -XRD) and micro x-ray fluorescence ( $\mu$ -XRF) spectroscopic analyses have previously indicated that uranium occurs as U(VI) through the 300 Area NPP and SPP depth profile (Catalano et al. 2006b). The speciation of uranium, however, was observed to change as a function of depth. Over-neutralization of the waste ponds promoted the formation of mobile aqueous uranyl species, which allowed permeation into the deeper vadose zone and groundwater. These uranium complexes exist in the deeper vadose zone predominantly as sorbed uranium to phyllosilicates, chlorite, and smectite (Qafoku et al. 2005). At shallower depths, EXAFS analyses suggest that the major uranium-controlling phase was meta-torbernite,  $Cu(UO_2)_2(PO_4)_2 \cdot xH_2O$  (Catalano et al. 2006b; Arai et al. 2007) with uranyl-carbonate

precipitates, predominantly consistent with uranium-rich calcite (Catalano, personal communication). Until recently, it had been speculated that the uranyl-silicate phase present in the 300 Area sediments was either Na-boltwoodite,  $\text{Na}(\text{UO}_2)(\text{SiO}_3\text{OH}) \cdot x\text{H}_2\text{O}$ , or uranophane,  $\text{Ca}(\text{UO}_2)_2[\text{SiO}_3(\text{OH})]_2 \cdot x\text{H}_2\text{O}$ —both minerals have the uranophane group structure (Liu et al. 2004; Liu et al. 2006; Zachara et al. 2005; McKinley et al. 2006; McKinley et al. 2007). The minute inclusions, which prevent bulk analyses, and similarities between the uranophane group structures had precluded conclusive identification of the uranyl-silicate phase. However,  $\mu$ -XRD spectroscopy has identified the presence of uranophane and uranium associated with muscovite (Arai et al. 2007). Near-surface sediments exhibited high calcite concentrations (35 wt%), which exceeded those in comparable Hanford sediments, as a result of over-neutralization events. High calcite concentrations resulted in near-surface uranium speciation being dominated by uranyl-carbonate coprecipitation with calcite (Catalano et al. 2004; Catalano et al. 2006b). Enhancing the natural paragenetic sequence for sorbed uranium phases, uranyl-carbonate, and uranyl-silicate phases present in the Hanford 300 Area vadose zone and capillary fringe through polyphosphate remediation would attenuate the continuing source of groundwater uranium contamination and enhance the proposed polyphosphate remediation within the 300 Area aquifer (Wellman et al. 2007b).

## 2.4 Polyphosphate Remediation Technology

Numerous approaches have been proposed to sequester uranium, *in situ*, with solid-phase hydroxyapatite,  $\text{Ca}_5(\text{PO}_4)_3\text{OH}$ , (Conca 1996; Arey et al. 1999; Wright et al. 1995; Seaman et al. 2001; Moore et al. 2001; Gauglitz and Holterdorf 1992). These proposals put forth the common idea to apply solid-phase phosphate (generally hydroxyapatite) directly to the contaminated soil or surface water or to use it as a trench fill emplaced in the pathway of migrating contaminant plumes. These strategies have merit and represent a feasible technology for near-surface treatment, yet cannot accomplish remediation of pore waters that are situated in deep aquifers or under conditions such as those found in the Hanford deep vadose zone and smear zone where the plume can extend 90 meters below ground surface.

Alternative strategies use water-soluble phosphate compounds that could be injected into the plume from strategically placed wells. However, one challenge about deploying a soluble phosphate amendment into the subsurface is the unwanted rapid precipitation of phosphate phases, which occlude the injection wells and pore space within the formation. Lee et al. (1995) proposed using tribasic sodium phosphate,  $\text{Na}_3(\text{PO}_4) \cdot n\text{H}_2\text{O}$ , as a chemical stabilizer for uranium and radiostrontium. However, even in relatively dilute groundwater solutions, there are enough dissolved cations to form Al-, Fe-, Ca-, and Na-phosphates. Nash and colleagues (1993; 1994; 2000; 1998a; 1997; 1998b; 1999) attempted to circumvent this shortcoming by proposing that a water-soluble organophosphate compound, phytic acid, be injected into the contaminated groundwater. The key advantage of this method is that the hydrolyzation kinetics of the molecule are slow, such that release of orthophosphate is delayed, allowing the injected amending solution to disperse and mix throughout the target plume. However, Wellman et al. (2006b) demonstrated that rapid agglomeration of Ca-phytate occluded 30% of the fluid-filled pore space within the formation. Rapid reduction in the hydraulic conductivity will have a significant effect on additional injections of phytic acid solution, the targeted groundwater plume, or both, by deflecting flow from the natural path. Moreover, phytic acid is an organophosphate molecule that would serve as a source of both carbon and phosphorus to the subsurface environment. This may serve to detrimentally biostimulate the oligotrophic subsurface environment present at the Hanford Site.

An alternative to the phosphate amendments previously described is the use of soluble long-chain polyphosphate materials that have been demonstrated to delay the precipitation of phosphate phases (Wellman et al. 2006b) (Figure 2.5). Phosphate minerals precipitate when phosphate compounds hydrolyze to yield the orthophosphate molecule ( $\text{PO}_4^{3-}$ ); the longer the polyphosphate chain, the slower the hydrolysis reaction that leads to orthophosphate production (Figure 2.6). Accordingly, use of a long-chain polyphosphate compound allows controlled deployment and precipitation within the subsurface, thereby minimizing changes in hydraulic conductivity.

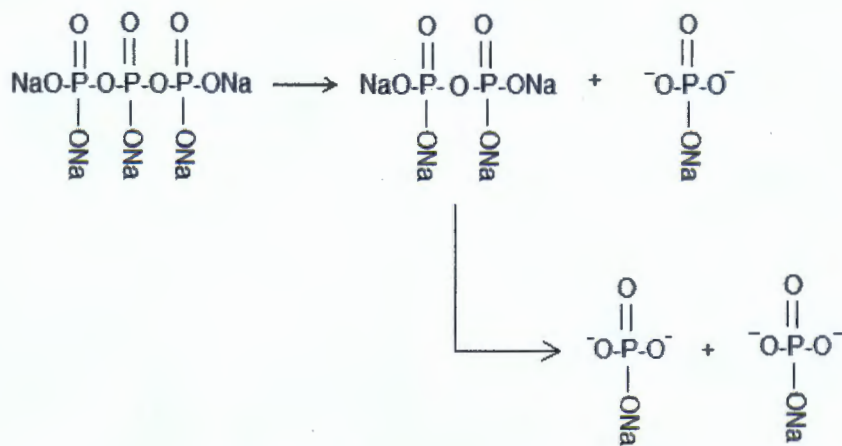


Figure 2.5. Schematic Depicting the Step-Wise Hydrolysis of Sodium Tripolyphosphate

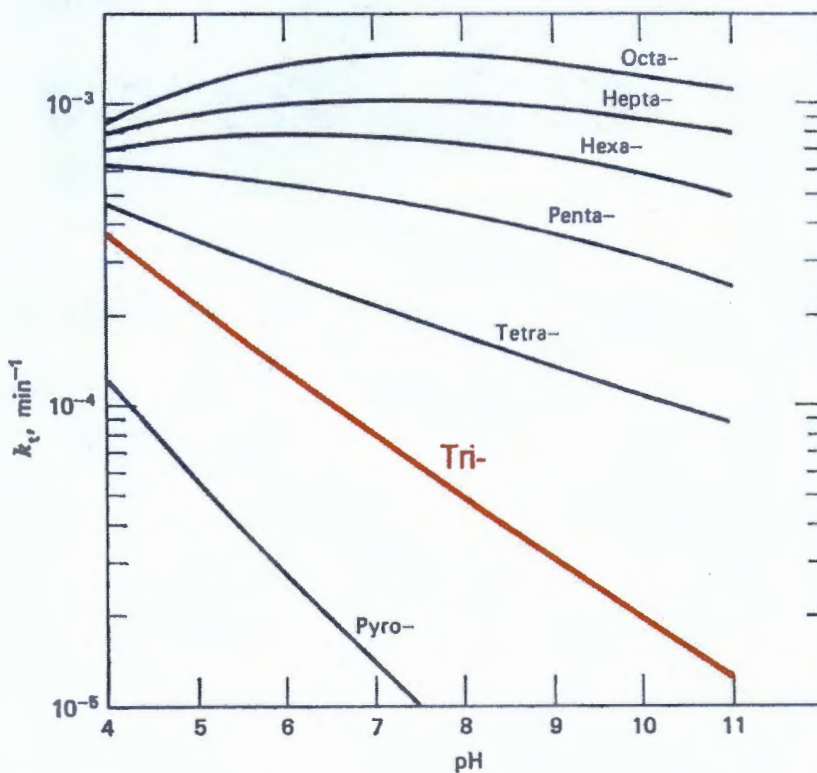
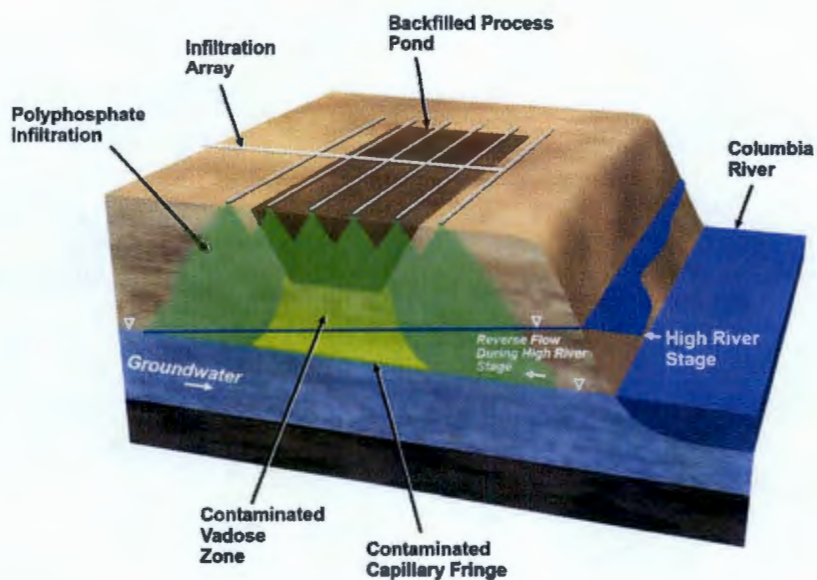


Figure 2.6. Hydrolysis Rate of Polyphosphate Molecules as a Function of pH (Shen and Morgan 1973)

The focus of this investigation is to evaluate the efficacy of using the polyphosphate treatment technology to treat uranium contamination within the deep vadose zone and capillary fringe (i.e., zone of water table fluctuation or “smear zone”) above the 300 Area aquifer. A conceptual design of a treatability test is the construction of an infiltration array at the ground surface above an area of potential contamination such as one of the process ponds, which has been previously excavated and backfilled, but may contain some unknown amount of contamination in the vadose zone and capillary fringe beneath the lower extent of the excavation activities (e.g., Figure 2.7). Infiltration of polyphosphate technology is expected to enhance the paragenesis of uranium solid phases by increasing the weathering and transformation of these phases to uranium-phosphate phases. This is expected to mitigate the continuing source of groundwater contamination and enhance the proposed polyphosphate remediation within the 300 Area aquifer (Wellman et al. 2007b). Data obtained from this study will be used to develop implementation cost estimates, identify implementation challenges, and investigate the capability of the technology to meet remedial objectives. This information will be used to establish the viability of the method and determine how best to implement the technology in the field.



**Figure 2.7.** Schematic Depicting a Proposed Treatability Test of Polyphosphate to Stabilize Uranium in the Vadose Zone and Capillary Fringe

### 3.0 Laboratory-Scale Testing – Materials and Methods

Laboratory-scale tests were conducted to evaluate technical issues, including:

- Quantify the mobility of polyphosphate under water content and pore water velocities relative to the vadose zone and capillary fringe.
- Evaluate uranium-phosphate formation via the reaction between uranium-bearing solid phases and aqueous polyphosphate remediation technology as a function of polyphosphate composition and concentration.
- Develop an understanding of the mechanism of autunite formation via the reaction of solid-phase calcite-bound uranium and aqueous polyphosphate remediation technology.
- Develop an understanding of the transformation mechanism and reaction kinetics between uranyl-carbonate and -silicate minerals with the polyphosphate remedy under advective conditions.
- Quantify the stability of uranyl-carbonate, -silicate, and -phosphate phases controlling uranium in the vadose zone and capillary fringe under site specific conditions and during polyphosphate remedial actions.
- Quantify the extent and rate of uranium released and immobilized as a function of polyphosphate composition, concentration, and based on the infiltration rate of the polyphosphate remedy.
- Provide the fundamental geochemical and thermodynamic data associated with polyphosphate technology and remediation necessary for incorporation into reactive transport codes to allow predictive simulations of polyphosphate remedial actions.

All experiments were conducted with sediments and groundwater from the 300 Area to verify that testing conditions are representative of the remediation area.

#### 3.1 Behavior of Polyphosphate Amendment Under Unsaturated Conditions

Unsaturated-column experiments were conducted using an unsaturated flow apparatus (UFA). The experimental centrifugation system and method used to conduct unsaturated transport experiments are described in detail elsewhere (Gamerding and Kaplan 2000; Gamerding and Kaplan 2001; Gamerding et al. 1998; Gamerding et al. 2001b; a; Wellman et al. 2008a). Therefore, only a brief description will be provided here. Interested readers should consult previous publications for a more comprehensive explanation of the technique. Columns (length,  $L = 6.0$  cm, radius,  $r = 2.25$  cm, bulk volume,  $V_{bulk} = 95.43$  cm<sup>3</sup>) were packed with Hanford vadose zone sediment in approximately 10-g increments which were tamped and the surface was scored prior to adding subsequent layers. The columns were saturated with Hanford groundwater. The process of fully saturating the column and reducing the water content to the desired level minimizes preferential flow paths and hysteresis; establishes the most consistent, uniform attainment of water content within a series of unsaturated columns; and affords a consistent method for establishing unsaturated conditions. Sediment bulk density,  $\rho_b$  (g cm<sup>-3</sup>), and volumetric water content,  $\theta$  (cm cm<sup>-3</sup>), were determined from the mass of the sediment and water. The percent saturation was calculated from the ratio of the volumetric water content to the total porosity,  $\phi$ , which was calculated from the bulk density and particle density,  $\rho_p$  (g cm<sup>-3</sup>).

The saturated column was placed in a temperature-controlled ultracentrifuge (Model L8-UFA, Beckman Coulter, Inc., Fullerton, CA), which has been modified to provide constant flow to two specimens through a rotating seal assembly (Figure 3.1). Steady-state water content was attained at the desired degree of saturation. The centrifugation method uses a combination of the centrifugal force and the fluid flux,  $q$  ( $\text{cm h}^{-1}$ ), where  $q$  is equal to the flow rate,  $F$  ( $\text{cm}^3 \text{h}^{-1}$ ), per cross-sectional area,  $A$  ( $\text{cm}^2$ ). The flow rate and centrifugal force were optimized to attain a fluid residence time of three to four hours. Infusion pumps (AVI 210A, 3M, St. Paul, MN) were used to control the flow rate. Water that was forced from the column by centrifugal force was replaced by fluid delivery via the pump (water was held in the sediment column by matric potential). Unsaturated transport experiments were initiated when the sediment columns reached a steady-state average water content.

Breakthrough curves were determined by changing the influent solution to Hanford groundwater spiked with phosphate compound of interest (Table 3.1) and the non-reactive tracer pentafluorobenzoic acid (PFBA) until complete breakthrough was attained. Subsequently, the influent solution was changed to unspiked Hanford groundwater, which was displaced through the column until all phosphate had been displaced from the column. The conservative tracer within the influent solution was used to provide an estimate of the water flow patterns in the columns.

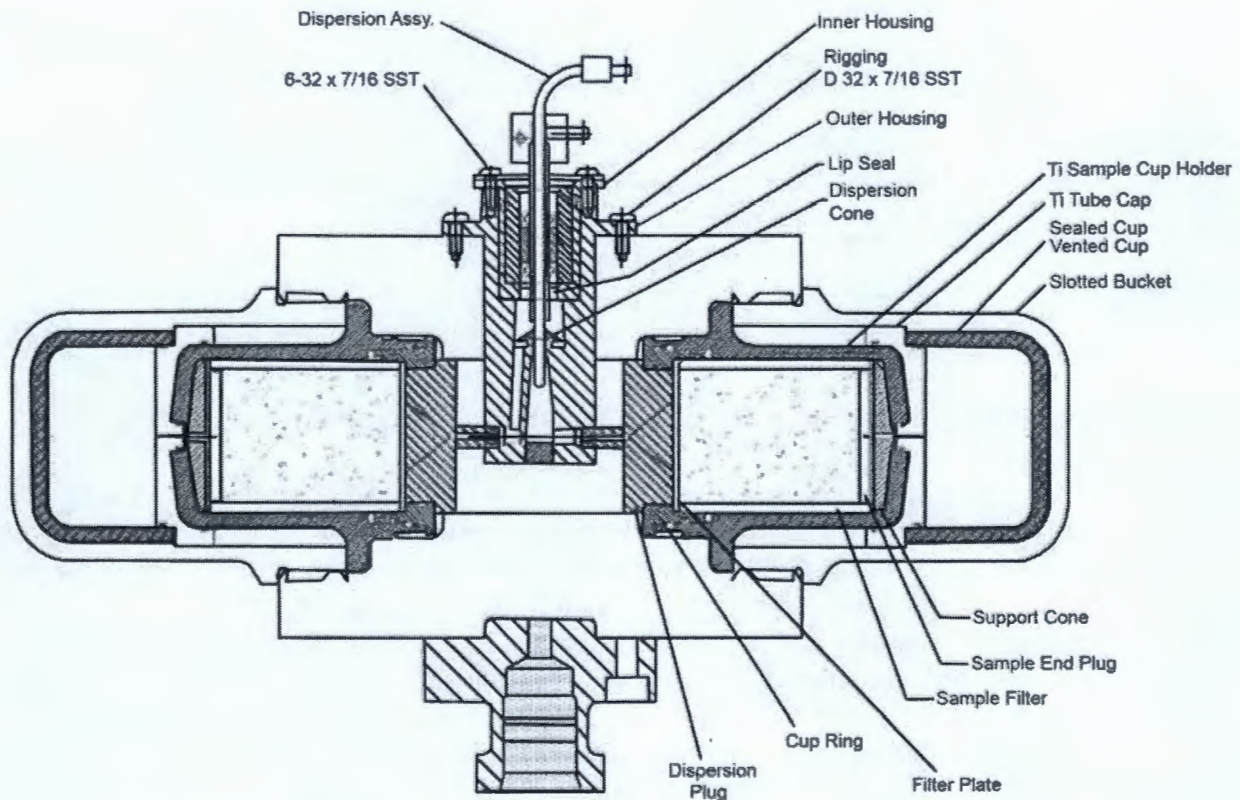


**Figure 3.1.** Schematic of UFA Constant Flow Rotor and Rotating Seal Assembly

**Table 3.1.** Experimental Conditions for the Quantification of Polyphosphate Mobility as a Function of Water Content and Pore Water Velocity

Phosphate amendment	150 ppm as tripolyphosphate, $\text{Na}_3\text{P}_3\text{O}_{10}$	150 ppm as pyrophosphate, $\text{Na}_4\text{P}_2\text{O}_7 \cdot 10\text{H}_2\text{O}$	150 ppm as orthophosphate, $\text{Na}_3\text{PO}_4 \cdot 12\text{H}_2\text{O}$	Polyphosphate formulation: 25% ortho-, 25% pyro-, and 50% tripolyphosphate
Conservative Tracer	PFBA	PFBA	PFBA	PFBA
Water Content, wt%	15% and 25%	15% and 25%	15% and 25%	15% and 25%
Pore Water Velocity	20 and 2 cm $\text{hr}^{-1}$	20 and 2 cm $\text{hr}^{-1}$	20 and 2 cm $\text{hr}^{-1}$	20 and 2 cm $\text{hr}^{-1}$

The average water content is determined gravimetrically by weighing the column at each sampling time; the cumulative effluent volume is determined by summing the mass of each effluent sample and dividing by the specific density of the influent solution. Inductively coupled plasma-mass spectrometry (ICP-OES) was used to measure the concentration of total phosphorus in solution. The centrifuge method is especially suited to this research, which was directed toward testing specific hypotheses using disturbed sediments under a variety of moisture conditions and pore water velocities. Sampling of the effluent is a manual process that requires stopping the centrifuge and flow to the column. Thus, one potentially confounding factor with the centrifuge method is a bias in the kinetic measurements because of flow interruption for sampling (the centrifuge must be stopped to access the sampling cup and remove the effluent solutions). The magnitude of this problem depends on the ratio of the stop interval to the flow rate (Gamerdinger et al. 2001b) and was minimized for these tests. Previous investigations have indicated there is no significant effect for stopping flow to nonsorptive tracers (Gamerdinger and Kaplan 2000), colloids (Kaplan and Gamerdinger 1999), or uranium (Gamerdinger et al. 2001b, 2001a).

## 3.2 Sequestration of Uranium with Calcite

To determine the extent to which calcite can serve as a host for uranium it is necessary to quantify the uptake of uranium by calcite and characterize whether uranium is bound via sorption or incorporated into the structure. If uranium is partitioned with the calcite phase via a sorption mechanism, the retention of uranium will be minimal and subject to desorption. However, if uranium is incorporated into the calcite structure, the release of uranium will be governed by dissolution of the uranium-rich calcite phase.

### 3.2.1 Calcite Pre-Equilibration

To assess only the interaction between aqueous uranium and solid calcite, the calcite must be in a state of thermodynamic equilibrium with the aqueous matrix. The aqueous matrix used for all experiments was prepared by equilibrating Hanford groundwater with calcite for 1 week, followed by vacuum filtration using a 0.45- $\mu\text{m}$  Nalgene filter. The solutions were pH adjusted using Optima nitric acid (Fisher),  $\text{HNO}_3$ , or 1M sodium hydroxide (Alfa Aesar),  $\text{NaOH}$ .

Prior to experimental testing, calcite was equilibrated with the respective test solution by shaking overnight, centrifuging, measuring the pH, and decanting the supernatant. This was repeated until the pH of the added solution was constant after contacting the calcite. The process of pre-equilibration isolated the reaction of uranium with calcite from any other reaction that may have occurred while the calcite and aqueous solutions equilibrated.

### 3.2.2 Kinetic Experiments

Kinetic experiments were conducted to evaluate the rate of uranium uptake by calcite. Nalgene high-density polyethylene (HDPE) bottles contained 500 mL of calcite-equilibrated Hanford groundwater, at respective pH values ranging from 6.5 to 8, containing 100 mg/L of uranyl-nitrate and 0.25 g of calcite (100-200 mesh) washed with ethanol. Control solutions were prepared using the same testing conditions in the absence of calcite to evaluate the loss of uranium to the test apparatus. There was no measurable sorption of uranium to the test containers over the pH range investigated. All solutions were placed on a shaker table for predetermined time intervals ranging from 2 to 1440 minutes, and then centrifuged at 2100 rpm for 5 minutes to remove any colloidal material from suspension. Immediately after centrifugation 5-mL aliquots of the supernatant were removed and filtered through a 0.2- $\mu$ m syringe filter. Inductively coupled plasma-mass spectrometry (ICP-MS) was used to measure the concentration of aqueous uranium; ICP-OES was used to quantify the aqueous concentration of calcium.

### 3.2.3 Loading Experiments

Loading experiments were conducted in a manner similar to kinetics experiments (ASTM 2001). Calcite-equilibrated Hanford groundwater, at respective pH values ranging from 6.5 to 8, was spiked with uranyl-nitrate to the desired concentration. The respective solutions were added to Nalgene HPDE bottles containing calcite. The solution-to-solid ratio for loading experiments varied from 50 to 10,000. The initial aqueous uranium concentration was 100 mg/L. Control solutions were prepared using the same testing conditions in the absence of calcite to evaluate the loss of uranium to the test apparatus. Sorption of uranium to the test containers was not measured over the pH range investigated. All solutions were placed on a shaker table for 24 hours. The samples were centrifuged at 2100 rpm for 5 minutes to remove any colloidal material from suspension prior to removing 3-mL aliquots of the supernatant. The supernatant was filtered through a 0.2- $\mu$ m syringe filter and analyzed using ICP-MS to measure the concentration of aqueous uranium.

The percent sorption was calculated as follows:

$$\% \text{ Sorption} = \frac{C_i - C_f}{C_i} * 100 \quad (3.1)$$

where  $C_i$  and  $C_f$  = the initial and final concentrations of aqueous uranium (mg/L)

Determining the standard deviation requires accounting for the uncertainty associated with each parameter in Equation 3.1.

The standard deviation of a function for uncorrelated random errors is given by

$$\sigma_f = \sqrt{\sum_{i=1}^n \left( \frac{\partial f}{\partial x_i} \right)^2 \sigma_i^2} \quad (3.2)$$

where  $\sigma_f$  = standard deviation of the function  $f$ ,  
 $x_i$  = parameter  $i$ ,  
 $\sigma_i$  = standard deviation of parameter  $i$ .

Substituting Equation 3.1 into 3.2 and converting to relative standard deviations,  $\hat{\sigma}_r = \sigma_f/\bar{x}$ , yields

$$\hat{\sigma}_r = \sqrt{\frac{(\hat{\sigma}_{c_i} c_i)^2 + (\hat{\sigma}_{c_f} c_f)^2}{(c_i - c_f)^2} + \hat{\sigma}_{c_i}^2 c_i^2} \quad (3.3)$$

Errors for  $\hat{\sigma}_{c_i}$ ,  $\hat{\sigma}_{c_f}$ ,  $\hat{\sigma}_V$ , and  $\hat{\sigma}_m$  are 10%, 10%, 5%, and 5%, respectively. This error analysis results in typical  $2\sigma$  uncertainties. All experiments were conducted in duplicate to ensure that the system yielded reproducible results.

### 3.2.4 Equilibrium Partition Coefficient, $K_d$ , Experiments

$K_d$  experiments were conducted in a manner similar to kinetics and loading experiments (ASTM 2001). The calcite-equilibrated Hanford groundwater was pH adjusted to values ranging from 6.5 to 8 and spiked with uranyl-nitrate to achieve concentrations ranging from 10 ppb to 10 ppm uranyl-nitrate. A 10-mL aliquot of each solution was added to a test tube containing 0.2 g of calcite. All solutions were placed on a shaker table for one week. The samples were centrifuged at 2100 rpm for 5 minutes to remove any colloidal material from suspension prior to removing 5-mL aliquots of the supernatant. The supernatant was filtered through a 0.2- $\mu$ m syringe filter and analyzed using ICP-MS to measure the concentration of aqueous uranium.

The distribution coefficient was calculated as follows:

$$K_d = \frac{(C_i - C_f)V}{C_f M} \quad (3.4)$$

where  $K_d$  = distribution coefficient  
 $C_i$  and  $C_f$  = initial and final concentrations of aqueous uranium (mg/L)  
 $V$  = volume of solution (mL)  
 $M$  = mass of calcite (g).

## 3.3 Synthesis of Uranium Minerals

The synthesis of uranium-bearing calcite and uranophane are described in the following sections.

### 3.3.1 Synthesis of Uranium-Bearing Calcite

Uranium-bearing calcite was precipitated by modification of the method of Reeder et al. (2000), which is similar to the method of Tesoriero and Pankow (1996). A 1.5-mM solution of aqueous uranyl nitrate,  $(\text{UO}_2(\text{NO}_3)_2 \cdot 6\text{H}_2\text{O})$ , International BioAnalytical Laboratories) was prepared in 18-M $\Omega$ /cm distilled, deionized (DDI) water. Two solutions were prepared in DDI water; one was a solution of 300-mM calcium ( $\text{CaCl}_2$ , Alfa Aesar) and the other was a 300-mM bicarbonate ( $\text{NaHCO}_3$ , Alfa Aesar) solution. A 0.9 molal solution of sodium chloride ( $\text{NaCl}$ , Alfa Aesar) was prepared and added to both the calcium chloride and sodium bicarbonate solutions as the background electrolyte to yield solutions with a total ionic strength of 0.5 molal. The calcium chloride and sodium bicarbonate solutions were simultaneously delivered to the uranyl-nitrate solution at a constant rate of 250 mL/hr using infusion pumps (AVI 210A, 3M, St. Paul, MN). The solutions were constantly stirred and air was continuously bubbled to maintain a consistent concentration of  $\text{CO}_2$  for a period of four days. The concentrations of Ca and  $\text{HCO}_3$  were maintained at approximately 100 mM. The pH initially increased until calcite nucleation was observed. Subsequently, the pH decreased to 8.1-8.2 and remained constant throughout the duration of the co-precipitation experiment. The precipitate was recovered via centrifugation at 2000 rpm, washed three times with boiled DDI water, and dried at room temperature for seven days.

The synthetic product was characterized using EXAFS spectroscopy, chemical digestion with concentrated nitric acid (Fisher Optima) followed by ICP-MS for elemental analyses, X-ray diffraction (XRD), scanning electron microscopy (SEM), and multi-point Brunauer-Emmett-Teller (BET) analyses. EXAFS spectroscopy was used to confirm whether the uranium-carbonate bond environment was consistent with reference uranium co-precipitated with calcite; chemical analyses were used to ensure chemical composition; XRD was used to confirm mineralogy; SEM was used to evaluate morphology; and krypton (Kr)-adsorption BET was used to measure sample surface area.

### 3.3.2 Synthesis of Uranophane

Uranophane was synthesized by adding 4.2 g of uranyl-acetate dihydrate ( $\text{UO}_2(\text{C}_2\text{H}_3\text{O}_2)_2 \cdot 2\text{H}_2\text{O}$ , International BioAnalytical Laboratories), 2.3 g of sodium silicate nanohydrate ( $\text{Na}_2\text{SiO}_3 \cdot 9\text{H}_2\text{O}$ , Fisher Scientific), 2.8 g of calcium acetate ( $\text{Ca}(\text{C}_2\text{H}_3\text{O}_2)_2 \cdot 2\text{H}_2\text{O}$ , JT Baker), and 48 mL of prepared DDI water, to a 125 mL Teflon cup (Parr Instrument Co.). The DDI water, 18 M $\Omega$ /cm, was boiled for 20 minutes then allowed to cool while nitrogen was continuously bubbled into the water. The pH of the solution was adjusted to 5.5 using high pressure liquid chromatography (HPLC)-grade glacial acetic acid ( $\text{CH}_3\text{COOH}$ , Fisher Scientific). A Teflon lid was placed on the Teflon cup and then inserted into a 125-mL digestion reactor (Parr Instrument Co.). The reactor was heated for 24 hours at 100°C and then cooled to room temperature. The product was recovered via centrifugation at 1800 rpm, washed five times with boiled DDI water, then returned to the Teflon cup along with 50 mL of prepared DDI water. The lid and cup were inserted into the digestion reactor and heated at 175°C for 5 days. After cooling to room temperature, the product was recovered via centrifugation and dried at room temperature.

## 3.4 Characterization of Pristine and Reacted Uranium Minerals – Uranium-Rich Calcite, Uranophane, and Meta-Torbernite

Synthetic uranium-rich calcite and uranophane, and natural meta-torbernite obtained from Katanga, Zaire via Excalibur Minerals, were characterized using EXAFS spectroscopy, XRD, SEM, and multi-

point BET analyses. EXAFS spectroscopy was used to confirm whether the uranium-carbonate bond environment was consistent with reference uranium co-precipitated with calcite; XRD was used to confirm mineralogy; SEM was used to evaluate morphology; and N<sub>2</sub>-adsorption BET was used to measure sample surface area.

### **3.4.1 X-Ray Diffraction**

X-ray diffraction was performed using material ground in an agate mortar and pestle to <500 mesh (<25 μm) (using standard sieves of the American Society for Testing Materials [ASTM]) to improve the diffraction patterns by removing the effects of preferred orientation. Spectrometry was performed using a Scintag Inc. Model 3520 PAD-V x-ray diffractometer, operated at 45 kV and 40 mA using a XGEN-4000 generator. Tungsten-filtered copper radiation  $K_{\alpha} = 1.54 \text{ \AA}$  was used with a Peltier cooled Scintag Inc. Si(Li) solid-state detector. The sample was analyzed using a 2-theta ( $2\theta$ ) range from 2 to 65°, a step size of 0.02° and a 4-second count time at each step. In addition to identification of the main phase on the basis of its structure, these methods also should identify any contaminating crystalline minerals that constitute  $\geq \sim 5 \text{ wt\%}$  of the bulk composition.

### **3.4.2 Scanning Electron Microscopy – Energy Dispersive Spectrometry**

Photomicrographs of hydroxylapatite were obtained by means of a SEM JEOL 840 equipped with a Robinson 6.0 backscatter detector. The beam conditions were 20 KeV acceleration and a 1 nA beam current. The samples were mounted on an aluminum plate using double-sided tape and were carbon-coated under a vacuum. The carbon coat provides a conductive path for the electrons and helps secure the particles. Images were acquired using GATAN DM software version 3.2, 1996.

An Oxford ISIS 300 series energy dispersive spectrometer (EDS) was used to determine chemical composition. EDS spectra were stored electronically using Oxford ISIS 300 version 3.2 software. An EDS spectrum represents the chemical composition of a particle found within a sample. While not all particles are counted for the same live-/dead-time period, a typical EDS spectrum is counted for 100 seconds with 30% dead-time.

### **3.4.3 N<sub>2</sub>-Adsorption BET Surface Area**

Surface area measurements were determined based on the multi-point BET N<sub>2</sub>-adsorption method (Brunauer et al. 1938). A Micromeritics ASAP 2020 Gas Sorption System was used to measure the surface area of the uranium-calcite sample. A reference alumina standard (lot number 46F-BA106-24) was used to verify instrument calibration and ensure consistent sample preparation. Grab samples, ~0.5g, of each of the materials (reference standard and sample) were weighed and placed in tared sample flasks. A vacuum was pulled on each sample flask for 100 hours at 100°C to remove all physi-sorbed contaminants from the mineral surfaces and provide a clean solid surface onto which a monolayer of gas molecules would absorb. The surface area for the minerals was then measured by the adsorption of nitrogen on the sample surface.

### 3.4.4 Extended X-Ray Absorption Fine Structure Spectroscopy

EXAFS analysis was conducted on pristine uranium phases including synthetic uranium-rich calcite and natural meta-autunite, as well as uranium-rich calcite samples reacted with ortho-, pyro-, and tripolyphosphate; calcite samples reacted with uranium at pH 7, 7.5, and 8; and reacted materials extracted from pressurized unsaturated flow (PUF) columns. EXAFS results were compared to previously published spectra of uranium-bearing calcite (Reeder et al. 2000; Reeder et al. 2001). The spectra of meta-ankoleite and meta-autunite were previously published by Thompson et al. (1998) and the spectra of saléeite and metatorbernite by Catalano and Brown (2004). Uranium L<sub>III</sub>- EXAFS measurements of the uranium-calcite samples were conducted at room temperature on the Molecular Environmental Sciences Beamline 11-2 (Bargar et al. 2002) at the Stanford Synchrotron Radiation Laboratory (SSRL) using a cryogenically cooled Si (220),  $\phi = 0^\circ$ , double-crystal monochromator. Fluorescence-yield data were collected using an argon-filled Stern-Heald-type detector (Lytle et al. 1984). A collimating mirror before the monochromator was used for harmonic rejection, with a cutoff of 19.6 keV. Yttrium metal foil was mounted between two ionization chambers downstream of the sample for energy calibration; the first inflection point in the yttrium K-edge was set to 17038 eV. Background-subtracted  $k^3$ -weighted EXAFS data were analyzed using the SixPACK (Webb 2004) interface to IFEFFIT (Newville 2001). The data were fit as linear combinations of the  $\chi$  data from  $k = 3$ -12,  $k^3$  weighted.

## 3.5 Stability of Uranium Minerals – Uranium-Rich Calcite, Uranophane, and Meta-Torbernite

Single-pass flow-through test methods and rate calculations and uncertainty associated with evaluating the dissolution of uranium-bearing calcite, uranophane, and meta-torbernite are discussed in the following sections.

### 3.5.1 Single-Pass Flow-Through Test Methods

Evaluation of the dissolution of uranium-bearing calcite, uranophane, and meta-torbernite was performed with the single-pass flow-through (SPFT) test method. The SPFT apparatus provides for experimental flexibility, allowing each of the kinetic test parameters to be isolated and quantified. Temperature, flow rate, solution composition, and sample mass and size can be manipulated to assure accurate rate determinations.

The SPFT method has been described in detail elsewhere (McGrail et al. 1997b; Wellman et al. 2006a; Wellman et al. 2005); therefore, only a brief description will be provided here and interested readers should consult the noted references for additional information. In general, the SPFT system (Figure 3.2) consists of a programmable pump (Kloehn; model 50300) that transports solutions from an influent reservoir via Teflon lines. Solution is transferred into 60-mL capacity *perfluoroalkoxide* (PFA) reactors (Savillex). The reactors are situated within constant temperature ovens (VWR Scientific Products), whose temperature is controlled to  $\pm 2^\circ\text{C}$  by tested and calibrated thermocouples (Glas-Col; model TC105). The powdered specimen rests at the bottom of the reactor and influent and effluent solutions enter and exit, respectively, from fluid transfer lines that protrude through two separate ports at the top of the reactor. The residence time of aqueous solutions in the reactor varies with the flow rate, which is adjusted in accordance with the needs of the experiment. The effluent line carries solution to collection vials that are positioned outside the oven.

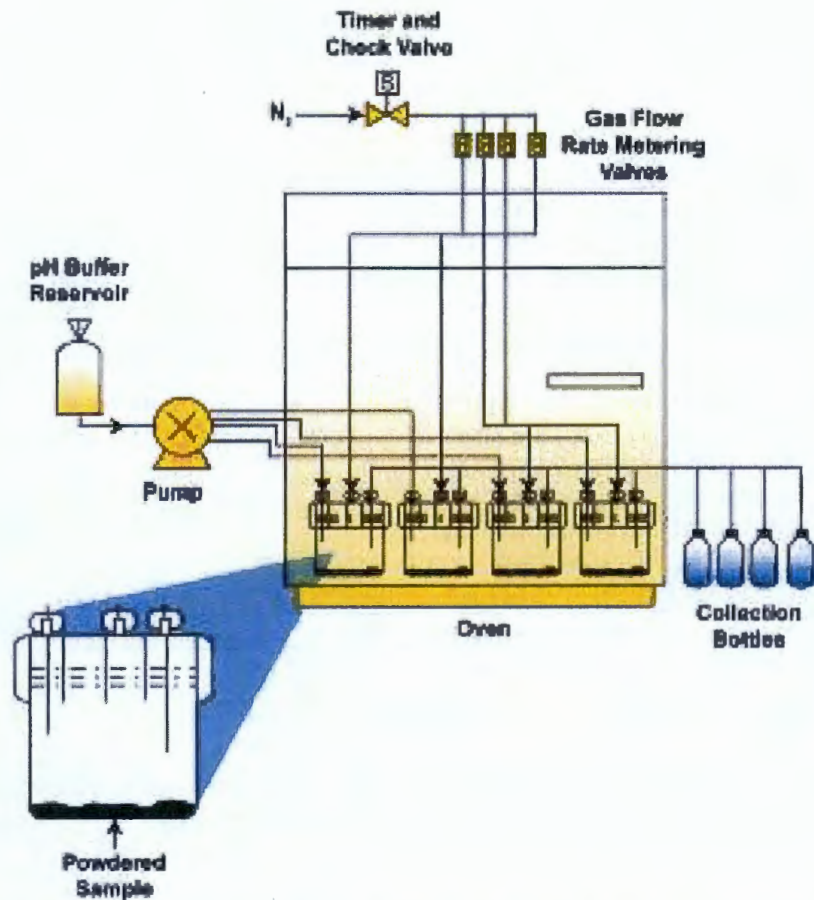


**Figure 3.2.** Schematic of the Single-Pass Flow-Through Dissolution Test System

Effluent solution was collected continuously and aliquots of the fluid sample were retained for both pH measurement and analysis of dissolved element concentrations by ICP-OES and ICP-MS. Solutions earmarked for analysis by ICP-OES and ICP-MS methods were preserved in Optima™ nitric acid. Concentrations of aqueous calcium and phosphorus were used to quantify the dissolution rates as a function of pH and temperature. Before the sample specimens were added to the reactor, blank solution samples were collected and used to establish the concentration of background analytes. The blank samples were treated in exactly the same manner as the samples.

The solutions used to control the pH during the SPFT experiments are summarized in Table 3.2. Table 3.2 also lists the *in situ* pH values computed at each test temperature using EQ3NR (Wolery 1992). It is important to take into account the change in pH that occurs at different temperatures when computing dissolution rates from SPFT data because the *in situ* pH can vary by as much as 1.5 pH units over the temperature range from 23° to 90°C. By quantifying temperature and pH-dependent rate parameters the dissolution rate of relevant minerals can be extrapolated to conditions representative of the subsurface. Buffer solutions were prepared by adding small amounts of the organic *tris* hydroxymethyl aminomethane (THAM) buffer to DDI water and adjusting the solution to the desired pH value using 15.8M HNO<sub>3</sub> or 1 M LiOH.

**Table 3.2.** Composition of Solutions Used in Single-Pass Flow-Through Experiments. Solution pH values above 23°C were calculated using the EQ3NR Code V7.2b database.

Solution	Composition	pH @			
		23°C	40°C	70°C	90°C
1	0.01 M THAM + 0.00143 M LiOH + 0.0111 M HNO <sub>3</sub>	6.05	5.96	5.55	5.23
2	0.01 M THAM + 0.00914 M HNO <sub>3</sub>	6.86	6.59	6.02	5.67
3	0.01 M THAM + 0.0032 M HNO <sub>3</sub>	8.06	7.83	7.33	6.99
4	0.01 M THAM + 0.000274 M HNO <sub>3</sub>	9.09	8.86	8.42	8.10
5	0.01 M THAM	10.04	9.59	8.90	8.53
6	0.01 M THAM + 0.00514 M LiOH	10.97	10.87	10.45	10.09
7	0.01 M THAM + 0.0143 M LiOH	12.06	11.62	10.90	10.52
8	0.05 M THAM + 0.0375 M HNO <sub>3</sub>	5.91	5.99	6.06	5.99
9	0.05 M THAM + 0.047 M HNO <sub>3</sub>	7.01	6.57	5.91	5.55
10	0.05 M THAM + 0.02 M HNO <sub>3</sub>	8.32	7.90	7.25	6.89
11	0.05 M THAM + 0.0041 M HNO <sub>3</sub>	8.99	8.67	8.08	7.72
12	0.05 M THAM + 0.003 M LiOH	9.99	9.55	8.88	8.52
13	0.1 M NH <sub>4</sub> OH + 0.00256 M HNO <sub>3</sub>	11.09	10.67	9.92	9.51
14	0.1 M NH <sub>4</sub> OH + 0.0175 M LiOH	12.00	11.13	9.81	9.06

THAM = *tris* hydroxymethyl aminomethane buffer.

### 3.5.2 Rate Calculations and Uncertainty

Dissolution rates, based on steady-state concentrations of elements in the effluent, are normalized to the amount of the element present in the sample by the following formula:

$$r_i = \frac{(C_i - \bar{C}_{i,b})q}{f_i S} \quad (3.5)$$

- where
- $r_i$  = the normalized dissolution rate for element  $i$  ( $\text{g m}^{-2} \text{d}^{-1}$ )
  - $C_i$  = the concentration of the element  $i$  in the effluent ( $\text{g L}^{-1}$ )
  - $\bar{C}_{i,b}$  = the average background concentration of the element of interest ( $\text{g L}^{-1}$ )
  - $q$  = the flow rate ( $\text{L d}^{-1}$ )
  - $f_i$  = the mass fraction of the element in the metal (dimensionless)
  - $S$  = the surface area of the sample ( $\text{m}^2$ ).

The surface area of uranium-bearing calcite, uranophane, and meta-torbernite were determined using N<sub>2</sub>-adsorption BET analysis (Table 3.3) (Brunauer et al. 1938).

**Table 3.3.** Surface Area of Uranium Minerals as Measured by BET N<sub>2</sub>-Adsorption

Uranium Mineral	Surface Area, m <sup>2</sup> /g
Uranium-calcite	0.30
Uranophane	74.88
Meta-torbernite	1.28

The value of  $f_i$  was calculated from the chemical composition of the sample. Flow rates are determined by gravimetric analysis of the fluid collected in each effluent collection vessel upon sampling. The background concentration of the element of interest is determined, as previously discussed, by analyses of the starting input solution and three blank solutions. Typically, background concentrations of elements are below their respective detection threshold. The detection threshold of any element is defined here as the lowest calibration standard that can be determined reproducibly during an analytical run within 10%. In cases where the analyte is below the detection threshold, the background concentration of the element is set at the value of the detection threshold.

Determining the experimental uncertainty of the dissolution rate takes into account uncertainties of each parameter in Equation (3.8). For uncorrelated random errors, the standard deviation of a function  $f(x_1, x_2, \dots, x_n)$  is given by

$$\sigma_f = \sqrt{\sum_{i=1}^n \left( \frac{\partial f}{\partial x_i} \right)^2 \sigma_i^2} \quad (3.6)$$

where  $\sigma_f$  = the standard deviation of the function  $f$   
 $x_i$  = parameter  $i$   
 $\sigma_i$  = the standard deviation of parameter  $i$ .

Substituting Equations (3.5) into (3.6) results in the following:

$$\sigma_{r_i} = \sqrt{\left( \frac{q}{f_i S} \right)^2 (\sigma_{C_i}^2 + \sigma_{\bar{C}_{i,b}}^2) + \left( \frac{C_i - \bar{C}_{i,b}}{f_i S} \right)^2 \sigma_q^2 + \left( \frac{(C_i - \bar{C}_{i,b})q}{f_i^2 S} \right)^2 \sigma_{f_i}^2 + \left( \frac{(C_i - \bar{C}_{i,b})q}{f_i S^2} \right)^2 \sigma_S^2} \quad (3.7)$$

Equation (6) can also be expressed in terms of the relative error,  $\hat{\sigma}_{r_i} = \sigma_{r_i} / r_i$ , and is given by

$$\hat{\sigma}_{r_i} = \sqrt{\frac{(\hat{\sigma}_{C_i} C_i)^2 + (\hat{\sigma}_{\bar{C}_{i,b}} \bar{C}_{i,b})^2}{(C_i - \bar{C}_{i,b})^2} + \hat{\sigma}_q^2 + \hat{\sigma}_{f_i}^2 + \hat{\sigma}_S^2} \quad (3.8)$$

Relative errors of 10%, 10%, 5%, 3%, and 15% for  $C_i$ ,  $\bar{C}_{i,b}$ ,  $q$ ,  $f_i$ , and  $S$ , respectively, are typical for measurements conducted at PNNL. However, to reduce the error associated with mass fraction ( $f_i$ ), the samples to be used in these experiments will be ground, homogenized, sub-sampled, and analyzed at least three times to obtain a more accurate composition with a better estimate of the uncertainty. The conservative appraisal of errors assigned to the parameters in Equation (3.8), in addition to the practice of imputing detection threshold values to background concentrations, results in typical uncertainties of approximately  $\pm 35\%$  on the dissolution rate.

### 3.6 Interaction of Polyphosphates with Uranium Minerals – Uranium-Rich Calcite, Uranophane, and Meta-Torbernite

The interaction of ortho-, pyro-, and tripolyphosphate with uranium-rich calcite was evaluated through a series of static and dynamic tests to determine the effect of polyphosphate amendments on the stability of uranium-rich calcite, uranophane, and meta-torbernite. ICP-OES and ICP-MS were used to quantify the concentration of aqueous cations and anions; x-ray absorption spectroscopy was used to determine the spatial variation in U(VI) solid-phase concentration and speciation with micrometer resolution and identify the resulting uranium phase(s) formed as a function of the during phosphate remediation formulation and treatment.

#### 3.6.1 Kinetic Experiments

Kinetic experiments were conducted to evaluate the rate of interaction of ortho- ( $\text{Na}_3\text{PO}_4 \cdot 12\text{H}_2\text{O}$ ), pyro- ( $\text{Na}_4\text{P}_2\text{O}_7 \cdot 10\text{H}_2\text{O}$ ), and tripolyphosphate ( $\text{Na}_5\text{P}_3\text{O}_{10}$ ) with uranium-bearing calcite. Nalgene HDPE bottles had 500 mL of DDI water, which was spiked with ortho-, pyro-, or tripolyphosphate to the desired concentration (Table 3.4) and adjusted to pH values ranging from 6.5 to 8. Control solutions were prepared using the same testing conditions in the absence of uranium-rich calcite to evaluate the loss of ortho-, pyro-, and tripolyphosphate to the test apparatus. Sorption of ortho-, pyro-, and tripolyphosphate to the test containers was not measured over the pH range investigated. Five grams of uranium-rich calcite was added to the groundwater solutions and all solutions were placed on a shaker table for predetermined time intervals ranging from 1 to 1440 minutes. ICP-MS was used to measure the concentration of aqueous uranium; ICP-OES was used to measure the concentration of total phosphate and calcium.

**Table 3.4.** Conditions for Quantification of the Kinetic Interaction of Polyphosphate with Uranium-Bearing Calcite

Temperature, °C	23
pH	6.5, 7, 7.5, 8
Phosphate amendment	500 ppm $\text{PO}_4$ as tripolyphosphate, pyrophosphate, or orthophosphate, respectively
Time, min	1, 2, 4, 6, 10, 15, 30, 60, 120, 480, 1440

#### 3.6.2 Loading Experiments

Loading experiments were conducted in a manner similar to kinetics experiments (ASTM 2001). DDI water, at respective pH values ranging from 6.5 to 8, was spiked with ortho-, pyro-, or tripolyphosphate to the desired concentration (Table 3.5). The respective solutions were added to Fisher 50-mL centrifuge tubes containing uranium-rich calcite to achieve the desired solution-to-solid ratios (Table 3.5), which varied from 100 to 2500. Control solutions were prepared using the same testing conditions in the absence of uranium-rich calcite to evaluate the loss of ortho-, pyro-, or tripolyphosphate to the test apparatus. Sorption of ortho-, pyro-, and tripolyphosphate to the test containers was not measured over the pH range investigated. All solutions were placed on a shaker table. The samples were centrifuged at 2000 rpm for 5 minutes to remove any colloidal material from suspension prior to removing 3-mL aliquots of the supernatant. The supernatant was filtered through a 0.2- $\mu\text{m}$  syringe filter and analyzed using ICP-MS to measure the concentration of aqueous uranium, and using ICP-OES to measure the total concentration of aqueous phosphate and calcium.

**Table 3.5.** Experimental Conditions for Quantifying the Loading of Polyphosphate on Uranium-Bearing Calcite

Temperature, °C	23
pH	6.5, 7, 7.5, 8
Phosphate amendment	500 ppm PO <sub>4</sub> as triphosphate, pyrophosphate, and orthophosphate, respectively
Solution-to-Solid Ratio	50, 100, 200, 500, 1000, 2500

### 3.6.3 Unsaturated Weathering of Uranium Minerals During Polyphosphate Remediation

Dynamic tests were conducted under unsaturated conditions using the PUF system (McGrail et al. 1997a; 1999; Pierce et al. 2006; Wierenga and Van Genuchten 1989). The UFA and PUF systems are equally suited to conducting comparable unsaturated flow experiments. However, the PUF system allows controlled dynamic changes in water content that simulate the periodic wet-dry cycling experienced in the deep vadose zone and smear zone. Additionally, slight changes in pH, conductivity, and water content that occur during dissolution and precipitation reactions are continuously logged via the PUF system. As such, the PUF system is better suited to conducting unsaturated weathering and precipitation experiments than the UFA system (Pierce et al. 2006; McGrail et al. 1997a; 1999) (Figure 3.3).

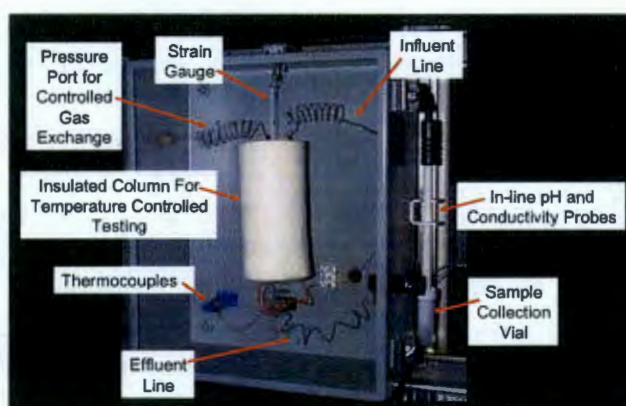


**Figure 3.3.** Photo of PUF Column Assembly

The PUF system, which is similar to a Wierenga column (McGrail et al. 1997a; 1999), consists of a polyetheretherketone column ( $r = 0.96$  cm,  $L = 7.62$  cm) with a porous titanium plate; it has a nominal pore size of  $0.2 \mu\text{m}$  and is sealed in the bottom of the column. Once the porous titanium plate is water saturated, water, but not air, is allowed to flow through the  $0.2\text{-}\mu\text{m}$  pores, as long as the applied pressure differential does not exceed the air entry relief pressure, referred to as the bubble pressure of the Ti-plate. If the pressure differential is exceeded, air will escape through the plate and compromise the capability to maintain unsaturated flow conditions in the column (McGrail et al. 1997a; 1999). The PUF test computer control system runs LabVIEW™ (National Instruments Corporation) software for logging test data from several thermocouples, pressure sensors, inline sensors that measure effluent pH and conductivity, and from an electronic strain gauge that measures column weight to accurately track water mass balance and saturation level. The column also includes a PUF port, which is an electronically actuated valve that periodically vents the column gases. The purpose of column venting is to prevent reduction in the partial pressure of important gases, especially O<sub>2</sub> and CO<sub>2</sub>, which may be consumed in a variety of chemical reactions.

Columns were packed with Hanford vadose zone sediment and uranium-bearing minerals (uranium-rich calcite, uranophane, and meta-torbernite) previously identified as controlling phases in 300 Area sediments (Catalano et al. 2004; Catalano and Brown, Jr. 2004; Catalano et al. 2006b; Dong et al. 2005; Wang et al. 2005a; Wang et al. 2005b; Zachara et al. 2007; Zachara et al. 2005; Arai et al. 2007) in approximately 5-g increments that were tamped and the surface was scored prior to adding subsequent layers (Table 3.6). The columns were saturated with Hanford groundwater. The process of fully saturating the column and reducing the water content to the desired level minimizes preferential flow paths and hysteresis verifies the most consistent, uniform attainment of water content within a series of unsaturated columns, and affords a consistent method for establishing unsaturated conditions. Sediment bulk density,  $\rho_b$  ( $\text{g cm}^{-3}$ ), and volumetric water content,  $\theta$  ( $\text{cm}^3 \text{cm}^{-3}$ ), were determined from the mass of the sediment and water. The percent saturation was calculated from the ratio of the volumetric water content to the total porosity,  $\phi$ , which was calculated from the bulk density and particle density,  $\rho_p$  ( $\text{g cm}^{-3}$ ).

**Table 3.6.** Sediment and Uranium Mineral Composition of Columns Used in the Evaluation of Polyphosphate Remediation Under Vadose Zone Conditions

Sediment	Uranium Mineral	Polyphosphate Amendment
North Process Pond		100% tripolyphosphate in Hanford Groundwater
North Process Pond		Hanford Groundwater
Uncontaminated 300 Area	Uranium-rich calcite	25% ortho-, 65% pyro-, 10% tripolyphosphate in Hanford Groundwater
Uncontaminated 300 Area	Uranium-rich calcite	70% ortho-, 20% pyro-, 10% tripolyphosphate in Hanford Groundwater
Uncontaminated 300 Area	Uranium-rich calcite	90% ortho- and 10% tripolyphosphate in Hanford Groundwater
Uncontaminated 300 Area	Uranium-rich calcite	Hanford Groundwater
Uncontaminated 300 Area	Uranophane	90% ortho- and 10% tripolyphosphate in Hanford Groundwater
Uncontaminated 300 Area	Meta-Torbernite	90% ortho- and 10% tripolyphosphate in Hanford Groundwater
Uncontaminated 300 Area	Meta-Torbernite	Hanford Groundwater

Flow was initiated through the columns with Hanford groundwater until steady-state water content was attained at the desired degree of saturation. After the attainment of hydraulic and chemical equilibrium, the influent solution was changed to Hanford groundwater containing the polyphosphate formulation. The effect of wet-dry cycling was simulated by periodically resaturating the column, with continuous flow, and then desaturating the column to the initial water content. All effluent solutions were monitored for pH with in-line sensors. Prior to starting the experiments, the in-line pH probe was calibrated with National Bureau of Standards pH buffers (pH 7.00, 10.00, or 12.00 at 25°C). Precision of pH measurement was  $\pm 0.02$  pH units. Concentrations of Al, Ca, Cd, Co, Cr, Fe, K, Mg, Na, P, S, Sr, and Si in the effluent solutions samples were monitored with ICP-OES methods; whereas the concentration of uranium was determined by ICP-MS methods. After passing through the 0.2- $\mu\text{m}$  Ti porous plate and the inline sensors, aliquots of the effluent solutions were acidified with ultra-high-purity concentrated  $\text{HNO}_3$  and analyzed using ICP-OES and ICP-MS methods.

Upon termination of the column tests, the solid-phase speciation of U(VI) was assessed using XRD and EXAFS to develop a mechanistic understanding of the formation and/or transformation and identity of resulting uranium phase(s) during phosphate remediation. The thermodynamic database and reaction code EQ3/6 (Wolery and Jarek 2003) was used to evaluate the uranium aqueous speciation and saturation state of the effluent solutions with respect to uranium solid phases using an updated thermodynamic database for uranium.

### **3.6.3.1 Polyphosphate Remediation of North Process Pond Sediment**

Experiments were conducted with a grab sample of sediment collected from the 300 Area NPP located on the Hanford Site. A 5-gal container with a shovel was used to collect the sample from an excavated trench approximately 8 m beneath the current ground surface. These sediments were collected prior to the excavation activities being completed and overlaid a U(VI) groundwater plume containing U(VI) concentrations that range from ~0.042 to 1.05  $\mu\text{mol/L}$ ; fluctuations in the Columbia River stage can cause the groundwater elevation to vary significantly. The cobble size and material >0.635-cm were removed during field collection.

#### **3.6.3.1.1 Mineralogical Analyses**

Mineralogical analyses were performed on the bulk sediment and clay fraction (<2  $\mu\text{m}$ ) using XRD. All XRD measurements on the bulk material were performed at room temperature for 4 hours with a Scintag® automated powder diffractometer (Model 3520) with  $\text{CuK}_\alpha$  radiation x-ray tube ( $\lambda = 1.54 \text{ \AA}$ ). The bulk samples were analyzed with a  $2^\circ$  to  $65^\circ$   $2\theta$ , a step size of  $0.04^\circ$ , and a 40-second dwell time at each step. For the bulk sample, approximately 1 g of oven-dried sediment was crushed into a fine powder in an agate mortar and pestle and hand packed into a specialized XRD holder. Clays from the untreated sediment were analyzed initially with the randomly oriented mount and later with the preferentially oriented mount techniques. For the randomly mounted samples, the clays were Mg-saturated, air dried, and gently crushed with an agate mortar and pestle before being mounted into a bulk powder holder and analyzed. The preferentially oriented mounts were prepared by saturating the clay fraction with 1.0 mol/L MgCl, vacuum filtering, and transferring the sample onto an aluminum slide. The sample was then solvated with ethylene glycol and stored in a desiccator. Diffractograms for both the randomly and preferentially oriented mounts were collected at room temperature from  $2$  to  $45^\circ$   $2\theta$  and processed with JADE software (Materials Data Inc. (MDI) Livermore, California) combined with the Joint Committee on Powder Diffraction Standards (JCPDS) International Center for Diffraction Data (ICDD) (Newtown Square, Pennsylvania) database. For additional details on sediment characterization and selective extractions see (Serne et al. 2002b; Brown et al. 2005).

#### **3.6.3.1.2 X-Ray Absorption Spectroscopy**

Approximately, 100 mg of untreated B11494 sediment were packed in Teflon® sample holders sealed with 10-mil Kapton® tape, and then heat-sealed in polyethylene bags in preparation for XANES and EXAFS analysis. Uranium  $L_{III}$ -edge x-ray absorption fine structure (XAFS) measurements were performed on B11494 untreated sediments to determine the oxidation state and identity of the uranium phase or phases. X-ray absorption fine structure is an element-specific, short-range structural probe that provides information on the local structure and composition of the element of interest (Brown et al. 1988). The XANES region of the spectrum provides information about the oxidation state and local coordination

environment of the element, whereas the EXAFS region provides information on the type, distance to, and number of neighboring atoms.

The XAFS measurements of untreated B11494 sediments were conducted at room temperature on the Molecular Environmental Sciences beam line 11-2 (Bargar et al. 2002) at the SSRL with a cryogenically cooled Si(220) double-crystal monochromator. Fluorescence yield data were collected with a high-throughput 30-element solid-state Ge detector equipped with a Sr filter to minimize x-ray scatter.

The XAFS data were processed with the computer code SixPACK (Webb 2004) interface to the IFEFFIT XAFS analysis package (Newville 2001). The XANES spectra were background-subtracted and normalized to an edge-step of one. After background-subtraction, the EXAFS data were extracted and  $K^3$ -weighted.

## 4.0 Results and Discussion

The following sections discuss 1) transport of polyphosphate under unsaturated conditions, 2) the stability of uranium-rich calcite, uranophane, and meta-torbernite as a function of pH, temperature, and aqueous activity of phosphate, 3) formation via the reaction of solid-phase calcite-bound uranium and aqueous polyphosphate remediation technology, 4) the kinetics of the reaction between uranyl-carbonate and -silicate minerals with the polyphosphate remedy, 5) the interaction and effect of polyphosphate technology on uranium weathering as a function of polyphosphate composition, concentration, and infiltration rate, under hydraulically unsaturated conditions, 6) STOMP predictive simulations of intermediate- and field-scale infiltration, and 7) intermediation-scale infiltration test.

### 4.1 Transport of Polyphosphate Under Unsaturated Conditions

The transport of phosphate has been previously investigated in detail under hydraulically saturated conditions (van Der Zee et al. 1989; van Der Zee and van Riemsdijk 1986; Sakadevan and Bavor 1998; Ho and Notodarmojo 1995; Robertson and Harman 1999; Gerritse 1993; Tofflemire and Chen 1977; Nagpal 1985; 1986; Arias et al. 2001; Sawhney and Hill 1975; Lin and Banin 2005; Akinremi and Cho 1991).

The mobility of phosphate within subsurface environments is dependent upon the mineralogy and geochemistry of the environment including the following:

- Fe and Al oxides (Hsu 1964; 1965; 1968; Hsu and Rennie 1962; Hamad et al. 1992; Kuo and Lotse 1974; Bolan et al. 1985; Willett et al. 1988; Madrid and de Arambarri 1985; van Riemsdijk et al. 1984; Parfitt et al. 1975; van Der Zee and van Riemsdijk 1986; Sakadevan and Bavor 1998; Violante et al. 1991; Toor et al. 1997; Freese et al. 1992)
- clay content (Lin and Banin 2005; Ho and Notodarmojo 1995; Muljadi et al. 1966; Kuo and Lotse 1972; Toor et al. 1997; Johnston et al. 1991)
- calcite (Lewis and Racz 1969; Samadi and Gilkes 1999; Cole and Olsen 1959; Cole et al. 1953; Kuo and Lotse 1972; Hamad et al. 1992; Akinremi and Cho 1991; Arambarri and Talibudeen 1959; Bertrand et al. 2003)
- organic carbon (Arambarri and Talibudeen 1959; Nagpal 1986; Daly et al. 2001), pH (van Der Zee et al. 1989; Olsen and Watanabe 1957; Sawhney and Hill 1975; Barrow 1984)
- ionic strength (Rajan and Fox 1972)
- sand content (Arias et al. 2001; Lin and Banin 2005; Ho and Notodarmojo 1995; Del Bubba et al. 2003; Tofflemire and Chen 1977; Yuan and Lucas 1982; Leclerc et al. 2001).

The predominant mechanisms of phosphate retention in sediments are sorption and surface complexation to Fe, Al, and Mn oxides, clay minerals and calcite.

Typical of the arid western United States, Hanford sediments are dominated by gravel and sand, which generally exhibit a lower sorption capacity than more finely textured sediments (Kaplan et al. 2000). Hanford groundwater is dominated by calcium, magnesium, sodium, sulfate, and carbonate and has a pH ranging from approximately 7.5 to 8.5 (Wellman et al. 2008b). The most dominant condensed polyphosphates, ortho-, pyro-, and tripolyphosphate, readily dissociate protons. At pH 7.5 the predominant species are  $\text{H}_2\text{PO}_4^-$ ,  $\text{HPO}_4^{2-}$ ,  $\text{HP}_3\text{O}_{10}^{4-}$ , and  $\text{HP}_2\text{O}_7^{3-}$  (Jenkins et al. 1971). All of these phosphate species form dissolved ion pair complexes with metal ions (e.g.,  $\text{Ca}^{2+}$  and  $\text{Mg}^{2+}$ ). Calcite can limit the decrease in solubility of phosphate above pH 7 (Garrels and Christ 1965). However alternatively, at pH values between 7.5 and 8.5, calcium-induced precipitation of phosphate has been shown to be one of the main processes responsible for its removal (Arias et al. 2001; Cole and Olsen 1959; Cole et al. 1953; Lewis and Racz 1969; Samadi and Gilkes 1999). This is a significant consideration under alkaline pH conditions (Jenkins et al. 1971; Gregory et al. 1970; Clark and Peech 1955; Racz and Soper 1967) and particularly under conditions present in the Hanford subsurface. For example, at pH 7.5, a total calcium concentration of  $2 \times 10^{-3}$  M and phosphate concentrations of  $1.6 \times 10^{-4}$  M ortho-,  $1.6 \times 10^{-5}$  M pyro-, and  $3.2 \times 10^{-5}$  M tripoly-, approximately 50% of the ortho- would be complexed as  $\text{CaHPO}_4$ , 80% of the pyro- would be complexed as  $\text{CaHP}_2\text{O}_7^-$ , and approximately 90% of the tripoly- would be complexed as  $\text{CaHP}_3\text{O}_{10}^{2-}$  (Jenkins et al. 1971). Sorption of anionic complexes such as these is limited under alkaline conditions, particularly in sand and gravel sediments. Demonstration of a small degree of sorption will have a significant impact on retardation during transport in unsaturated sediments and on infiltration design, rate, and remedial performance of polyphosphate technology to stabilize uranium source terms in the vadose zone and capillary fringe.

The mobility of polyphosphate species has been the subject of far fewer investigations, which have focused on understanding the degree of polyphosphate fixation as a function of time following its application to soil columns (Hashimoto and Lehr 1973; Philen and Lehr 1967; Takefuji 1967), and the effect of the counter cation on fixation and uptake by plants (Tsuge and Yoshida 1958; Sutton and Larsen 1964; Malquori and Radaelli 1967; Blanchar and Hossner 1969b; a; Lucci 1967; Takefuji 1967; Kartseva 1969). Application of polyphosphate technology to vadose zone and capillary fringe environments for remediation requires understanding the effects of water content and pore water velocity on polyphosphate mobility, both of which have been previously shown to be significant influences on the mobility of reactive species within the subsurface (Gamerdinger and Kaplan 2000; Gamerdinger et al. 1998; Gamerdinger et al. 2001b; a; Lindenmeier et al. 1995; McGraw 1996; McGraw and Kaplan 1997; Wellman et al. 2008a). The only identified investigation of phosphate mobility under hydraulically unsaturated conditions indicated that phosphate application to sediments increased the water retention properties of the sediments as a result of the increase in the negative charge of the soil particles (Lutz et al. 1966). However, there are no known investigations quantifying the mobility of polyphosphate species under advective conditions in unsaturated, alkaline environments. The objective of this investigation was to quantify the migration of ortho-, pyro-, and tripolyphosphate as a function of water content within 300 Area vadose zone and smear zone sediments.

#### **4.1.1 Ortho-, Pyro-, and Tripolyphosphate Transport Under Unsaturated Conditions**

The conditions and measured parameters for all of the polyphosphate transport experiments are summarized in Table 4.1. Experiments are designated by the abbreviated phosphate type, percent saturation, and average pore water velocity; for example, Ortho-22-20 indicates an experiment at 22%

saturation and 20 cm h<sup>-1</sup>. Recovery is the percentage of phosphorus introduced into the column that was recovered in the effluent;  $R_{ef}$  is the effective retardation determined by moment analysis; and,  $K_{d-ap}$  is the apparent distribution coefficient calculated from  $R_{ef}$ . Transport experiments were initially conducted at ~22% water saturation at average pore water velocities of ~20 cm hr<sup>-1</sup> to evaluate the effect of polyphosphate chain length on the retardation of various polyphosphate compounds. Subsequent experiments were conducted at a lower percent of saturation, ~15%, at average pore water velocities of ~20 cm hr<sup>-1</sup> to evaluate the effect of water content, and at 2 cm hr<sup>-1</sup> to evaluate the effect of pore water velocity on the transport and fate of polyphosphate. Lower water contents can result in possible decreased sorption because of 1) incomplete sorption due to rate limitations, 2) decreased availability of sorption sites induced by two-region flow at the lower water contents, and 3) reduced effective pore volume.

**Table 4.1.** Polyphosphate Transport Parameters in <2-mm Fraction from Hanford 300 Area Vadose Sediments Determined by Direct Measurement or Analysis of Breakthrough Curves

Experiment	$F$ , cm <sup>3</sup> h <sup>-1</sup>	rpm	$\rho_b$ , g cm <sup>-3</sup>	$\theta$	$V_w$ , mL	$v$ , cm h <sup>-1</sup>	$t_0$ ( $V_w$ )	% Rec.	$R_{ef}$	$K_{d-ap}$ , mL g <sup>-1</sup>
Ortho-22-20	30.4	900	1.52	0.105	10.07	18.12	30.19	98.17	5.23	0.29
Ortho-15-20	20.5	900	1.52	0.069	6.57	18.73	31.12	92.05	4.94	0.18
Ortho-15-2	1.8	3000	1.52	0.055	5.21	2.07	37.51	97.65	4.95	0.14
Pyro-22-20	31.4	900	1.50	0.100	9.56	19.70	31.61	93.21	8.64	0.51
Pyro-15-20	20.7	900	1.50	0.064	6.15	20.21	30.36	98.56	2.16	0.05
Pyro-15-2	2.1	3000	1.51	0.065	6.16	2.05	29.59	88.56	6.24	0.22
Tripoly-22-20	32.3	900	1.52	0.098	9.37	20.68	32.93	101.94	8.44	0.48
Tripoly-15-20	22.7	900	1.52	0.066	6.26	21.75	33.34	96.12	5.22	0.18
Tripoly-15-2	1.8	3000	1.52	0.055	5.21	2.07	35.29	93.39	7.54	0.22
Tri-soln-22-20	33.8	900	1.51	0.110	10.46	19.39	31.40	94.33	7.56	0.48
Tri-soln-15-20	22.3	900	1.51	0.072	6.85	19.55	33.16	94.27	4.41	0.16
Tri-soln-15-2	1.9	3000	1.50	0.057	5.41	2.11	30.77	82.40	4.64	0.14

(a)  $F$  = flow rate;  $\rho_b$  = bulk density;  $\theta$  = average volumetric water content (standard deviation);  $V_w$  = average pore volume;  $v$  = average pore water velocity;  $t_0$  = step input;  $R_{ef}$  = effective retardation factor;  $K_{d-app}$  = apparent sediment water distribution coefficient based on  $R_{ef}$ .

Transport of ortho-, pyro-, tripoly-, and the polyphosphate formulation at ~20% moisture content and an average pore water velocity of 20 cm hr<sup>-1</sup> are shown in Figure 4.1. Recovery of phosphate in the effluent was ~100%. The apparent sorption,  $K_{d-ap}$ , for pyro-, tripol-, and the polyphosphate formulation was comparable between the compounds,  $K_{d-ap}$  0.48 – 0.51 (Table 4.1 and Figure 4.1). The  $K_{d-ap}$  for ortho- was 57% less than the higher-chain polyphosphate species,  $K_{d-ap}$  = 0.29. Comparable results demonstrating greater sorption of pyrophosphate and tripolyphosphate, relative to orthophosphate, have been previously observed through the results of static sorption tests (Blanchar and Hossner 1969b; a; c; MacIntire et al. 1937; Scott 1958).

Decreasing the pore water content from ~22% to 15% resulted in a >60% decrease in sorption for all polyphosphate compounds (Table 4.1 and Figure 4.2). Additionally, breakthrough curves (BTCs) for pyro-, tripoly-, and the polyphosphate formulation exhibited increased asymmetry and tailing, characteristic of non-equilibrium behavior. Gamerdinger et al. (2001b) recently suggested the formation

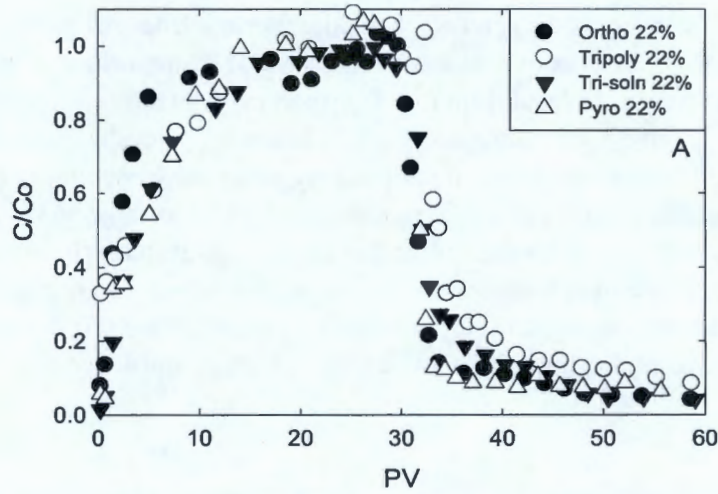


**Figure 4.1.** Observed Phosphate Transport at (a) ~22% an Average  $v$  of  $20 \text{ cm hr}^{-1}$

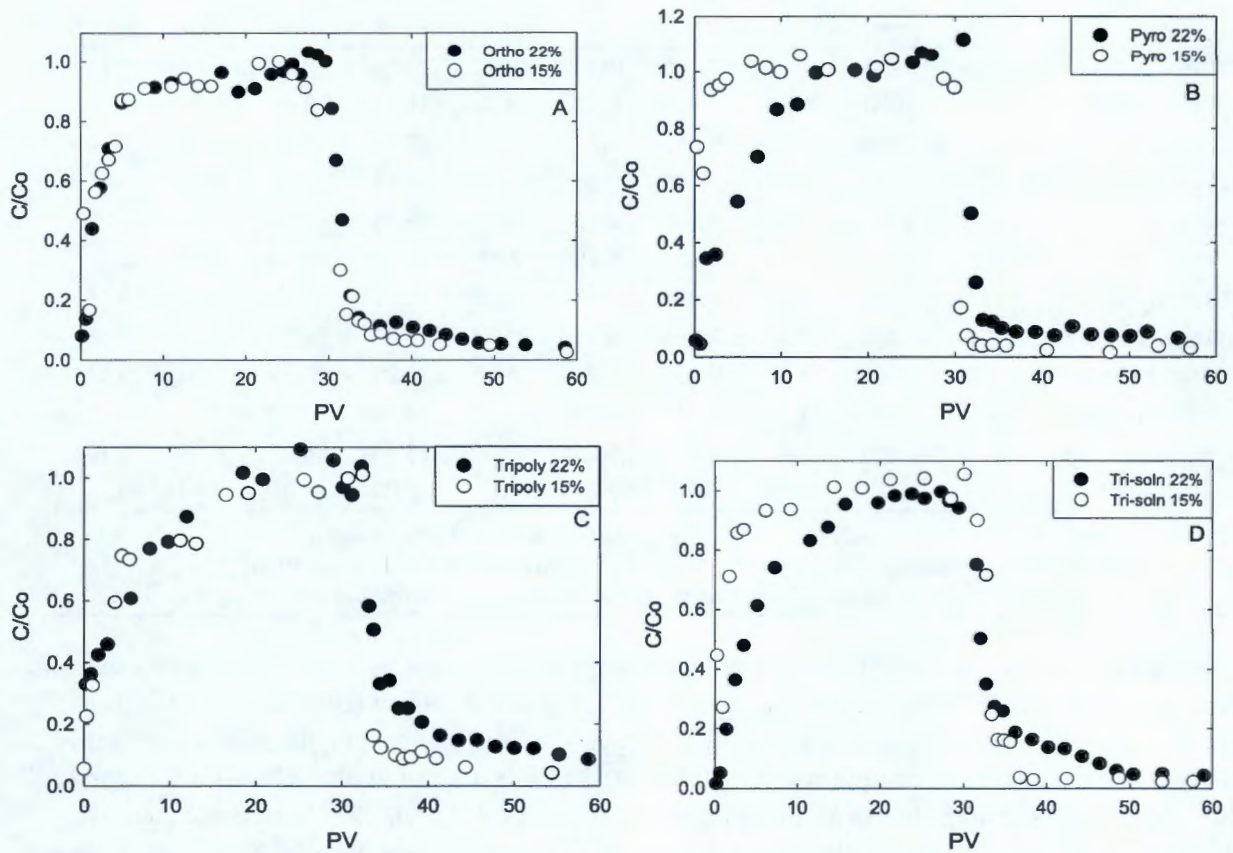


**Figure 4.2.** Observed Phosphate Transport at ~22% and 15% Water Saturation for (a) Orthophosphate, (b) Pyrophosphate, (c) Tripolyphosphate, and (d) Phosphate Formulation at an Average  $v$  of  $20 \text{ cm hr}^{-1}$

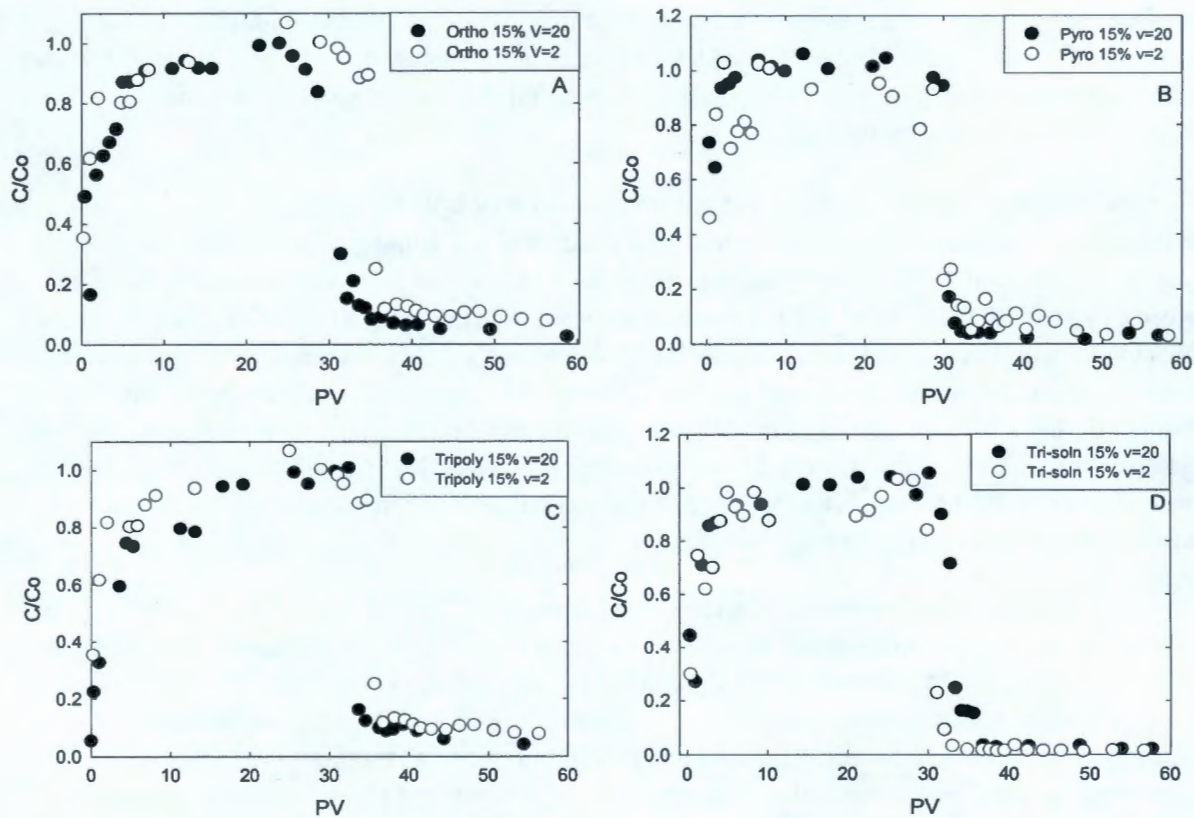
of immobile-water regimes under unsaturated conditions may 1) restrict access to a fraction of the reactive sites or 2) effectively increase the velocity of water in the mobile domain, as a result of reducing the effective pore volume. The relative importance of these factors was assessed by considering phosphate transport at a slower velocity.

Figure 4.3 displays the results of unsaturated transport experiments for ortho-, pyro-, tripolyphosphate, and the polyphosphate formulation conducted at 2 cm hr<sup>-1</sup>. The hydrodynamic conditions were the same as those conducted at 20 cm hr<sup>-1</sup>. The results show that decreasing the pore water velocity from 20 to 2 cm hr<sup>-1</sup> did not result in an increase in the apparent sorption of ortho- or the polyphosphate formulation (Table 4.1). The lack of increase in  $K_{d-ap}$  with decreasing pore water velocity indicates that exclusion from a fraction of the pore space is more important than velocity in determining the sorption during transport. This agrees with previous findings demonstrating comparable behavior for uranium transport under unsaturated conditions (Gamerding et al. 2001b; a; Wellman et al. 2008a; Wellman et al. *in press*) and support a reduction in the accessible volumetric domains as a function of decreasing water content and systematic variations in the pore water velocity.

Alternatively, decreasing in the pore water velocity from 20 to 2 cm hr<sup>-1</sup> did result in an increase in the apparent sorption of pyrophosphate and tripolyphosphate (Table 4.1). This suggests that chemical reaction nonequilibrium may influence the migration of polyphosphate compounds. Similar results were previously observed under saturated conditions (Wellman et al. 2007c). Possible mechanisms that may have resulted in increased rate-limited sorption are 1) sorption of degradation products onto sediment-bound polymerized phosphate molecules, 2) degradation of polymerized phosphate compounds and subsequent sorption to the sediment matrix, or 3) rapid precipitation of heavy, fast-settling solid phases.

Schmid and McKinney (1969) previously identified key processes involved in the formation of apatite from mixtures of ortho-, pyro-, and tripolyphosphate. Results of sorption studies illustrated that orthophosphate sorbs onto polyphosphate near pH ~7 to 9. Although, tripolyphosphate does not readily precipitate in the absence of orthophosphate, sorption of orthophosphate onto tripolyphosphate serves as a heterogeneous nucleating surface to promote precipitation. As orthophosphate begins to precipitate, the pH of the solution increases slightly, while the degradation of tripolyphosphate is accelerated to form ortho- and pyrophosphate. This further enhances precipitation by providing additional orthophosphate. Furthermore, pyrophosphate produces a heavy, fast-settling precipitate with aqueous cations. Identification of the exact mechanism(s) of retardation was beyond the scope of the present study.

The apparent retardation factor and equilibrium partition coefficients calculated from the <2-mm fraction were adjusted for field conditions. The field-corrected  $K_d$  and retardation values (Table 4.2) were calculated assuming retardation was caused by the <2-mm fraction, which composed ~10% of the total sediment matrix and using an average bulk density value of 2.19 previously quantified within the 300 Area limited-field investigation (LFI) (Williams et al. 2007).



**Figure 4.3.** Observed Phosphate Transport at an Average  $v$  of 20 and 2  $\text{cm hr}^{-1}$  for (a) Orthophosphate, (b) Pyrophosphate, (c) Tripolyphosphate, and (d) Phosphate Formulation at an Average Water Saturation of  $\sim 15\%$

**Table 4.2.** Field Transport Parameters Calculated from Laboratory-Derived Transport Parameters

Experiment	$v$ , $\text{cm h}^{-1}$	$R_{ef}$	$K_{d-app}$ , $\text{mL g}^{-1}$
Ortho-22-20	18.12	1.42	0.020
Ortho-15-20	18.73	1.39	0.019
Ortho-15-2	2.07	1.40	0.019
Pyro-22-20	19.70	1.76	0.037
Pyro-15-20	20.21	1.12	0.006
Pyro-15-2	2.05	1.52	0.025
Tripoly-22-20	20.68	1.74	0.036
Tripoly-15-20	21.75	1.42	0.020
Tripoly-15-2	2.07	1.65	0.031
Tri-soln-22-20	19.39	1.66	0.031
Tri-soln-15-20	19.55	1.02	0.001
Tri-soln-15-2	2.11	1.36	0.017

Based on the field-corrected values presented in Table 4.2, polyphosphates will exhibit little retardation during infiltration of the vadose zone and capillary fringe. Thus, the infiltration array layout, infiltration rate, water content, and pore water velocity require particular consideration during polyphosphate infiltration through the vadose zone and capillary fringe. The results of intermediate-scale testing will evaluate the effects of Hanford sediment properties, infiltration type (e.g., ponded, pulsed injection, constant-rate injection), and infiltration volume at a scale that bridged the gap between the small-scale UFA studies and the field-scale.

## 4.2 Interaction of Polyphosphate with Calcite-Bound Uranium

Detailed understanding of the rate and mechanism of the interaction between polyphosphate and uranium-rich calcite will allow a more effective design of the infiltration strategy to minimize the mobilization of uranium during remediation. The objective of this investigation was to evaluate the interaction of polyphosphate species with uranium-rich calcite to determine the effects of geochemical conditions on the partitioning of polyphosphate and its degradation products with uranium-rich calcite, quantify the release of uranium from uranium-rich calcite based on the identity and concentration of aqueous polyphosphate species, and quantify the rate and mechanism of uranium immobilization based on the identity and concentration of aqueous polyphosphate species. The information obtained from this line of inquiry is essential to effectively develop phosphate-based remediation strategies for uranium in calcareous environments.

### 4.2.1 Sequestration of Uranium with Calcite

Calcite is a ubiquitous mineralogical component in many sediments that commonly exists as a coating material that can aggregate other minerals. Calcite serves as a known sorbent for many aqueous cations, including  $\text{Am}^{3+}$ ,  $\text{Ba}^{2+}$ ,  $\text{Cd}^{2+}$ ,  $\text{Co}^{2+}$ ,  $\text{Cu}^{2+}$ ,  $\text{Mn}^{2+}$ ,  $\text{Nd}^{3+}$ ,  $\text{Sr}^{2+}$ ,  $\text{Zn}^{2+}$ , and U (VI) (Bruno et al. 1989; Davis et al. 1987; Franklin and Morse 1982; Lorens 1981; Jurinak and Bauer 1956; McBride 1979; Milton and Brown 1987; Morse et al. 1984; Mucci and Morse 1983; Pingitore 1986; Pingitore and Eastman 1984; Pingitore et al. 1988; Shanbhag and Morse 1982; Zachara et al. 1988; Zachara et al. 1989). At the Hanford Site, calcite is a significant mineral component with which the pore waters are at equilibrium (Liu et al. 2004). Calcite can affect the transport and fate of uranium within the subsurface, indirectly, by the release of aqueous  $\text{Ca}^{2+}$  and carbonate to form aqueous neutral and anionic  $\text{Ca-UO}_2\text{-CO}_3$  complexes (Bernhard et al. 2001; Kaplan et al. 1998; Kalmykov and Choppin 2000) and directly through its role as a sorbent. However, to date, there are no known investigations quantifying the uptake of uranium by calcite as a function of pH, stability of the resulting phase, or the effect of aqueous phosphate.

#### 4.2.1.1 Uptake of Uranium by Calcite

Figure 4.4 displays the dependence of uranium uptake in the presence of calcite. The calcite solid phase was pre-equilibrated with the aqueous matrix, which was in equilibrium with calcite. This eliminated the need to consider geochemical reactions that could occur between calcite and the aqueous matrix (e.g., dissolution). The uptake of uranium from the aqueous matrix increased linearly with increasing aqueous uranium concentration over the pH values of 6.5 to 7. At pH = 7.5 the mass of uranium removed reached a maximum value of 0.6  $\mu\text{g}$  uranium/g calcite. The mass of uranium removed further decreased at pH 8 reaching a maximum, 0.2  $\mu\text{g}$  uranium/g calcite, at an aqueous uranium concentration of  $\sim 100 \text{ g L}^{-1}$ .

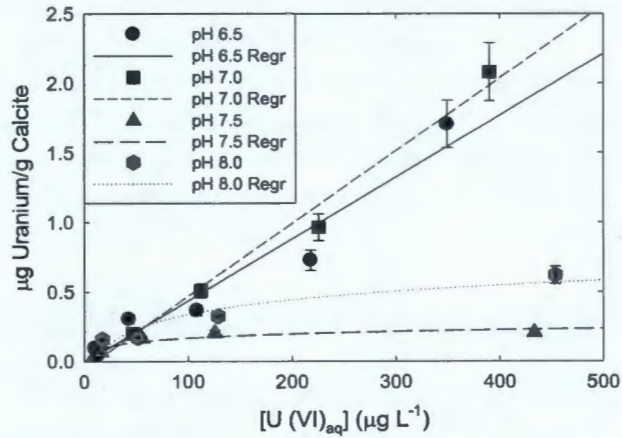


**Figure 4.4.** Uranium Loading ( $\mu\text{g}$  uranium/g calcite) on Calcite over the pH Range of 6.5 to 8 in Calcite-Equilibrated Groundwater

Sequestration of uranium depends on numerous environmental variables including aqueous pH, composition of the aqueous matrix, oxidation potential (Eh), and surface binding sites. Uranium sequestration processes include sorption and/or surface complexation, incorporation in the calcite structure, and precipitation of uranium-carbonates. Under oxidizing conditions, uranium is found as hexavalent uranium in surface and groundwater as the linear uranyl dioxo cation ( $\text{UO}_2^{2+}$ ). Aqueous ligands, including  $\text{OH}^-$ ,  $\text{CO}_3^{2-}$ ,  $\text{PO}_4^{3-}$ , will form stable complexes with U(VI) and are the basis for some remediation techniques. Under circumneutral to alkaline pH conditions uranium can form the aqueous species  $\text{UO}_2(\text{CO}_3)_3^{4-}$  and  $\text{Ca}_2\text{UO}_2(\text{CO}_3)_3$  (Bernhard et al. 2001; Kalmykov and Choppin 2000), a major species within Hanford vadose zone pore waters (Liu et al. 2004; Wang et al. 2005a; Qafoku et al. 2005). Complexation and hydrolysis have significant influence over the aqueous speciation of uranium, which may result in an increase or decrease in uptake by geologic media. Additionally, phosphate imparts significant influence on the aqueous speciation of uranium. Under common groundwater pH conditions of 4 to 10,  $[\text{PO}_4^{3-}] = 0.1$ , uranyl forms more stable complexes with phosphate than with any other ligand (Langmuir 1978). When the ratio of aqueous phosphate to carbonate is  $> 0.1$ , phosphate complexation of uranium is predominant within the system (Sandino and Bruno 1992).

The thermodynamic geochemical code MINTQA2 was used to evaluate the aqueous speciation of uranium in solution over the pH range being investigated using updated thermodynamic databases from various literature sources (Sergeyeva et al. 1972; Langmuir 1978; Alwan and Williams 1980; O'Hare et al. 1976; O'Hare et al. 1988; Vochten 1990; Nguyen et al. 1992; Grenthe et al. 1992; Finch 1997; Chen et al. 1999; Kalmykov and Choppin 2000). It is important to note that because of the complex chemistry of uranium, there is significant debate within the literature regarding the stoichiometry and the thermodynamic values assigned to aqueous uranium species and secondary mineral phases. As such, model predictions are based on current knowledge but may have significant uncertainty associated with them and are considered semi quantitative. Figure 4.5 illustrates the dominant aqueous species below pH 7.5 is predicted by  $\text{UO}_2(\text{HPO}_4)_2^{2-}$ . As pH increases, the aqueous speciation of uranium changes such that the proportion of the neutral ternary calcium carbonate species,  $\text{Ca}_2\text{UO}_2(\text{CO}_3)_2$ , increases and ultimately becomes the main aqueous uranyl complex. The results demonstrate the complexity of the U(VI) speciation in Hanford Site groundwaters and the impact calcium, as the  $\text{Ca}_2\text{UO}_2\text{CO}_3$  complex, can have on the speciation of U(VI). This complex is expected to be the dominant U(VI) form under the conditions expected in the Hanford subsurface. Similar to  $\text{Ca}^{2+}$ , the presence of  $\text{Mg}^{2+}$  has been suggested

to also form a  $Mg_2UO_2CO_3$  complex. However, this complex was not included in the calculations displayed because of a lack of thermodynamic data, but the presence of this complex could have a profound effect on the U(VI) distribution, given the concentration of  $Mg^{2+}$  in Hanford groundwater (15 ppm).

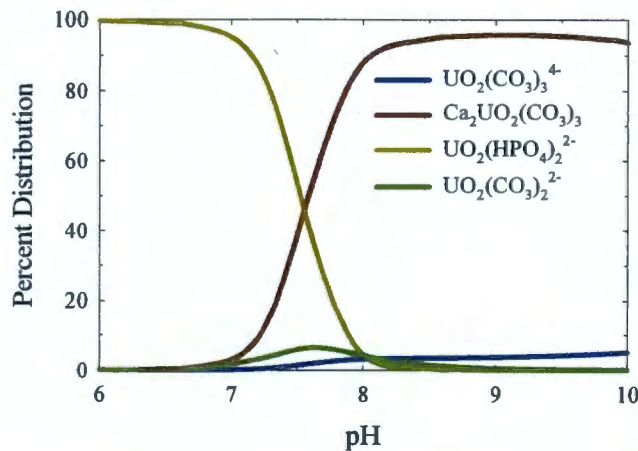


**Figure 4.5.** Percent Distribution of U(VI) Species Calculated with MINTEQA2 at 25°C, Ionic Strength = 0.1 M, and  $pCO_2 = 10^{-3.5}$  Bar for a Total U(VI) =  $1 \times 10^{-6}$  M in Hanford Groundwater Well-699-S3-25

Calcite is proposed to have two primary hydration sites,  $\equiv CaOH$  and  $\equiv CO_3H$  (van Cappellen et al. 1993; Stipp and Hochella Jr. 1991; Stipp 1999), which results in the formation of  $\equiv CaOH_2^+$ ,  $\equiv CaHCO_3$ ,  $\equiv CaCO_3^-$ ,  $\equiv CO_3Ca^+$ , and  $\equiv CO_3^-$  surface species (Pokrovsky et al. 2000; Vdovic 2001). Under the pH range 6 to 8.5, the fraction of cationic surface sites decreases while the proportion of anionic and neutral species increases (Figure 4.6) (Pokrovsky et al. 2000). Coupling the predicted aqueous and surface speciation, the uptake of uranium can be explained, in part by the dominance of the anionic aqueous species and cationic surface site at  $pH < 7.5$ . The increasing proportion of neutral aqueous species and anionic and neutral surface sites affords a decreased affinity and uptake of uranium with  $pH$  values  $\geq 7$ .

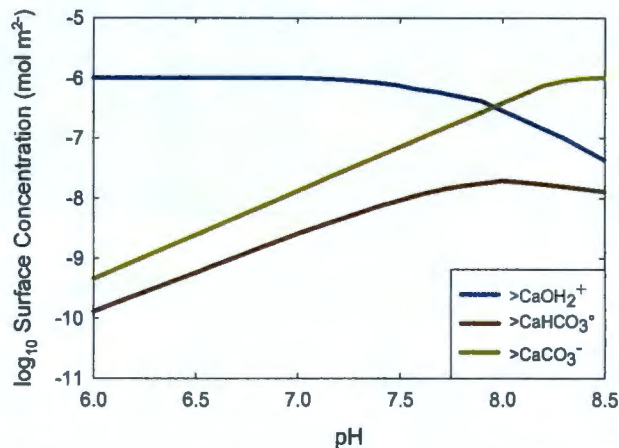


**Figure 4.6.** Speciation of Dominant Calcite Surface Sites at 25°C,  $I = 0.01$  M,  $[Ca^{2+}]_{tot} = 10^{-3}$  M, and  $pCO_2 = 10^{-3.5}$  atm (adapted from Pokrovsky et al. (2000))

The long-term retention of uranium is dependent on the chemical state and mechanism of retention. Figure 4.7 displays the U  $L_{III}$ -edge EXAFS spectrum of calcite reacted with 60 ppm uranium under static conditions. The spectra are consistent with those presented by Reeder et al. (2001) for uranium-rich calcite.

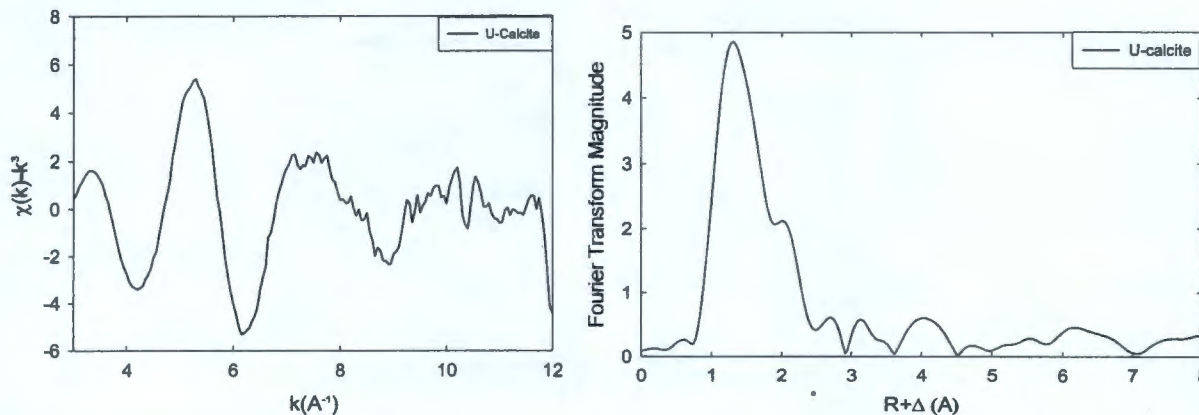


**Figure 4.7.** EXAFS (left) and Fourier Transform (right) Spectra of Calcite Reacted with 60 ppm Uranium

Figure 4.8 displays scanning electron microscopy images of well-formed rhombohedral uranium-calcite crystals. Energy dispersive spectrometry indicates the crystals contain  $\sim 0.5 - 1.0$  wt% uranium. Results presented here illustrating the formation of uranium-rich calcite are consistent with numerous experimental studies conducted previously to discern the mechanisms of direct uranium sequestration by calcite, including sorption and co-precipitation (Carroll et al. 1992; Kaplan et al. 1998; Dong et al. 2005; Elzinga et al. 2004; Savenko 2001; Noubactep et al. 2006; Reeder et al. 2004; Reeder et al. 2000; Reeder et al. 2001; Kelly et al. 2003a). These investigations have illustrated that coprecipitation and formation of a solid solution are likely the dominant mechanisms of uptake and retention of uranium by calcite.



**Figure 4.8.** Scanning Electron Microscopy Image of Uranium-Rich Calcite

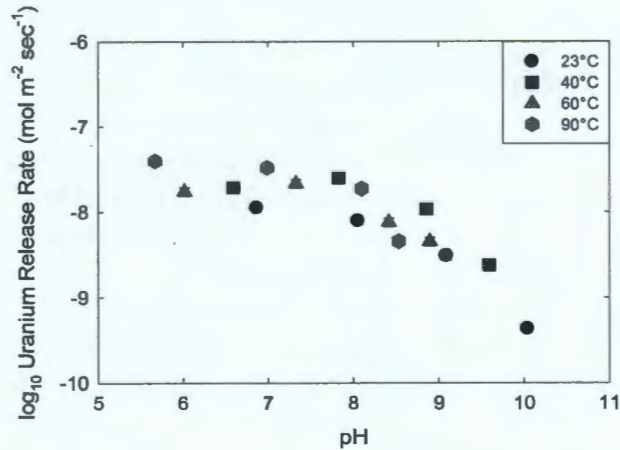
#### 4.2.2 Dissolution Kinetics of Uranium-Rich Calcite

The uptake of U(VI) and co-precipitation of uranium with calcite presents a significant process affecting the mobility and sequestration in subsurface environments, especially throughout the arid western United States at sites such as Hanford where the pore waters are in equilibrium with calcite, pH of 7.5 to 8.5 with a dissolved  $[CO_3^{2-}]$  of  $\sim 1.13 \times 10^{-3} \text{ mol L}^{-1}$  (Kaplan and Serne 1995). Numerous

experimental investigations have been conducted to discern the mechanism of uranium uptake by calcite (Carroll et al. 1992; Meece and Benninger 1993; Geipel et al. 1997; Reeder et al. 2000; Reeder et al. 2001; Kelly et al. 2003b; Savenko 2001; Elzinga et al. 2004; Noubactep et al. 2006; Dong et al. 2005). A key result of these works has been the understanding that co-precipitation and formation of that solid solution are the likely dominant mechanisms of uranium sequestration by calcite. Thus, given the significant concentrations of uranium that can be retained in calcite (Reeder et al. 2000), it is essential to understand the stability of this phase and the potential for remobilization under environmental conditions. However, the multiple modes of uranium incorporation into the calcite structure and challenges associated with precise characterization of the phase have thus far prevented any thermodynamic or kinetic investigations regarding uranium-rich calcite. The purpose of this investigation was to quantify the dissolution of uranium-rich calcite as a function of pH (6 to 10), temperature (23° to 90°C), and as a function of polyphosphate concentration. This information is critical to understanding and quantifying the stability of uranium-rich calcite in the 300 Area, providing insight into the continuing source of uranium to the 300 Area aquifer, and quantifying the effect of polyphosphate infiltration on the release and immobilization of uranium from uranium-rich calcite.

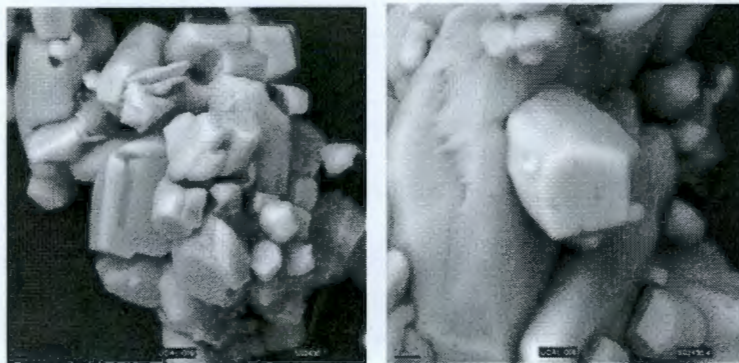
#### 4.2.2.1 Effect of pH and Temperature

Figure 4.9 illustrates the release rate of uranium from uranium-rich calcite across the pH range of 6 to 10 and the temperature range of 23° to 90°C. Under the pH range of 6 to 9 the release of uranium is independent of pH. At  $9 < \text{pH}$  the rate of uranium release begins to exhibit an inverse dependence on pH. Similar results have been observed for the dissolution of calcite (Morse 1983; Dolgaleva et al. 2005; van Cappellen et al. 1993). Dolgaleva et al. (2005) summarized the results of numerous experimental investigations to illustrate the dissolution behavior of calcite as a function of pH under the range of 2 to 14. It was shown that the dissolution of calcite displays a strong inverse correlation with increasing pH under the pH range of 2 to 5. Under the pH range of 5 to 10 the dissolution of calcite is nearly constant and further decreases above 10. This behavior has been attributed to the surface speciation of calcite. Relevant to this investigation, in the pH range of 5.5 to 8 the calcite surface possesses nearly equal fractions of  $\equiv\text{CaOH}_2^+$  and  $\equiv\text{CO}_3^-$  sites. The constant dissolution kinetics observed under these conditions as a function of pH are therefore controlled by the rate at which hydrated surface calcium ions bonded to deprotonated  $\equiv\text{CO}_3^-$  neighbors are detached from the lattice structure. The decrease in dissolution rate with  $9 < \text{pH}$  reflects the increasing fraction of  $\equiv\text{CaOH}^\circ$  sites produced through deprotonation of  $\equiv\text{CaOH}_2^+$  (van Cappellen et al. 1993). Uranium-rich calcite is dominantly calcite and the minor inclusion of uranium affords minimal change to the dissolution rate. Moreover, the ability to index the dissolution of uranium-rich calcite based on the release of uranium to solution supports previous results suggesting uranium is a structural component, regardless of whether the mechanism of uptake and retention is coprecipitation and formation of a solid solution, rather than sorption.



**Figure 4.9.** Log<sub>10</sub> Uranium Release Rate as a Function of Temperature-Corrected pH for Uranium-Rich Calcite in 0.01 M TRIS Solution

The dissolution of calcite has been shown to increase as a function of temperature, and thus, it was hypothesized that the dissolution of uranium-rich calcite would vary accordingly. However, uranium-rich calcite displayed minimal dependence on temperature. SEM was conducted on reacted materials to confirm there was no formation of secondary phases that would contribute to the observed dissolution behavior. SEM images do not indicate the formation of any secondary phases (Figure 4.10). Thus, it is postulated that the narrow temperature range used in this investigation limited observation of the effect of temperature on the dissolution of uranium-rich calcite. However, the temperature of the Hanford subsurface is ~15°C, which is less than 10° below the lowest temperature used here to quantify the dissolution kinetics of uranium-rich calcite. Given the minor dependence on temperature observed for uranium-rich calcite, it is believed that the values quantified here provide an accurate estimation for the dissolution of uranium-rich calcite in the subsurface.



**Figure 4.10.** Scanning-Electron Microscopy Image of Uranium-Rich Calcite After Single-Pass Flow-Through Dissolution Tests

#### 4.2.2.2 Effect of Solution Saturation State

The dissolution rate of uranium-rich calcite was quantified in the presence of the polyphosphate amendment consisting of 90% orthophosphate:10% tripolyphosphate. The release of uranium was quantified at pH = 7.5 and 23°C as a function of amendment concentration. The log<sub>10</sub> release rate of uranium as a function of [PO<sub>4</sub><sup>3-</sup><sub>(aq)</sub>] is shown in Figure 4.11. The rate of uranium release exhibits an ~10x

increase as a function of increasing phosphate concentration. However, the rate of uranium release is maintained at, or below, the minimum rate observed in the absence of aqueous phosphate, regardless of pH (Figure 4.9 and Figure 4.11). Thus, the concentration of uranium potentially released during the infiltration of polyphosphate remedial solution will be less than that released through the dissolution of uranium-rich calcite in natural pore waters, and polyphosphate remediation will not detrimentally impact the stability of uranium-rich calcite. The release of uranium as a function of phosphate can be predicted from Equation 4.1 obtained from a least-squares regression (solid line) of the experimental data in Figure 4.11:

$$\text{Log } r_{\text{dissol}} (\text{mol m}^{-2} \text{sec}^{-1}) = 2.1 \times 10^{-9} + 1.0 \times 10^{-7} [\text{PO}_4^{3-}] \quad (4.1)$$

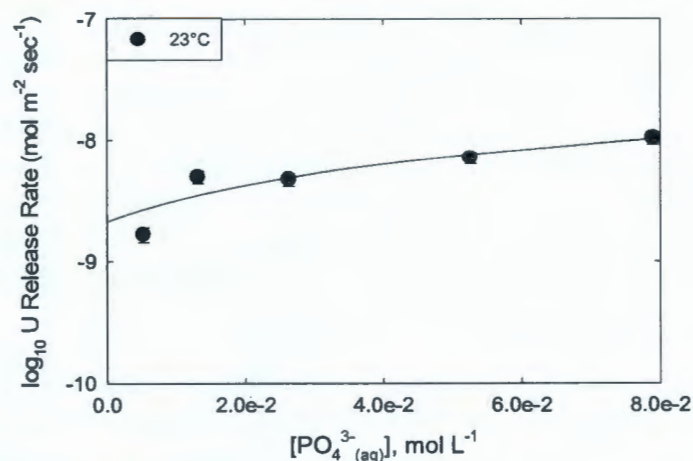


**Figure 4.11.** Log<sub>10</sub> Rate of Uranium Release from Uranium-Rich Calcite as a Function of [PO<sub>4</sub><sup>3-(aq)</sup>] at pH = 7.5, 23°C

### 4.2.3 Effect of Aqueous Phosphate on Uranium-Rich Calcite

Evaluating the interaction of polyphosphate with uranium-rich calcite (Dong et al. 2005; Zachara et al. 2005) is critical to understanding the potential rate and magnitude of uranium release during remedy infiltration and the rate and mechanism of uranium sequestration via polyphosphate remediation. There are no known investigations regarding the interaction of aqueous phosphate with uranium-rich calcite. However, the mechanism of phosphate uptake by calcite resulting in the formation of calcium-phosphate phases has been the subject of numerous investigations.

The reaction of phosphate in calcareous sediments involves complex adsorption and precipitation processes (Delgado et al. 2000; Pena and Torrent 1984; Castro and Torrent 1995; Cole et al. 1953; Kuo and Lotse 1972). The interaction of phosphate with calcite surfaces consists of rapid monolayer sorption. At lower aqueous phosphate concentrations, the amount of phosphate sorbed per gram of calcite is proportional to the amount of calcite present. In the presence of high phosphate concentrations, initial uptake of phosphate occurs similarly through the formation of a monolayer. However, the total amount of uptake is independent of the amount of calcite present. Following nucleation, the reaction of phosphate with calcite proceeds until the concentration of phosphate has been reduced to below a critical value, indicating calcium phosphate precipitates at the expense of calcite, which serves as a soluble source of calcium (Cole et al. 1953). Although hydroxylapatite is the most thermodynamically stable phase

precipitated in calcareous environments enriched with phosphate (Lindsay 1979; Lindsay and Moreno 1960), no direct measurement has been conducted on natural sediments to support this assertion because of the limited concentration of phosphate naturally occurring in sedimentary matrices. However, Cho (1991) noted the formation of  $\text{CaHPO}_4$  during the dissolution of calcite in the presence of phosphate. Additionally, Avnimelech (1980) described the formation of a calcium-carbonate-phosphate surface complex  $\text{Ca}_3(\text{HCO}_3)_3\text{PO}_4$  that subsequently leads to precipitation of dicalcium phosphate (DCP) (Cole et al. 1953), octacalcium phosphate (OCP) (Clark and Peech 1955), hydrolytic conversion of DCP to OCP (Arvieu and Bouvier 1974), or OCP disproportionates to reform DCP and hydroxyapatite (Stumm and Leckie 1970).

Based on the results of these investigations, it may be postulated that the reaction of uranium-rich calcite with aqueous phosphate may occur by a similar mechanism. It has been previously shown that uranium will form strong complexes with O-containing ligands, including carbonate, hydroxide, and phosphate (Langmuir 1978; 1997), of which phosphate will form the most stable complexes (Sandino and Bruno 1992). Moreover, sorption occurring via inner-sphere complexes is believed to be an important precursor step in surface precipitation of uranyl minerals (Sutton et al. 2003). It may be hypothesized, then, that the interaction of phosphate with uranium-rich calcite may afford the formation of a  $\text{Ca-UO}_2\text{-PO}_4$  surface complex that may undergo subsequent transformation resulting in the formation of autunite. However, there are no known such investigations.

EXAFS was conducted on calcite reacted under static conditions with  $60 \text{ mg L}^{-1}$  uranium in the presence of  $340 \text{ } \mu\text{g L}^{-1}$  phosphate at pH 7, 7.5, and 8. Evaluation of the uranium  $L_{III}$ -edge EXAFS spectra (Figure 4.12) suggests that the chemical speciation of uranium changed systematically as a function of pH and meta-autunite stability. Figure 4.12 displays the U  $L_{III}$ -edge EXAFS spectrum of an autunite mineral phase  $X_{3-n}^{(n)+}[(\text{UO}_2)(\text{PO}_4)]_2 \cdot x\text{H}_2\text{O}$  where  $X$  is any mono- or divalent cation, U-calcite, and calcite reacted under static conditions with 60 ppm uranium in the presence of  $340 \text{ } \mu\text{g L}^{-1}$  phosphate at pH 7, 7.5, and 8. The data were well fit using a linear combinations of the  $\chi$  data from  $k = 3\text{-}12$ ,  $k^3$  weighted for U-calcite and autunite-group minerals (Table 4.3). The fitted data indicate the formation of an autunite mineral phase under the pH range of 7 to 8. This suggests that the sorption of phosphorus to uranium-rich calcite may serve as an initial step in the formation of Ca-autunite. However, the fraction of autunite formed decreases as a function of pH and increasing carbonate concentration.

The thermodynamic geochemical code Geochemist's Workbench was used to evaluate the stability of meta-autunite over the pH range being investigated using updated thermodynamic databases from various literature sources (Bernhard et al. 2001; Brooks et al. 2003; Sergeeva et al. 1972; Langmuir 1978; Alwan and Williams 1980; O'Hare et al. 1976; O'Hare et al. 1988; Vochten 1990; Nguyen et al. 1992; Grenthe et al. 1992; Finch 1997; Chen et al. 1999; Kalmykov and Choppin 2000; Delaney and Lundeen 1990). Figure 4.13 presents the stability of Ca-meta-autunite as calculated in Hanford groundwater as a function of pH and the log of the ratio of phosphate to bicarbonate. Formation of the uranyl-phosphate phase is most prominent, under the given test conditions, within the pH range of 7.0 to 7.5. Above 7.5, the ternary carbonate complex exerts a greater influence on the speciation of uranium. As such, the amount of phosphate required for meta-autunite precipitation increases as a function of increasing pH and bicarbonate. Results presented here demonstrate the ability of autunite-group phases to form in the presence of minimal phosphate concentrations, and underscore the significance of pH and the  $\text{HPO}_4^{2-}/\text{HCO}_3^-$  ratio on the formation of autunite.

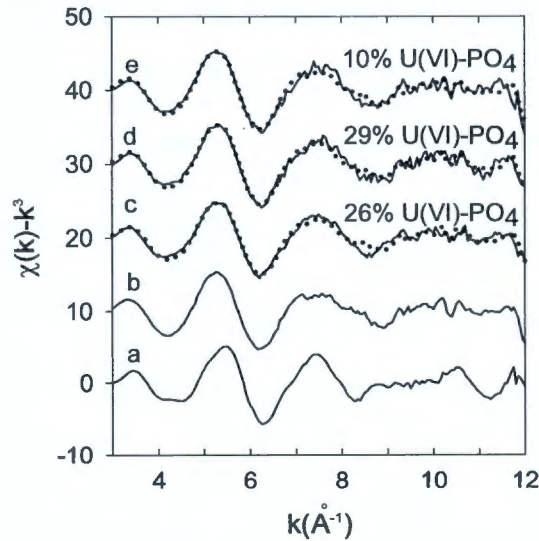


**Figure 4.12.** EXAFS of (a) Autunite-Group Mineral,  $X_{3-n}^{(n)+} [(UO_2)(PO_4)]_2 \cdot xH_2O$ , (b) U-Calcite, and Calcite Reacted with 60 ppm Uranium in the Presence of 340 ppb Phosphate at (c) pH 7, (d) pH 7.5, and (e) pH 8. The dashed line is the best fit to the EXAFS spectra using linear combination of U-calcite and autunite-group mineral.

**Table 4.3.** Standard Fits as Measured from  $k = 3-12, k^3$  Weighted

	U-Calcite	Autunite-Group Mineral
pH 7	0.74	0.26
pH 7.5	0.71	0.29
pH 8	0.90	0.10

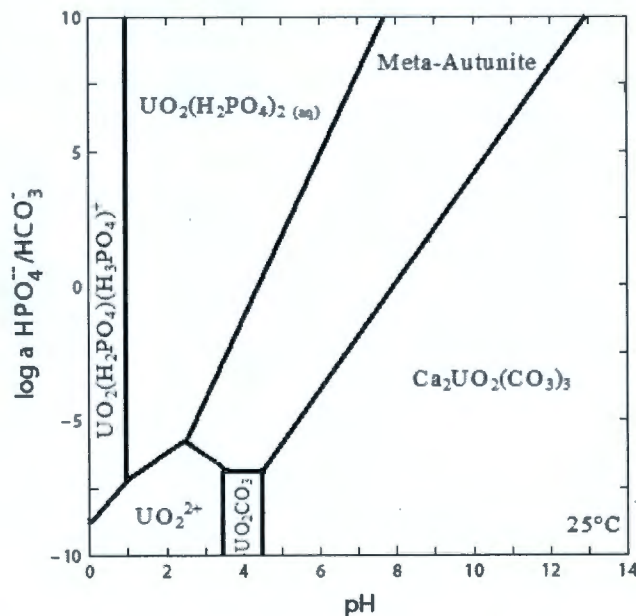


**Figure 4.13.** Activity/Activity Diagram Showing the Stability of Ca-Meta-Autunite Calculated with Geochemist's Workbench®

#### 4.2.4 Stabilization of Uranium-Bearing Calcite with Polyphosphates

As has been shown previously, injection of a 100% orthophosphate solution into a calcite-equilibrated porous media results in rapid precipitation and occlusion of the effective pore volume (Wellman et al. 2006b). However, balancing degradation kinetics of polyphosphate molecules with the complex interactions between ortho-, pyro-, and tripolyphosphate (Wellman et al. 2007c) can allow for development of a polyphosphate formulation providing rapid stabilization of uranium-solid phases under advective conditions through the vadose zone and capillary fringe. Therefore, it is critical to understand the interaction of ortho-, pyro- and tripolyphosphate with uranium solid phases and the subsequent effect on immobilization through the formation uranyl phosphates.

Figure 4.14 displays the aqueous concentration of uranium released through the reaction of ortho-, pyro-, and tripolyphosphate with uranium-rich calcite as a function of pH and the ratio of  $\text{g } [\text{PO}_4^{3-}]_{\text{aq}}/\text{g}$  uranium-calcite. Under the pH range of 6.5 to 8.0, the aqueous concentration of uranium is generally greatest upon reaction with the pyrophosphate, followed by tripolyphosphate. Orthophosphate affords the greatest control over the aqueous concentration of uranium under all pH conditions, maintaining aqueous uranium concentrations less than  $30 \mu\text{g/L}$  at a  $\text{g } [\text{PO}_4^{3-}]_{\text{aq}}/\text{g}$  uranium-calcite ratio of  $\leq 0.05$ . Pyrophosphate and tripolyphosphate required  $\text{g } [\text{PO}_4^{3-}]_{\text{aq}}/\text{g}$  uranium-calcite ratios of  $\sim 0.15$  to maintain aqueous uranium concentrations  $< 30 \mu\text{g/L}$ . Results presented here suggest the most rapid, complete stabilization of uranium-rich calcite would be observed through treatment with 100% orthophosphate.

There are no known investigations of the complexation of uranyl by linear polyphosphate molecules. However, the dependence of metal ion interactions with various polyphosphates has been the subject of several investigations (Onaka et al. 1981; van Wazer 1950; van Wazer et al. 1955; van Wazer et al. 1952). Based on results presented in Figure 4.14 and through analogy to the complexation of other cations by linear polyphosphate compounds, it can be postulated that the stability of uranyl orthophosphates is the most stable and readily precipitate to afford uranyl-phosphate solids (Baes and Schreyer 1953b; Baes and Schreyer 1953a; Baes et al. 1953; Sandino and Bruno 1992). The solubility of pyrophosphate metal complexes, however, are greater than those of tripolyphosphate (Onaka et al. 1981; van Wazer and Callis 1958). Thus, reaction of uranium-rich calcite with 100% pyrophosphate results in the formation of more stable aqueous uranium complexes that limit precipitation and results in greater mobilization of uranium during polyphosphate-based remediation.

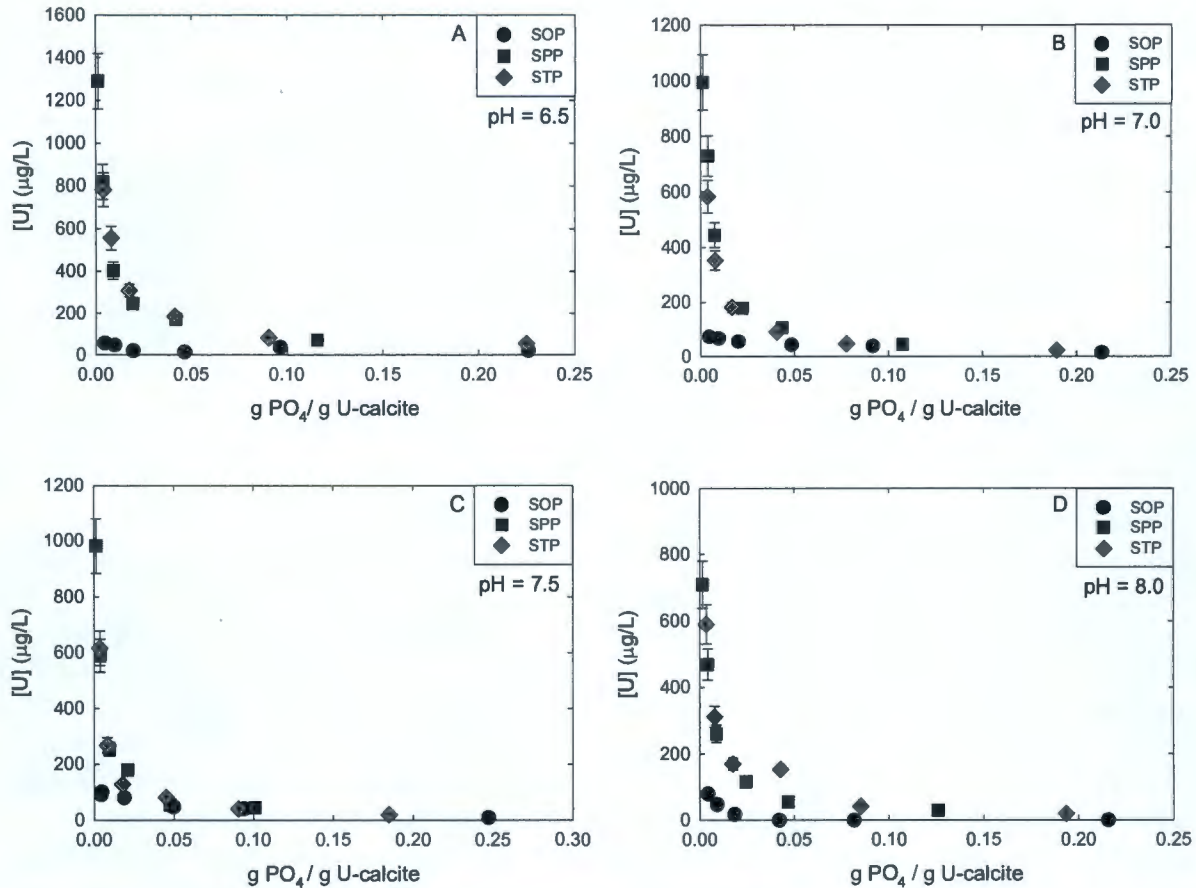


**Figure 4.14.** Concentration of Aqueous Uranium ( $\mu\text{g/L}$ ) Released Through the Reaction of Ortho-, Pyro-, and Tripolyphosphate with Uranium-Rich Calcite as a Function of pH and the Ratio of  $\text{g} [\text{PO}_4^{3-}]_{\text{aq}}/\text{g}$  Uranium-Calcite

### 4.3 Effect of Polyphosphate on Uranium Mineralogy

The vadose zone and capillary fringe is composed of unconsolidated sediment ranging in grain size from boulder to pebble gravel, and includes coarse to fine sand with minor amounts of silty sand and silt. Most often these sediments exhibit a clast-support structure; matrix between clasts is normally a poorly sorted mixture of sand and silt. Additionally, the water table at the 300 Area is very dynamic because of fluctuations in the Columbia River stage and leads to the very high permeability of the Hanford Formation sediments. Large daily, weekly, and seasonal fluctuations in the Columbia River stage are caused by the operation of hydroelectric dams on the river and seasonal trends (i.e., spring freshet). The dynamics of river stage fluctuations and the water table elevation cause a mixing zone of river and groundwater within the aquifer. During relatively high river stage periods river water enters the aquifer and the capillary fringe and lower vadose zone experience wet-dry cycling.

Weathering and paragenesis of uranyl minerals typically follow the thermodynamic progression of precipitating those that have the lowest solubility, for which precipitation kinetics do not present significant barriers to nucleation, followed by precipitation of advanced uranium minerals, which occurs over a considerable time frame (Smith 1984; Finch et al. 1999). The general sequence begins with the

uranyl-hydroxides, followed by the uranyl-carbonates, uranyl-silicates and finally, the highly stable uranyl-phosphates. Many arid and semiarid environments have exhibited accelerated corrosion of uranium phases because of cycling between wet and dry periods (Finch et al. 1992; Finch and Ewing 1992). Wet-dry cycling increases swelling and cracking of the minerals, resulting in an increase in the amount of reactive surface area. This increased surface area accelerates weathering of initial uranium minerals and favors the formation of advanced uranium-minerals, such as uranyl-phosphates (Sowder et al. 1999) if a sufficient source of phosphate is present. Evaluating the rate and extent of 1) reaction between polyphosphate and the uranium mineral phases present within the 300 Area vadose zone and capillary fringe and 2) autunite formation as a function of polyphosphate formulation and concentration is critical to identifying the optimum infiltration rate and controlling the flux of uranium from the vadose zone and capillary fringe during remediation.

### 4.3.1 Dissolution Kinetics of Uranophane

The formation of uranyl-silicate minerals most commonly occurs in nature through the oxidized weathering of uraninite. Natural ore deposits including the Oklo deposit in Gabon, Africa (Jensen and Ewing 2001) and the Shinkolobwe deposit in Zaire, Africa (Finch et al. 1992) demonstrate the significance of uranyl-silicate minerals as the primary minerals persisting in the far-field environment in maintaining control of long-term uranium migration. Additionally, uranyl-minerals have been found to be significant in anthropogenically contaminated areas. Within the Hanford Site 300 Area, uranium entered the subsurface environment through purposeful discharges of basic sodium aluminate and acidic uranyl-copper waste streams from the dissolution of nuclear fuel and fuel rod cladding. The North and South Process Ponds (NPP and SPP, respectively) received approximately 58,000 kg of uranium, 238,000 kg of copper, 1,156,000 kg of fluoride, 243,000 kg of nitrate and large amounts of aluminum hydroxide (McKinley et al. 2007). Additionally, sodium hydroxide was added to neutralize the acidic waste stream, resulting in a temporal variation in pH ranging from 1.8 to 11.4 (over-neutralization). Detailed XANES and EXAFS, electron and x-ray microprobe, SEM-EDS, synchrotron-based  $\mu$ -XRD and  $\mu$ -XRF spectroscopic analyses have previously indicated that uranium occurs as U(VI) through the 300 Area NPP and SPP depth profile (Catalano et al. 2006b). Micro-scale X-ray spectroscopy also identified uranophane  $\text{Ca}(\text{UO}_2)_2[\text{SiO}_3(\text{OH})]_2 \cdot x\text{H}_2\text{O}$  as a uranium-solid phase contributing to the flux of uranium from the vadose zone and capillary fringe into the aquifer (Arai et al. 2007; Zachara et al. 2007).

Liu et al (2004) conducted a series of saturated dynamic leach tests on NPP sediments. The release of uranium was observed to be a kinetic process characterized by an initial fast rate. The calculated solubility values were within the reported ranges of previous literature values (Liu et al. 2004). It was postulated that the observed behavior was a result of the coupled dissolution of uranophane and solute mass transfer from intraparticle spaces. However, quantification of dissolution rates for uranophane were confounded by mass transfer limitations. An increase in the release was quantified as a function of increasing bicarbonate concentration. Bicarbonate-promoted dissolution has been observed with numerous uranium minerals including uranophane (Casas et al. 1997b; Perez et al. 2000), soddyite (Perez et al. 1997; Casas et al. 1997b), uraninite (Casas et al. 1998; Casas et al. 1994; Pierce et al. 2005; Grandstaff 1976; de Pablo et al. 1999), becquerelite (Casas et al. 1997a; Sowder et al. 2000b; Hering and Schnoor 2000), and autunite-group minerals (Sowder et al. 2000b). Casas et al. (Perez et al. 2000; Casas et al. 1997b) quantified the solubility of uranophane through a series of static tests and provide a solubility constant of  $\log K^{\circ}_{\text{so}} = 11.7 \pm 0.6$ . This value is well within the range reported in the literature,  $K^{\circ}_{\text{so}} = 9.4 \pm 0.5$  to  $K^{\circ}_{\text{so}} = 17.4$ . Additionally, this investigation quantified the dissolution of uranophane

as a function of bicarbonate through static and flow-through tests, respectively. A clear dependence of uranophane dissolution was determined as a function of bicarbonate concentration (Equation 4.2).

$$\log r_{\text{dissol}} (\text{mol m}^{-2} \text{ sec}^{-1}) = -9.2 (\pm 0.4) + 0.7 (\pm 0.2) \log [\text{HCO}_3^-] \quad (4.2)$$

Although experimental studies have not agreed upon a mechanistic dissolution model, the dissolution rate of uranium solid phases has been shown to be a function of the concentration of natural oxygen-containing ligands including hydroxide, carbonate, and phosphate. In general, surface coordination and detachment of a uranium-ligand species from the surface promote dissolution. The extent to which ligand-promoted dissolution occurs is dependent upon the affinity of the complexing ligand for uranium and electron transfer. Under common groundwater pH conditions of 4 to 10,  $[\text{PO}_4^{3-}] = 0.1$ , uranyl forms more stable complexes with phosphate than with any other natural oxygen-containing ligand (Langmuir 1978).

Given the prevalence of uranophane in oxidizing environments, from either uranium ore deposits or nuclear fuel activities, quantitative knowledge of the kinetic and thermodynamic properties is required to understand the role and significance of uranophane in the uranium geochemical cycle. Moreover, this knowledge is necessary for remediation of oxidizing environments within which uranophane is a uranium-controlling phase. The purpose of this investigation was to quantify the dissolution of uranophane as a function of pH (6 to 12) at 23°C, and as a function of polyphosphate concentration. This information is critical to understanding and quantifying the stability of uranophane in the 300 Area, providing insight into the continuing source of uranium to the 300 Area aquifer, and quantifying the effect of polyphosphate infiltration on the release and immobilization of uranium from uranophane.

#### 4.3.1.1 Effect of pH and Temperature

Figure 4.15 illustrates the release rate of uranium from uranophane across the pH range of 6 to 12 at 23°C. The dissolution rate of uranophane displays an increase in dissolution rate from pH values 8 to 10. The pH dependence is  $\eta = 0.22 \pm 0.02$ . A decrease in uranophane dissolution rate is exhibited under the pH conditions of 6 to 8,  $\eta = -0.10 \pm 0.01$ . The dissolution of uranophane is in accordance with the general trend regarding the rate dependence of dissolution on pH: the pH decreases in the acidic pH range and increases under alkaline conditions. The minimum rate of dissolution is measured at pH (23°C) ~8. This is the  $\text{pH}_{\text{pzc}}$  for uranophane, or the conditions under which the net total particle charge is zero. Thus, it may be generalized that the dissolution rate of uranophane is related to the surface charge imparted to the surface by the sorption of  $\text{H}^+$  and/or  $\text{OH}^-$ , in the absence of other complexing ligands. The slow reaction rates under conditions approaching the  $\text{pH}_{\text{pzc}}$  are contributed to by the decrease in the rate of sorption of  $\text{H}^+$  and/or  $\text{OH}^-$  to the surface and the concomitant decrease in the rate-limiting hydrolysis of uranium within the uranophane sheet structure. Comparable dissolution behavior has been previously described for autunite sheet structures (Wellman et al. 2007a; Wellman et al. 2006a). The apparent dissolution behavior observed here agrees with the results of previous saturated dynamic leach tests conducted on NPP sediments (Liu et al. 2004). Results of this investigation suggested an increase in the release of uranium at pH values  $< 7.6$  or  $> 8.5$ . The values quantified here provide an accurate estimation for the dissolution of uranophane in the subsurface as a function of pH and provide critical information on the stability of uranophane under conditions relevant to the 300 Area.

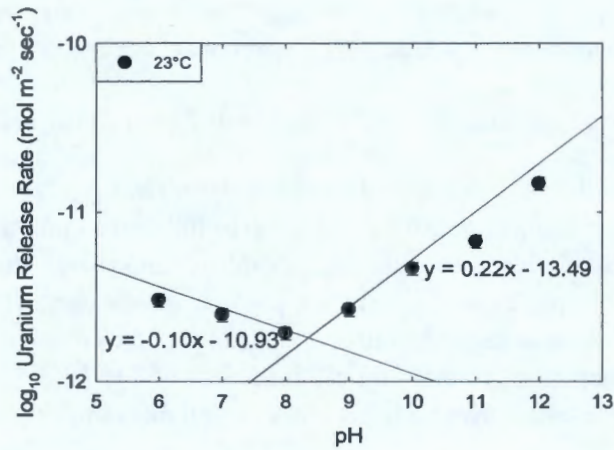


**Figure 4.15.** Log<sub>10</sub> Uranium Release Rate as a Function of pH for Uranophane in 0.05 M TRIS Solution

### 4.3.1.2 Effect of Solution Saturation State

The dissolution rate of uranophane was quantified in the presence of the polyphosphate amendment consisting of 90% orthophosphate:10% tripolyphosphate. The release of uranium was quantified at pH = 7.5, 23°C as a function of amendment concentration. The log<sub>10</sub> release rate of uranium as a function of [PO<sub>4</sub><sup>3-</sup><sub>(aq)</sub>] is shown in Figure 4.16. The rate of uranium release exhibits an ~5x increase as a function of increasing phosphate concentration over the concentration range of 500 to 1250 ppm phosphate. Subsequent increases in aqueous phosphate concentration have no measurable effect on the dissolution rate. The release of uranium as a function of phosphate can be predicted from Equation 4.3 obtained from a least-squares regression (solid line) of the experimental data in Figure 4.16:

$$\text{Log } r_{\text{dissol}} (\text{mol m}^{-2} \text{sec}^{-1}) = 6.6 \times 10^{-12} + 1.1 \times 10^{-10}[\text{PO}_4^{3-}] \quad (4.3)$$

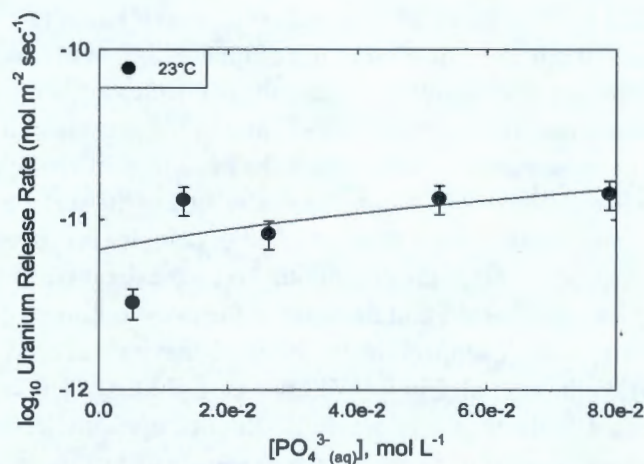


**Figure 4.16.** Log<sub>10</sub> Rate of Uranium from Uranophane Release as a Function of [PO<sub>4</sub><sup>3-</sup><sub>(aq)</sub>] at pH = 7.5, 23°C

### 4.3.2 Dissolution Kinetics of Meta-Torbernite, $\text{Cu}(\text{UO}_2)_2(\text{PO}_4)_2 \cdot x\text{H}_2\text{O}$

Uranyl phosphate phases are advanced secondary uranium minerals formed during the oxidized weathering of primary  $\text{UO}_2$  deposits (Garrels and Christ 1965). Characterization of sediments from uranium-contaminated sites including the 300 Area has identified discrete uranyl-phosphate, autunite, minerals (Bertsch et al. 1994; Buck et al. 1996; Buck et al. 1994; Buck et al. 1995; Morris et al. 1996; Tidwell et al. 1996; Catalano et al. 2004; Catalano et al. 2006b; Zachara et al. 2007; Zachara et al. 2005). Autunite minerals have been frequently identified in contaminated sediments as the long-term controlling phase of uranium. Under these conditions the mobility of uranium in subsurface pore waters is limited by the rate of dissolution of autunite and meta-autunite group minerals,  $X_{3-n}^{(n)+}(\text{UO}_2)_2(\text{PO}_4)_2 \cdot x\text{H}_2\text{O}$ .

The autunite-type sheet contains uranyl square bipyramids and phosphate tetrahedra. Each equatorial vertex of the uranyl square bipyramid is shared with a different phosphate tetrahedron, and each tetrahedron is linked to four different uranyl polyhedra (Figure 4.17) (Burns 1999). Although all autunite-group minerals contain uranyl phosphate sheets with the same topologies, the configurations of the constituents located between the sheets can vary dramatically. The interlayer sites can accommodate a wide variety of cations, ranging from octahedrally coordinated transition metals through monovalent cations in large irregular coordination polyhedra, including  $\text{K}^+$  and  $\text{H}_3\text{O}^+$  (Burns 1999). Substitution and the identity of the interlayer cation may also have a considerable impact on the stability of the mineral.

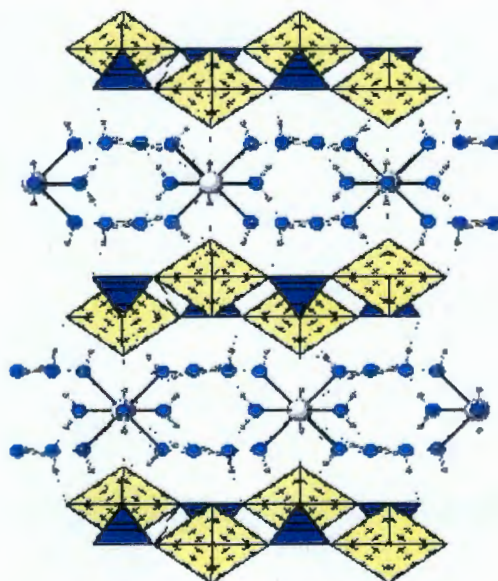


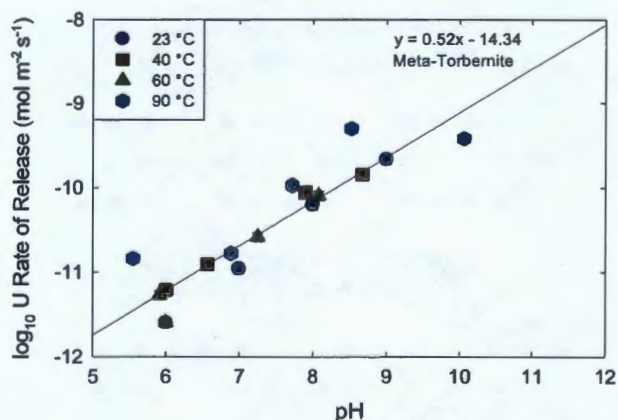
**Figure 4.17.** The Structure of Autunite-group Minerals, Determined by Single-Crystal X-Ray Diffraction (adapted from Locock and Burns 2002). Uranyl bipyramids are denoted in yellow, phosphate tetrahedral are dark blue, interlayer water molecules are light blue, and interlayer cations are white.

Previous experimental results have established the low solubility of many uranyl phosphate minerals (Moskvina et al. 1967; Vesely et al. 1965; Chukhlantsev and Stepanov 1956; Schreyer and Baes 1954; Karpov 1961). However, knowledge of the solubility of the uranyl phosphate phases is restricted to a narrow range of experimental conditions involving low pH media with high concentrations of phosphoric

acid (Scheyer and Baes 1954; Vesely et al. 1965; Karpov 1961) and all known solubility studies are based on synthetic, rather than natural phases (Giammar 2001; Sowder et al. 2000a; Vesely et al. 1965; Pekarek and Vesely 1965; Schreyer and Baes 1954; Karpov 1961). Moreover, few kinetic dissolution studies of autunite and meta-autunite group minerals have been reported (Wellman et al. 2007a; Wellman et al. 2006a; Giammar 2001) and these all have been conducted on Ca- and Na-meta autunite. Substitution of a copper cation,  $\text{Cu}^{2+}$ , into the interlayer of the autunite structure results in formation of meta-torbernite, for which the dissolution kinetics of have not been reported. Consequently, understanding of the long-term dissolution behavior of this important uranium-controlling solid is incomplete. The purpose of this investigation was to quantify the dissolution of meta-torbernite as a function of pH (6-10) and temperature (23° to 90°C), and as a function of polyphosphate concentration. This information is critical to understanding the persistence of meta-torbernite in the 300 Area and the effect of polyphosphate remediation on meta-torbernite.

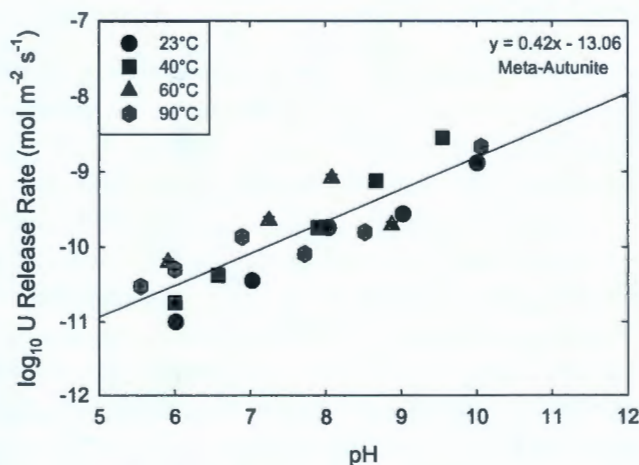
#### 4.3.2.1 Effect of pH and Temperature

Figure 4.18 illustrates the release rate of uranium from meta-torbernite across the pH range of 6 to 10 and the temperature range of 23° to 90°C. Release rates of uranium increase by ~100-fold over the pH interval and is quantified by the power law coefficient  $\eta = 0.52 \pm 0.08$ . The release of uranium is independent of temperature, which indicates that the power law coefficient,  $\eta$ , is independent of temperature.



**Figure 4.18.**  $\log_{10}$  Uranium Release Rate as a Function of Temperature-Corrected pH for Meta-Torbernite in 0.05 M TRIS Solution

Figure 4.19 illustrates the release rate of uranium from Ca-meta-autunite across the pH range of 6 to 10 and the temperature range of 23° to 90°C. Comparable to meta-torbernite, the release rates of uranium increase by ~100-fold over the pH interval and are independent of temperature. The increase in rate as a function of pH is quantified by the power law coefficient  $\eta = 0.42 \pm 0.05$ . The power law coefficient for meta-torbernite is slightly greater than that quantified for Ca-meta-autunite. This suggests 1) the stability of meta-torbernite is greater than that of meta-autunite, which is reflected in the predicted stability constants for each of these phases (Table 4.4); and, 2) release of the interlayer cation may be limited by the rate of matrix dissolution.



**Figure 4.19.** Log<sub>10</sub> Uranium Release Rate as a Function of Temperature Corrected pH for Ca-Meta-Autunite in 0.05 M TRIS Solution

**Table 4.4.** Table of Calculated or Measured Log  $K_{sp}$  Values of Uranyl Phosphate Solids (Langmuir 1997)

Log $K_{sp}$ of Autunite and Meta-Autunite Phases	
Phase	log $K_{sp}$
$H_2[(UO_2)(PO_4)]_2 \cdot nH_2O$	-48.4
$Na_2[(UO_2)(PO_4)]_2 \cdot nH_2O$	-47.6
$K_2[(UO_2)(PO_4)]_2 \cdot nH_2O$	-47.7
$Ca[(UO_2)(PO_4)]_2 \cdot nH_2O$	-41.7
$Mg[(UO_2)(PO_4)]_2 \cdot nH_2O$	-44.5
$Sr[(UO_2)(PO_4)]_2 \cdot nH_2O$	-43.8
$Cu[(UO_2)(PO_4)]_2 \cdot nH_2O$	-45.2
$Fe[(UO_2)(PO_4)]_2 \cdot nH_2O$	-47.2

Given the cessation of copper-bearing waste streams to the 300 Area in 1975 (McKinley et al. 2007), it could be hypothesized that exchange of the interlayer copper cation in meta-torbernite would occur with calcium under the geochemical conditions present in the 300 Area (i.e., pore is saturated with respect to calcite (Liu et al. 2004)) if the interlayer cation were readily exchangeable. However, meta-torbernite has remained a persistent phase in the 300 Area. The inhibition of interlayer cation release from meta-torbernite and meta-autunite, suggested here, further aids in understanding the persistence of meta-torbernite in the 300 Area.

Results of polyphosphate transport and unsaturated weathering experiments indicate the necessary infiltration rate is exceedingly low in comparison to the flow rate needed to produce a detectable release of uranium from meta-torbernite. In addition, the polyphosphate amendments use sodium-based phosphate compounds. If the interlayer copper cation in meta-torbernite were to exchange for sodium the resulting Na-meta-autunite phase would exhibit even greater stability than meta-torbernite (Table 4.4). Thus, controlled infiltration of polyphosphate amendments is not expected to mobilize uranium that is currently controlled by the meta-torbernite phase.

### 4.3.2.2 Effect of Solution Saturation State

The dissolution rate of meta-torbernite was quantified in the presence of the polyphosphate amendment consisting of 90% orthophosphate:10% tripolyphosphate. The release of uranium was quantified at pH = 7.5, 23°C as a function of amendment concentration. The log<sub>10</sub> release rate of uranium as a function of [PO<sub>4</sub><sup>3-</sup><sub>(aq)</sub>] is shown in Figure 4.20. The rate of uranium release exhibits an ~10x increase as a function of increasing phosphate concentration. However, the rate of uranium release is maintained at, or below, the minimum rate observed in the absence of aqueous phosphate, regardless of pH (Figure 4.19 and Figure 4.20). Thus, the concentration of uranium potentially released during the infiltration of polyphosphate remedial solution will be less than that released through the dissolution of meta-torbernite in natural pore waters and polyphosphate remediation will not detrimentally impact the stability of meta-torbernite. Furthermore, the release of uranium as a function of phosphate can be predicted from Equation 4.4 obtained from a least-squares regression (solid line) of the experimental data in Figure 4.20:

$$\text{Log } r_{\text{dissol}} (\text{mol m}^{-2} \text{ sec}^{-1}) = -4.7 \times 10^{-13} + 4.1 \times 10^{-10} [\text{PO}_4^{3-}] \quad (4.4)$$

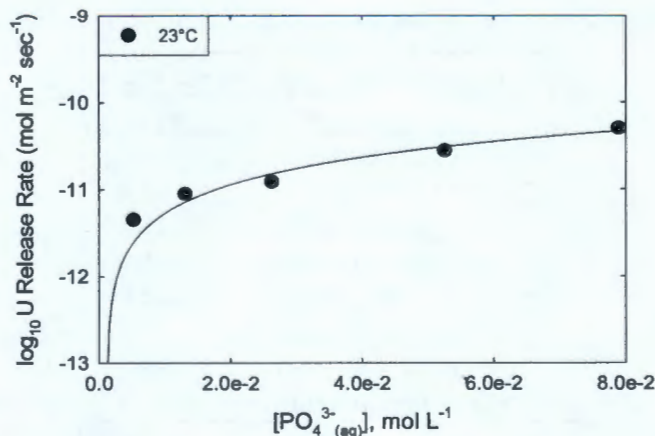


**Figure 4.20.** Log<sub>10</sub> Rate of Uranium Release from Meta-Torbernite as a Function of [PO<sub>4</sub><sup>3-</sup><sub>(aq)</sub>] at pH = 7.5, 23°C

### 4.3.3 Unsaturated Weathering of Uranium Minerals During Polyphosphate Remediation

The following sections address polyphosphate remediation of NPP sediment, polyphosphate formulation for vadose zone and capillary fringe infiltration, and polyphosphate remediation of uranium minerals.

#### 4.3.3.1 Polyphosphate Remediation of North Process Pond Sediment

To evaluate the efficacy of a long-chain polyphosphate for *in situ* stabilization of uranium under hydraulically unsaturated conditions, laboratory column tests were conducted at conditions expected within the 300 Area Hanford vadose zone and capillary fringe. Sediment columns were prepared with Hanford sediment B11494 removed from the North Process Pond (NPP) containing 540 mg kg<sup>-1</sup> uranium. The uranium-contaminated sediment used in these experiments will be referred to as B11494. The

columns were saturated with Hanford groundwater, desaturated, and treated with Hanford groundwater spiked with 1,000 ppm phosphate as sodium triphosphate. The purpose of this investigation was to determine the efficacy of using the polyphosphate amendment strategy for the remediation of uranium-contaminated sediments. Accordingly, two principal objectives were to evaluate the 1) efficacy of polyphosphate for immobilization and long-term stabilization of uranium within these sediments under conditions that simulate the unsaturated, open-flow, and transport conditions expected in the vadose zone; and 2) changes in uranium mineralogy due to polyphosphate treatment.

#### **4.3.3.1.1 Mineralogy**

The XRD analyses of the bulk sediment identified quartz as the dominant mineral, with lesser amounts of feldspar and hornblende, whereas the XRD analyses of the clay size fraction reveal minor amounts of illite and chlorite. The particle size distribution, determined by a combination of dry sieve and hydrometer methods, of the material collected can be characterized as 48% gravel (> 2-mm), 40% sand (0.06-mm to 2-mm), 4% silt (0.002-mm to 0.06-mm), and 8% clay (<0.002-mm). The air-dried moisture content was 8.92%, total carbon 1.11 mass%, which mainly consisted of organic carbon (0.97 mass%) with a minor amount of inorganic carbon (0.14 mass%). The uranium content was measured both by XRF (188 pCi/g) and gamma energy analysis (180 pCi/g) and corresponds to approximately 539 mg of uranium per kg of sediment. The majority of the uranium was determined to be associated with the < 2-mm size fraction, based on uranium gamma energy analysis (GEA) analyses of various size separates. In addition to uranium, elevated concentrations of Ga (47.6 µg/g) and Pb (30.7 µg/g), in comparison to uncontaminated Hanford sediment, were also identified by XRF. Results from selective chemical extractions (Tessier et al. 1979) with sodium acetate/acetic acid (pH ~ 5.0) and "TAMMS" reagent (0.12 M oxalic acid and 0.11 M ammonium oxalate at pH ~3.0) suggested that the majority of the uranium was associated with the carbonate solids (30.2% of the total U) and amorphous iron and aluminum hydroxide phases (55.0% of the total U), respectively (Serne et al. 2002a; Brown et al. 2005). The amount of uranium contained in these sediments exceeds the uranium concentration expected to be present in deep vadose zone sediments making these sediments a good model to evaluate the polyphosphate amendment strategy as a treatment technology for the treatment of uranium subsurface contamination.

#### **4.3.3.1.2 XANES and EXAFS**

The XANES spectrum of B11494 sediment sample indicates that only U(VI) is present in the sample, evident by the strong resonant feature located at roughly 17190 eV (Figure 4.21). This shoulder is due to the presence of the uranyl moiety ( $\text{UO}_2^{2+}$ ) (Farges et al. 1992; Catalano et al. 2006b; Bertsch et al. 1994). The EXAFS spectrum of the B11494 sediment sample (Figure 4.21) matched well with the spectrum of other near-surface samples collected from the 300 Area North Process Pond (Catalano et al. 2006a). In this previous study, uranium in these sediments was found to occur primarily in a form co-precipitated with calcite ( $\text{CaCO}_3$ ). The similarity of the B11494 spectrum with that of the near-surface North Process Pond samples suggests that uranium occurs primarily in a similar form (i.e., co-precipitated with  $\text{CaCO}_3$ ). Other uranium species also may be present in the sample, but only as minor components (< 10 mass%).

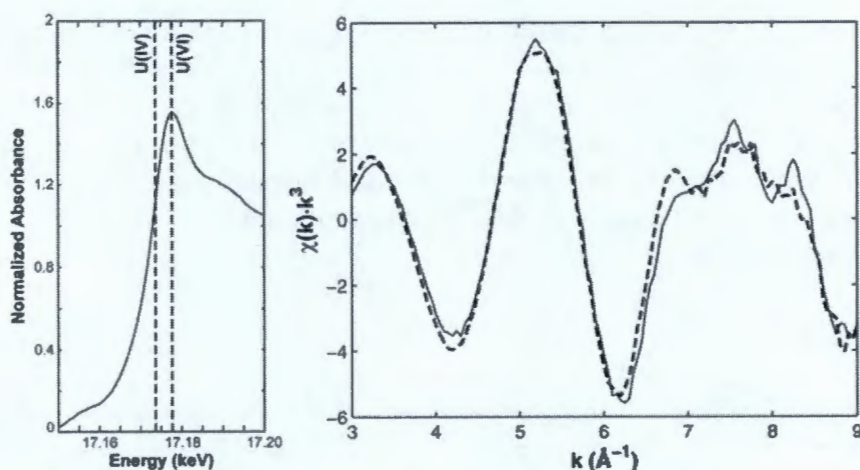


**Figure 4.21.** The XANES Spectrum of Sample B11494, Indicating the Presence of Only U(VI) (left). The EXAFS spectrum of B11494 sediment sample (solid line) compared to the spectrum of NP 4-1 sediment sample (dashed line) from Catalano et al. (2006). Uranium was previously found to occur coprecipitated with calcite in NP 4-1.

#### 4.3.3.1.3 Effluent Solution Chemistry

Results from the analyses of effluent samples from the  $1.0 \times 10^3 \mu\text{g/L}$  tripolyphosphate spiked Hanford Groundwater PUF column is provided in Figure 4.22. In the tripolyphosphate-treated column, the uranium concentration initiates at  $5.1 \times 10^3 \mu\text{g/L}$ , fluctuates over the first 20 pore volumes and subsequently exhibits a rapid decrease to  $7.0 \mu\text{g L}^{-1}$  within the succeeding 10 pore volumes. Effluent uranium concentrations remain well below drinking water standards through the duration of testing. Conversely, the concentration of phosphorus was below the limit of detection,  $< 6.3 \times 10^2 \mu\text{g/L}$ , for the first 15 pore volumes. Subsequently, the concentration of phosphorus increases rapidly until reaching a maximum,  $14.9 \times 10^4 \mu\text{g/L}$ , at  $\sim 25$  pore volumes. The final phosphorus concentration was approximately two-times lower than the initial spike concentration ( $24.6 \times 10^4 \mu\text{g/L}$ ), which suggests that once this experiment was terminated phosphorus was still being sequestered within the column. The increase in phosphorus concentration correlates with the observed decrease in uranium concentration. This correlation suggests that after approximately 20 pore volumes,  $\text{PO}_4^{3-}$  ions that are released from tripolyphosphate to form uranium-phosphate precipitate with the labile available fraction of U contained in the B11494 sediment. The concentrations of Ca, Mg, and Sr decreased slightly over time, whereas the concentrations of K, Na, S, and Si were relatively steady over the duration of the experiment. Aluminum ( $< 250 \mu\text{g/L}$ ), Cd ( $< 50 \mu\text{g/L}$ ), Co ( $50 \mu\text{g/L}$ ), Cr ( $30 \mu\text{g/L}$ ), and Fe ( $50 \mu\text{g/L}$ ) were all below the detection limits.

Comparatively, the effluent samples from the control column (i.e., the influent solution was Hanford groundwater without sodium tripolyphosphate) are shown in Figure 4.23. The concentration of uranium in the effluent from the control column initiates at  $8.1 \times 10^2 \mu\text{g/L}$  and increases to a maximum concentration of  $1.6 \times 10^5 \mu\text{g/L}$  over the first 20 pore volumes. Subsequently, the concentration of uranium exhibits a prolonged decrease to  $1.7 \times 10^3 \mu\text{g/L}$  during the remainder of the experiment. After 300 days of testing ( $\sim 50$  pore volumes) the concentration of uranium remain approximately 50 times greater than the maximum concentration limit (MCL) ( $30 \mu\text{g/L}$ ). The concentration of Ca, K, Mg, Na, Sr, and Si remained relatively constant, and Al, Cd, Co, Cr, Fe, and P concentrations were all below the sample limit of detection for the duration of the experiment without tripolyphosphate.

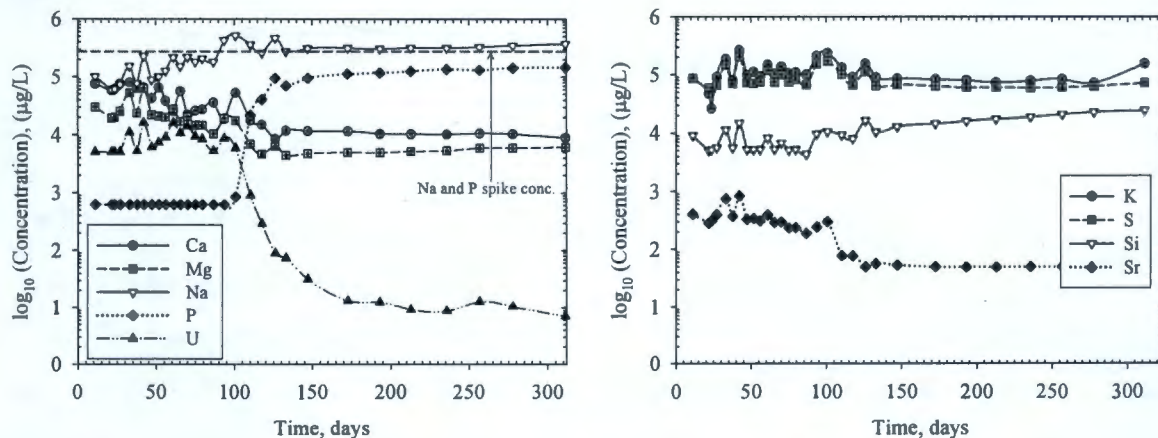


**Figure 4.22.** Log<sub>10</sub> Concentration of Elements, in µg/L, Released from the Tripolyphosphate (1000 µg/L) -Treated Column Measured in the Effluent Solutions as a Function of Time, in Days. The dashed line represents the initial concentration of Na and P measured in the Hanford groundwater-spiked groundwater.

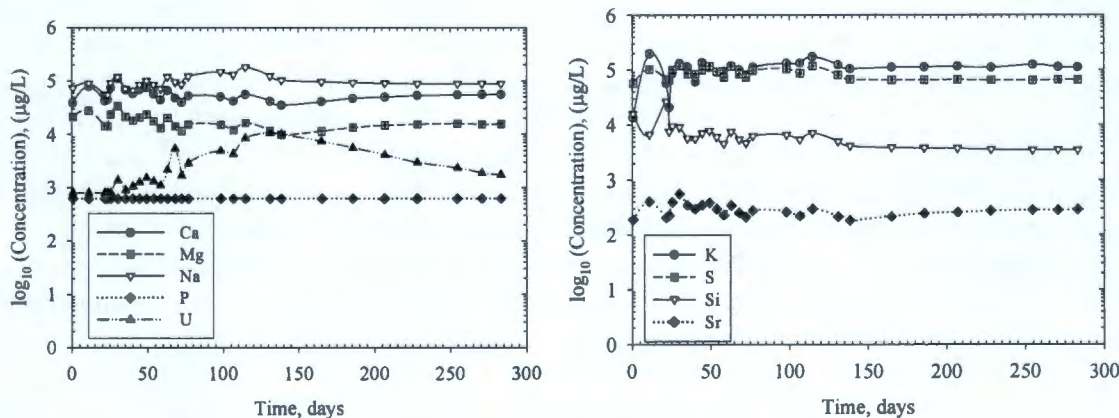


**Figure 4.23.** Log<sub>10</sub> Concentration of Elements, in µg/L, Released from the Control Column Measured in the Effluent Solutions as a Function of Time, in Days

Results of geochemical modeling conducted on effluent solution compositions measured at each sampling interval provided insight into the uranium solution speciation within the unsaturated columns (Figure 4.24). It is important to note that because of the complex chemistry of uranium, there is significant debate within the literature regarding the stoichiometry and the thermodynamic values assigned to aqueous uranium species and secondary mineral phases. As such, the model predictions are based on current knowledge, but may have significant uncertainty associated with them and are considered semi-quantitative. Geochemical predictions indicated that effluent from the control column was saturated with respect to liebigite [Ca<sub>2</sub>(UO<sub>2</sub>)(CO<sub>3</sub>)<sub>3</sub>·11(H<sub>2</sub>O)] (Figure 4.24). Liebigite is also the initial dominant uranium species predicted in the tripolyphosphate-amended column. During tripolyphosphate treatment, the aqueous species UO<sub>2</sub>(HPO<sub>4</sub>)<sub>2</sub><sup>2-</sup> becomes the dominant species at 100% of the predicted uranium distribution (Figure 4.24), whereas liebigite remains the predicted phase in the control column. Saturation indices calculated from the solution chemistry data further suggest that effluent solutions in the absence of the polyphosphate amendment remain oversaturated with CaCO<sub>3</sub>, while the solution with polyphosphate becomes undersaturated with respect to CaCO<sub>3</sub> (Figure 4.24).

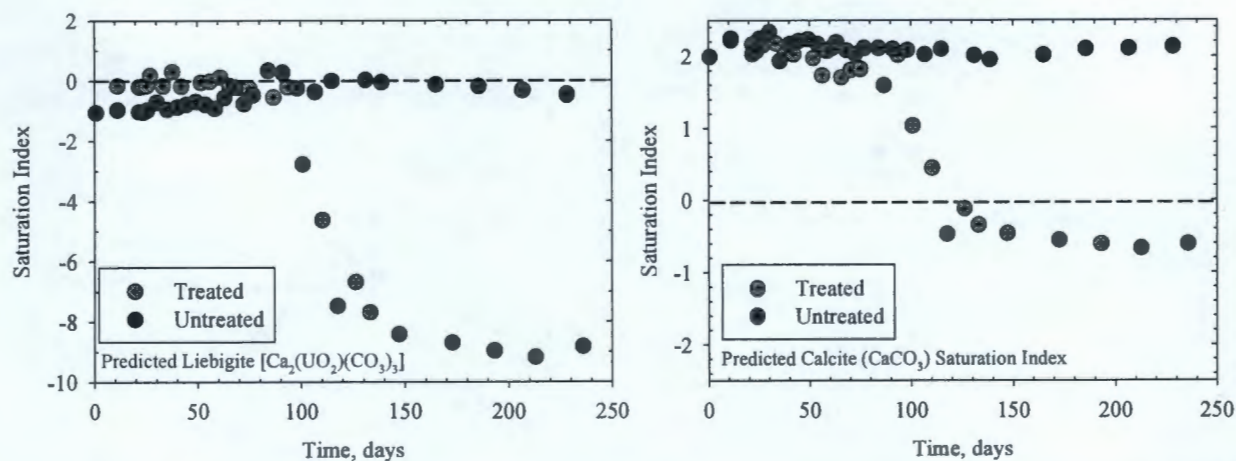


**Figure 4.24.** Geochemical Thermodynamic Modeling Results Depicting the Predicted Saturation Indices for Uranium Solid Phases (left) and Calcite (right) Based on Effluent Solution Compositions

Liebigite has been noted previously in other investigations as a possible phase existing in the NPP sediments (Catalano et al. 2006b). Further investigation suggested that uranium-rich calcite was a more realistic phase. However, thermodynamic and kinetic databases do not contain data for uranium-rich calcite, in part, because of the multiple modes of uranium incorporation into the calcite structure and challenges associated with precise characterization of the phase. Thus, thermodynamic geochemical predictions will not suggest the formation of uranium-rich calcite. As previously noted, the majority of uranium in this sediment is associated with uranium-rich calcite; therefore, although liebigite is predicted to occur, it is more likely uranium-rich calcite. Despite the limitations of current thermodynamic databases, the predicted results still clearly indicate that the saturation state of the system changes such that it is undersaturated with respect to the dominant uranyl-carbonate phases controlling uranium in sediment B11494 upon treatment with polyphosphate.

Results of EXAFS analyses conducted on reacted materials extracted from the polyphosphate treated and control columns. Figure 4.25 displays the U  $L_{III}$ -edge EXAFS spectrum of an autunite mineral phase  $X_{3-n}^{(n)+} [(UO_2)(PO_4)]_2 \cdot xH_2O$  where  $X$  is any mono- or divalent cation, U-calcite, sediment treated with tripolyphosphate and untreated sediment. Evaluation of the uranium  $L_{III}$ -edge EXAFS spectra (Figure 4.25) suggests that the chemical speciation of uranium changed upon treatment with tripolyphosphate. The data were well fit using a linear combination of the  $\chi$  data from  $k = 3-12$ ,  $k^3$  weighted for U-calcite and autunite-group minerals. The fitted data suggest that after more than 70 pore volumes of treatment ~14% of the uranium was present as an autunite-group mineral, while the remaining fraction was still uranium coprecipitated with calcite. The formation of an autunite-group mineral “rind” on the uranium-rich calcite surface decreased the flux of uranium from the column from ~5000  $\mu\text{g/L}$  to ~7  $\mu\text{g/L}$ , even though < 1% of the total uranium contained within the column had been removed. Subsequent release of uranium is limited by the rate of dissolution for autunite-group minerals. Because autunite sequesters uranium in the oxidized form, U(VI), rather than forcing reduction to U(IV), the possibility of re-oxidation and subsequent re-mobilization of uranium is negated.

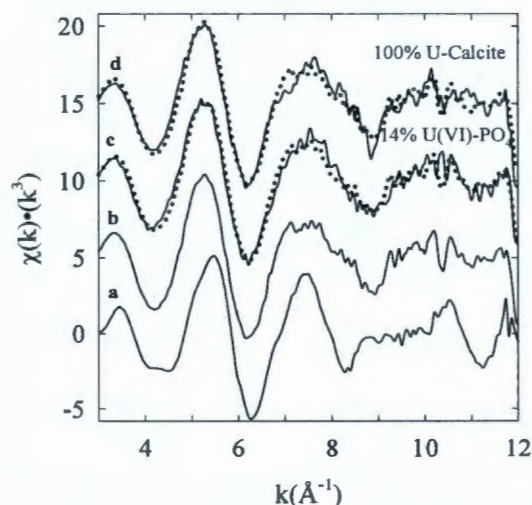


**Figure 4.25.** EXAFS of (a) Autunite-Group Mineral,  $X_{3-n}^{(n)+} [(UO_2)(PO_4)]_2 \cdot xH_2O$ , (b) U-Calcite, and 300 Area Sediment PUF Column Containing  $\sim 540$  mg/kg Uranium as Uranium Coprecipitated with Calcite Leached with (c) 1000 ppm Tripolyphosphate and (d) Hanford Groundwater. The dashed line is the best fit to the EXAFS spectra.

The initial increase in the concentration of aqueous uranium released from the tripolyphosphate-amended column is likely because of mobilization of readily labile uranium (i.e., water extractable), within the sediment, by the high sodium content of tripolyphosphate. Additionally, the degradation rate of tripolyphosphate and retardation of ortho-, pyro-, and tripolyphosphate within the sedimentary matrix delay reaction of phosphate with the uranium solid phase and the labile uranium, thereby affording the initial increase in aqueous uranium concentration. Adjusting the formulation of a polyphosphate amendment to include orthophosphate will minimize the release of labile uranium through precipitation as uranyl-phosphate. In the absence of the soluble polyphosphate amendment, the uranium concentration was sustained at a concentration approximately 50 times greater than the current drinking water standard. The results presented here illustrate the efficacy of using a soluble polyphosphate amendment to stabilize uranium-contaminated sediments through transformation of soluble uranium-bearing solid phases to uranium-phosphate phases resulting in reduction of the labile uranium concentrations to below the drinking water limits under hydraulically unsaturated conditions.

#### 4.3.3.2 Polyphosphate Formulation for Vadose Zone and Capillary Fringe Infiltration

The geology of the 300 Area vadose zone and capillary fringe is open framework sands and gravels, which are highly conductive. Based on the results presented above, the polyphosphate remedy developed for deployment within the 300 Area, which consisted of 25% orthophosphate, 25% pyrophosphate, and 50% tripolyphosphate (Wellman et al. 2007c), will not degrade and react with uranium solid phases present in the vadose zone and capillary fringe at a rate sufficient to control the flux of uranium into the aquifer. Additionally, the rate of transformation of uranyl-carbonate and uranyl-silicate phases with this formulation would require tens of pore volumes of treatment, which is impractical and would exacerbate the flux of uranium to the aquifer. Therefore, a series of unsaturated column tests were conducted on Hanford sediments containing  $\sim 900$  ppm uranium as uranium-rich calcite with three alternative polyphosphate formulations (Table 4.5). The polyphosphate formulations all contained 5000 ppm

phosphate, but the relative percent contributions of ortho-, pyro-, and tripolyphosphate were varied. Uranium-rich calcite is a highly soluble uranium-bearing phase. Aside from sorbed uranium, it is a highly labile form of uranium within the 300 Area. Therefore, it is critical that the selected polyphosphate formulation be capable of controlling the potential flux of uranium from this phase during remediation. Three principal objectives were to 1) quantify the ability of the polyphosphate formulations to attenuate the flux of uranium from the sedimentary matrices during remediation, 2) evaluate the immobilization of uranium within these sediments under conditions that simulate the unsaturated, open-flow and transport conditions expected in the vadose zone, and 3) evaluate changes in uranium mineralogy caused by polyphosphate treatment.

**Table 4.5.** Polyphosphate Formulations for Uranium Stabilization via Infiltration Under Unsaturated Conditions

Formulation	Nominal Percentage	Composition	Formula	Formula Wt, g/mol	Conc., g/L	Conc., M
1	25	Sodium phosphate, tribasic	$\text{Na}_3\text{PO}_4 \cdot 12\text{H}_2\text{O}$	380.13	5.003	$1.32 \times 10^{-2}$
	65	Sodium pyrophosphate	$\text{Na}_4\text{P}_2\text{O}_7 \cdot 10\text{H}_2\text{O}$	446.06	7.632	$1.71 \times 10^{-2}$
	10	Sodium tripolyphosphate	$\text{Na}_5\text{P}_3\text{O}_{10}$	367.86	0.646	$1.75 \times 10^{-3}$
2	70	Sodium phosphate, tribasic	$\text{Na}_3\text{PO}_4 \cdot 12\text{H}_2\text{O}$	380.13	14.009	$3.69 \times 10^{-2}$
	20	Sodium pyrophosphate	$\text{Na}_4\text{P}_2\text{O}_7 \cdot 10\text{H}_2\text{O}$	446.06	2.348	$5.26 \times 10^{-3}$
	10	Sodium tripolyphosphate	$\text{Na}_5\text{P}_3\text{O}_{10}$	367.86	0.646	$1.75 \times 10^{-3}$
3	90	Sodium phosphate, tribasic	$\text{Na}_3\text{PO}_4 \cdot 12\text{H}_2\text{O}$	380.13	18.011	$4.74 \times 10^{-2}$
	10	Sodium tripolyphosphate	$\text{Na}_5\text{P}_3\text{O}_{10}$	367.86	0.646	$1.75 \times 10^{-3}$

#### 4.3.3.2.1 Formulation 1: 25% Ortho-, 65% Pyro-, and 10% Tripolyphosphate

Because pyrophosphate displayed the greatest degree of retardation under unsaturated conditions, the initial reformulation of polyphosphate contained 25% ortho-, 65% pyro-, and 10% tripolyphosphate. Figure 4.26 presents effluent uranium concentrations. The initial uranium concentration measured in the Hanford groundwater effluent was  $\sim 6.0 \times 10^3 \mu\text{g/L}$ . Initial treatment of the column with the polyphosphate-amended Hanford groundwater resulted in a spike in uranium concentration of  $\sim 3.0 \times 10^5 \mu\text{g/L}$ . The effluent uranium concentration rapidly decreased during the subsequent 2 pore volumes of treatment and the total amount of uranium released during testing was  $\sim 1\%$ . The increase in pyrophosphate and decrease in tripolyphosphate, relative to the original polyphosphate formulation developed for treatment of the aquifer, decreases the necessary degradation time for production of orthophosphate. However, as previously noted, the solubility of pyrophosphate metal complexes are greater than those of tripolyphosphate (Onaka et al. 1981; van Wazer and Callis 1958). Thus, reaction of uranium-rich calcite with pyrophosphate can result in the formation of more stable aqueous uranium complexes, which limit precipitation and result in greater mobilization of uranium during polyphosphate-based remediation. Although results presented here suggest that the higher proportion of pyrophosphate does provide a more readily available source of orthophosphate for stabilization of uranium solid phases and attenuation of the aqueous uranium flux, the abundance of pyrophosphate in formulation 1 may produce a significant pulse of uranium to the aquifer during initiation of the remedial action.

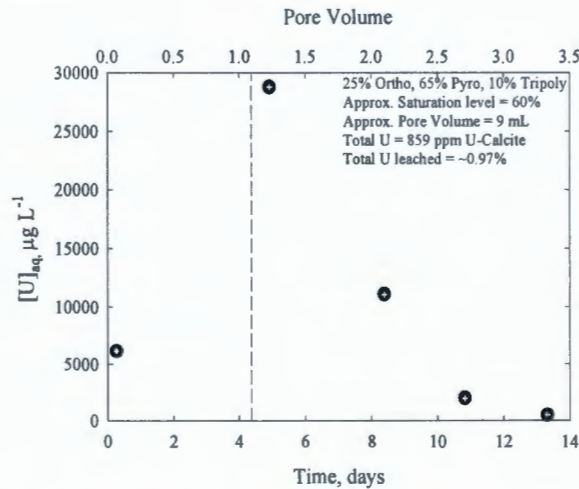


**Figure 4.26.** Concentration of Uranium,  $\mu\text{g/L}$ , Released from 25% Ortho-, 65% Pyro-, 10% Tripolyphosphate-Treated Column Measured in the Effluent Solutions as a Function of Time (days) and Pore Volume. The dashed vertical line represents the initiation of flow for the phosphate amended groundwater.

#### 4.3.3.2.2 Formulation 2: 70% Ortho-, 20% Pyro-, and 10% Tripolyphosphate

Figure 4.27 presents effluent uranium concentration from the 70% ortho-, 20% pyro-, 10% tripolyphosphate-amended column. The initial uranium concentration measured in the Hanford groundwater effluent was  $\sim 6.0 \times 10^3 \mu\text{g/L}$ . This concentration was comparable to that measured in Hanford groundwater effluent from the PUF column treated with formulation 1, 25% ortho-, 65% pyro-, 10% tripolyphosphate. Initial treatment of the column with the polyphosphate-amended Hanford groundwater resulted in a spike in uranium concentration of  $\sim 2.3 \times 10^5 \mu\text{g/L}$ . This increase in uranium concentration was  $\sim 24\%$  lower than that exhibited by the column treated with formulation 1. Comparable to the column treated by formulation 1, the effluent uranium concentration rapidly decreased during the subsequent 2 pore volumes of treatment. The total amount of uranium released during testing was  $\sim 1\%$ .

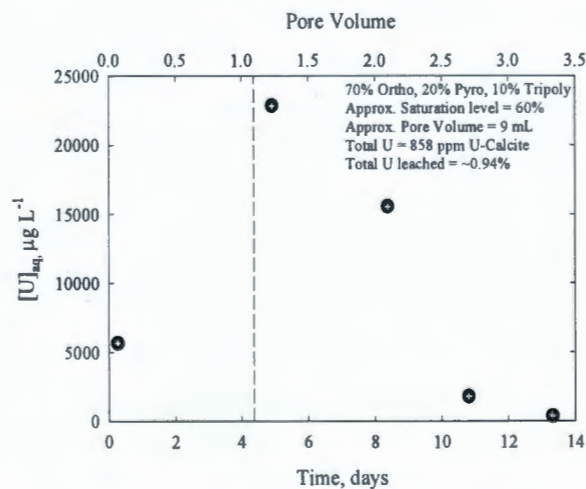


**Figure 4.27.** Concentration of Uranium,  $\mu\text{g/L}$ , Released from the 70% Ortho-, 20% Pyro-, 10% Tripolyphosphate-Treated Column Measured in the Effluent Solutions as a Function of Time (days) and Pore Volume. The dashed vertical line represents the initiation of flow for the phosphate amended groundwater.

#### 4.3.3.2.3 Formulation 3: 90% Ortho- and 10% Tripolyphosphate

Figure 4.28 presents effluent uranium concentration from the 90% ortho- and 10% tripolyphosphate-amended column. The initial uranium concentration measured in the Hanford groundwater effluent was  $\sim 7.5 \times 10^3 \mu\text{g/L}$ . Because of challenges establishing steady-state unsaturated flow conditions, flow of Hanford groundwater through the column continued for the first three pore volumes. In comparison, Hanford groundwater was only displaced for approximately one pore volume through unsaturated columns used to evaluate formulations 1 and 2. The effluent uranium concentration increased to  $\sim 1.8 \times 10^5 \mu\text{g/L}$  over the first three pore volumes, prior to treatment with polyphosphate formulation 3. Contrary to formulations 1 and 2, there was no spike in uranium concentration upon initial treatment of the column with the polyphosphate-amended Hanford groundwater. Rather the effluent uranium concentration decreased from  $\sim 1.8 \times 10^5 \mu\text{g/L}$  to  $\sim 1.4 \times 10^5 \mu\text{g/L}$ . Comparable to the column treated by formulations 1 and 2, the effluent uranium concentration rapidly decreased during the subsequent two pore volumes of treatment. The total amount of uranium released during testing was  $\sim 1.3\%$ . The increased amount of uranium released, relative to columns treated with formulation 1 and 2, was a result of two additional pore volumes of leaching with Hanford groundwater, prior to initiation of the polyphosphate amendment.

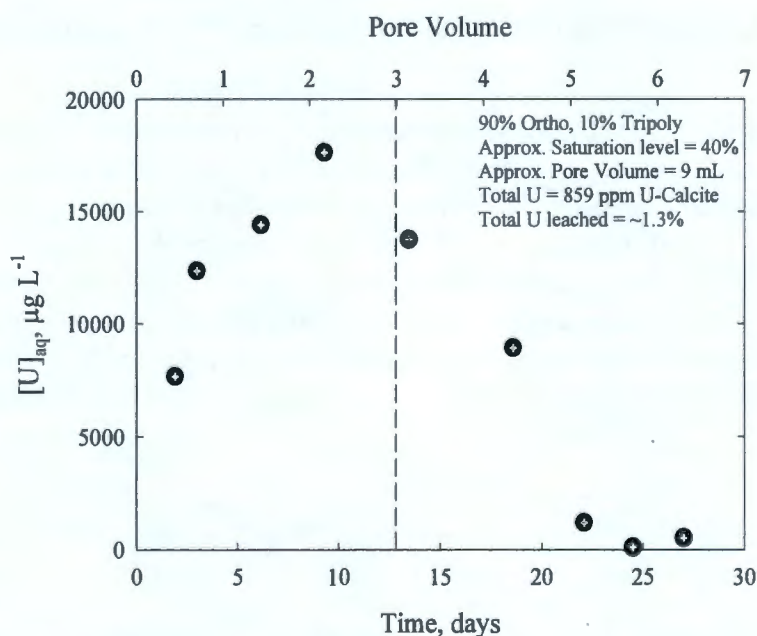


**Figure 4.28.** Concentration of Uranium,  $\mu\text{g/L}$ , Released from 90% Ortho- and 10% Tripolyphosphate-Treated Column Measured in the Effluent Solutions as a Function of Time (days) and Pore Volume. The dashed vertical line represents the initiation of flow for the phosphate amended groundwater.

EXAFS analyses were conducted on reacted materials extracted from the uranium-rich calcite columns treated with the three different polyphosphate formulations. Evaluation of the uranium  $L_{III}$ -edge EXAFS spectra (Figure 4.29) suggests that the chemical speciation of uranium changed upon treatment with polyphosphate. The data were well fit using a linear combinations of the  $\chi$  data from  $k = 3-12$ ,  $k^3$  weighted for U-calcite and autunite-group minerals. The fitted data suggest that treatment with formulation 1 (consisting of 25% ortho-, 65% pyro-, and 10% tripolyphosphate), resulted in only 1%

conversion of the uranium to a uranium-phosphate phase after ~3 pore volumes of treatment; the remaining fraction was still uranium coprecipitated with calcite. EXAFS results indicated that in the uranium-calcite rich column treated with formulation 2 (consisting of 70% ortho-, 20% pyro-, and 10% tripolyphosphate), 10% of the uranium was converted to a uranium-phosphate phase after nearly a comparable ~3 pore volumes of treatment. The remaining fraction was still coprecipitated with calcite. Treatment of uranium-rich calcite under unsaturated conditions was best achieved using polyphosphate formulation 3, 90% ortho- and 10% tripolyphosphate. After 3 pore volumes of treatment, 40% of the uranium was converted to uranium-phosphate. Even though < 1% of the total uranium contained within the column had been removed, the formation of an autunite-group mineral “rind” on the uranium-rich calcite surface decreased the flux of uranium from the column. Subsequent release of uranium is limited by the rate of dissolution for autunite-group minerals. Because autunite sequesters uranium in the oxidized form, U(VI), rather than forcing reduction to U(IV), the possibility of re-oxidation and subsequent re-mobilization of uranium is negated.

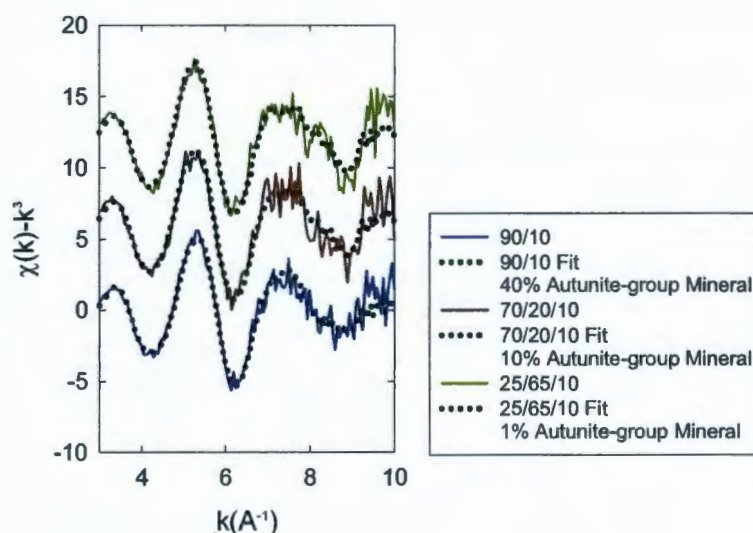


**Figure 4.29.** EXAFS of Uranium-Rich Calcite Reacted with (a) 90% Ortho-/10% Tripolyphosphate, (b) 70% Ortho-/20% Pyro-, and 10% Tripolyphosphate, and (c) 25% Ortho-/65% Pyro-, and 10% Tripolyphosphate. The dashed line is the best fit to the EXAFS spectra.

The results of unsaturated column tests conducted as a function of polyphosphate composition indicate that a formulation consisting of 90% orthophosphate and 10% tripolyphosphate will provide the most rapid and complete stabilization of uranium-solid phases through transformation to uranium-phosphate phases and mitigate the flux of uranium from the vadose zone and capillary fringe during infiltration. A polyphosphate formulation consisting of 100% orthophosphate is not permissible in Hanford groundwater because in the absence of 10% tripolyphosphate, the orthophosphate rapidly precipitates with cations present in Hanford groundwater. This results in the formulation of a slurry of phosphate phases that will rapidly occlude pore space, limiting infiltration. Moreover, attempting to prepare a polyphosphate amendment consisting of 100% orthophosphate in an aqueous media other than Hanford groundwater, such as deionized water, to reduce precipitation with cations, will not mitigate the rapid precipitation that will occur within the subsurface pore water (Wellman et al. 2006b).

### 4.3.3.3 Polyphosphate Remediation of Uranium Minerals

To evaluate the ability of the revised polyphosphate formulations consisting of 90% orthophosphate and 10% triphosphate *in situ* stabilization of uranium minerals under hydraulically unsaturated conditions, laboratory column tests were conducted at conditions expected within the 300 Area Hanford vadose zone and capillary fringe. Sediment columns were prepared with the < 2 mm of uncontaminated 300 Area sediment. The amount of uranium mineral dispersed throughout the column was equivalent to 300 ppm uranium, which is the approximate maximum concentration of uranium quantified within 300 Area sediment borehole analyses. The columns were saturated with Hanford groundwater, desaturated, and treated with Hanford groundwater spiked with the polyphosphate formulation. The principal objectives were to evaluate the ability of an orthophosphate-dominated solution to be infiltrated within an unsaturated sedimentary matrix and the efficacy of the polyphosphate for immobilization and long-term stabilization of uranium.

#### 4.3.3.3.1 Stabilization of Uranium-Rich Calcite with Polyphosphate Remediation Technology Under Unsaturated Conditions

Figure 4.30 presents effluent uranium concentration from an unsaturated column containing uranium-rich calcite that was treated with the 90% ortho- and 10% triphosphate-amended column. The dashed vertical line on the graph indicates the start of polyphosphate treatment; the solid vertical line indicates the termination of polyphosphate treatment and the flow of Hanford groundwater. Prior to the infiltration of polyphosphate the uranium concentration measured in the Hanford groundwater effluent was  $\sim 3.9 \times 10^5 \mu\text{g/L}$ . The effluent uranium concentration rapidly decreased to  $\sim 2.9 \times 10^5 \mu\text{g/L}$  upon initial infiltration of polyphosphate. The effluent uranium concentration continued to decrease during the subsequent six pore volumes of treatment. After the cessation of polyphosphate infiltration, the effluent uranium concentration remained 2 to 3 orders of magnitude lower than that quantified in the effluent prior to treatment.

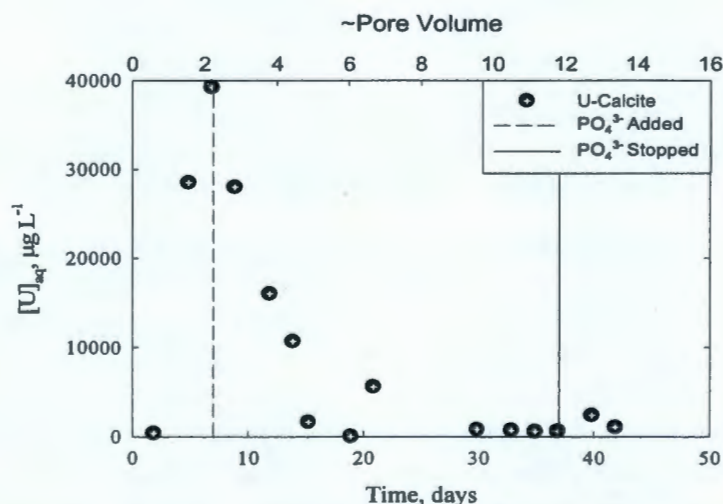


**Figure 4.30.** Concentration of Uranium,  $\mu\text{g/L}$ , in the Effluent Solutions as a Function of Time (days) and Pore Volume Released from Uranium-Calcite-Bearing Column Treated with 90% Ortho- and 10% Triphosphate. The dashed vertical line represents the initiation of flow for the phosphate-amended groundwater; the solid line represents the point at which polyphosphate infiltration was terminated and flow of groundwater was reinitiated.

#### 4.3.3.3.2 Stabilization of Uranophane with Polyphosphate Remediation Technology Under Unsaturated Conditions

Figure 4.31 presents the effluent uranium concentration from an unsaturated column containing uranophane that was treated with the 90% ortho- and 10% tripolyphosphate-amended column. The dashed vertical line on the graph indicates the start of polyphosphate treatment; the solid vertical line indicates the termination of polyphosphate treatment and the flow of Hanford groundwater. Prior to the infiltration of polyphosphate the uranium concentration measured in the Hanford groundwater effluent was  $\sim 2.5 \times 10^5 \mu\text{g/L}$ . Relative to the uranium-rich calcite column, the lower effluent concentration of uranium measured in the uranophane effluent reflects the higher stability of the uranyl-silicate mineral. As observed for polyphosphate remediation of uranium-rich calcite, the effluent uranium concentration rapidly decreased to  $\sim 4.8 \times 10^3 \mu\text{g/L}$  upon initial infiltration of polyphosphate. Following the cessation of polyphosphate infiltration the effluent uranium concentration remained 3 orders of magnitude lower than that quantified in the effluent prior to treatment.

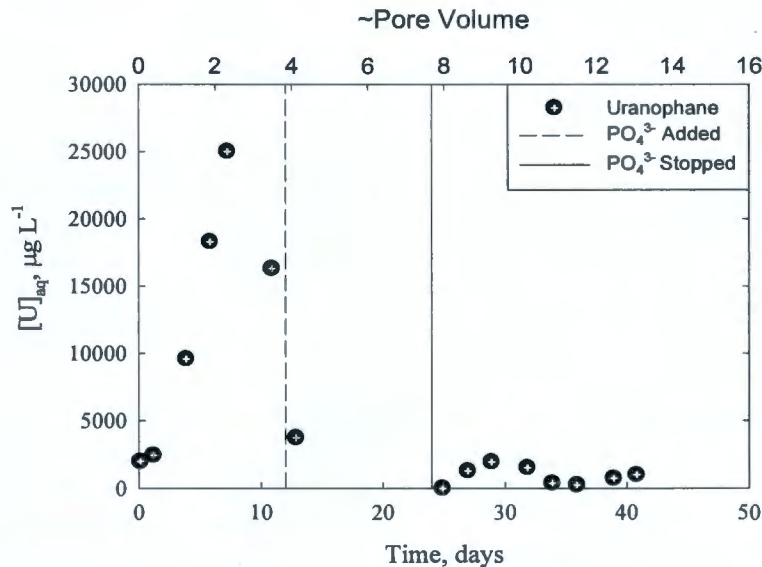


**Figure 4.31.** Concentration of Uranium,  $\mu\text{g/L}$ , in the Effluent Solutions as a Function of Time (days) and Pore Volume Released from the Uranophane-Bearing Column Treated with 90% Ortho- and 10% Tripolyphosphate. The dashed vertical line represents the initiation of flow for the phosphate-amended groundwater; the solid line represents the point at which polyphosphate infiltration was terminated and flow of groundwater was reinitiated.

#### 4.3.3.3.3 Stabilization of Meta-Torbernite with Polyphosphate Remediation Technology Under Unsaturated Conditions

Figure 4.32 presents effluent uranium concentration from an unsaturated column containing meta-torbernite that was treated with the 90% ortho- and 10% tripolyphosphate-amended column. The dashed vertical line on the graph indicates the start of polyphosphate treatment; the solid vertical line indicates the termination of polyphosphate treatment and the flow of Hanford groundwater. Prior to the infiltration of polyphosphate the uranium concentration measured in the Hanford groundwater effluent was  $\sim 4.5 \times 10^4 \mu\text{g/L}$ . Relative to the uranium-rich calcite or uranophane columns, the lower effluent concentration of uranium measured here, from meta-torbernite, reflects the high stability of the uranyl-

phosphate mineral. Upon infiltration of polyphosphate the effluent uranium concentration rapidly decreased within two pore volumes. Following the cessation of polyphosphate infiltration the effluent uranium concentration remained 2 orders of magnitude lower than that quantified in the effluent prior to treatment.

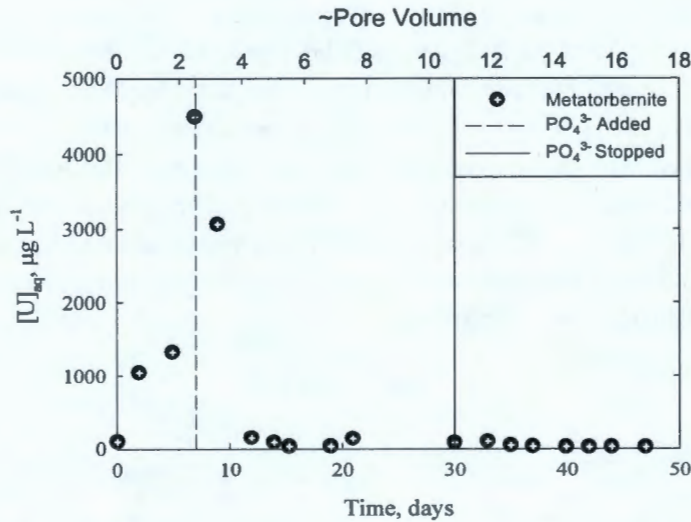


**Figure 4.32.** Concentration of Uranium,  $\mu\text{g/L}$ , in the Effluent Solutions as a Function of Time (days) and Pore Volume Released from the Meta-Torbernite-Bearing Column Treated with 90% Oortho- and 10% Tripolyphosphate. The dashed vertical line represents the initiation of flow for the phosphate-amended groundwater; the solid line represents the point at which polyphosphate infiltration was terminated and flow of groundwater was reinitiated.

#### 4.4 Hydraulic Properties of Sediment Mixtures

Saturated hydraulic conductivity and water retention parameters of three sediment mixtures were obtained in the Subsurface Flow and Transport Laboratory in the EMSL. The percentages of the coarse gravel, gravel, sand, and fines in these mixtures are shown in Table 4.6. Mixtures A, B, and C represent the average, a lower bound, and an upper bound of the sediment particle size distribution.

**Table 4.6.** Percentages of Coarse Gravel, Gravel, Sand, and Fines in Sediment Mixtures A, B, and C

Mixture	Coarse Gravel (4.75 – 12.7 mm)	Gravel (2 – 4.75 mm)	Total Gravel (2 – 12.7 mm)	Sand (0.053 – 2 mm)	Fines ( < 0.053 mm)
A	41	40	81	15	4
B	30	30	60	28	12
C	47	47	94	5.25	0.75

The saturated hydraulic conductivity is the proportionality constant in the Darcy equation that relates the flux density to a unit potential gradient. This property is measured using the constant head method (Klute and Dirksen 1986) with the fully automated IHCA (Integrated Hydraulic Conductivity Apparatus; Wietsma et al. 2008). For this method, a column with a diameter of 8.89 cm and a volume of 946 cm<sup>3</sup> was filled with 1750 g of one of the mixtures, yielding a dry bulk density of 1.85 g/cm<sup>3</sup> and a porosity of 0.302 for each packing. Three packings were analyzed using various constant head values. The average measured values for each packing and the average value for the three packings are listed in Table 4.7.

**Table 4.7.** Saturated Hydraulic Conductivity (cm/min) of the Three Sediment Mixtures

Mixture	Packing 1	Packing 2	Packing 3	Average
A	30.2	31.4	29.9	30.5
B	7.3	7.9	9.4	8.2
C	55.3	53.3	48.6	52.4

Water retention refers to the retention of water by the sediment at various capillary pressures. Mathematical functions are fit to the retention data and the resulting parameters are used directly in computer models for predicting water and contaminant movement. Several functions are available, but the van Genuchten function (Van Genuchten 1980) is most commonly used:

$$\theta = \theta_r + (\theta_s - \theta_r) \left[ 1 + (\alpha h)^n \right]^{-m} \quad (4.5)$$

where  $\theta_s$  = saturated water content (cm<sup>3</sup>/cm<sup>3</sup>)

$\theta_r$  = residual water content (cm<sup>3</sup>/cm<sup>3</sup>)

$h$  = capillary pressure (cm)

$\alpha, n, m$  = empirical fitting parameters ( $\alpha$  units are 1/cm;  $n$  and  $m$  are dimensionless).

Typically,  $m$  is approximated as  $m = 1 - 1/n$ .

Packing 3, used for the saturated hydraulic conductivity tests, was used to determine the water retention parameters with the multistep method (Eching and Hopmans 1993). The retention parameters listed in Table 4.8 were obtained by analysis of the capillary pressure and cumulative outflow as a function of time using the SFOPT program (Tuli et al. 2001).

**Table 4.8.** Parameters and Statistics for the van Genuchten Function Fitted to Data from the Multistep Method Using SFOPT (Tuli et al. 2001)

Mixture	$\alpha$ (1/cm)	$n$	$\theta_r$	$r^2$
A	0.82	2.68	0.024	0.982
B	0.13	2.53	0.041	0.978
C	1.52	2.44	0.012	0.968

## 4.5 Simulations of Intermediate-Scale Infiltration Experiments

Simulations of drip infiltration into an intermediate-scale facility box model were conducted with the STOMP simulator (White and Oostrom 2006). STOMP is a numerical model that simulates heat and mass transfer through multiple fluid phases in porous media systems. STOMP has been used to support several performance and risk assessments across the Hanford Site (Freedman et al. 2005; Zhang et al. 2004; Zhang et al. 2003), and meets NQA-1-2000 software requirements as well as those specified under DOE Order 414.1C for Safety Software.

For these simulations, the STOMP-W operational mode was used with courant-limited TVD solute transport. STOMP-W (Water mode) solves a single governing equation for the mass balance of liquid water under isothermal conditions and separate mass balance equations for advection and diffusion/dispersion of aqueous-phase solutes. The box was assumed to be 102 cm wide, 80 cm high, and 5.5 cm deep, and fully packed with Hanford sediment. Hydraulic properties used for the sediment in the simulations are listed in Table 4.9.

**Table 4.9.** Hydraulic and Solute Transport Properties Used for Hanford Sediment in Intermediate-Scale Simulations

Parameter	Value
Porosity, $\phi$ , %	30.2
Bulk density, $\rho_b$	1.85
Hydraulic conductivity, cm/min	30.5
van Genuchten $\alpha$ , 1/cm	0.82
van Genuchten $n$	2.68
Irreducible water saturation, $s_r$	0.08
Solute diffusion coefficient, $\text{cm}^2/\text{s}$	$1 \times 10^{-9}$
Longitudinal dispersion coefficient, cm	0.1

Initial conditions in the box assume a temperature of 20°C, atmospheric pressure of 101325 Pa, a hydraulic head of 20 cm, and a tracer concentration of 0 throughout. This results in the sediment being saturated with water below a height of 20 cm in the box, and close to the irreducible water saturation at heights above 24 cm (Figure 4.33).

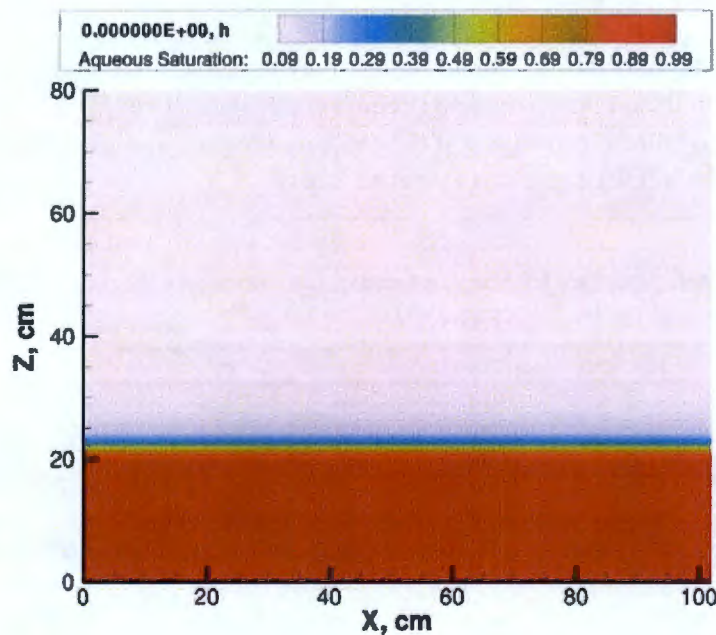


**Figure 4.33.** Initial Water Saturation for Simulations of Box Infiltration Experiment

To simulate the flow of groundwater below the water table, a constant flow rate of 1 L/hr was applied to the left boundary of the model, from 0 to 20 cm in height. Horizontal flow was allowed to equilibrate for 24 hours. Given a cross-sectional area of 20 cm x 5.5 cm, and a porosity of 0.302, this flow rate results in a horizontal average linear velocity of 30.1 cm/hr in the saturated zone of the model.

To simulate drip infiltration at the surface, a source of 1 L/hr, with a tracer concentration of 1 mol/L was applied as a point source at the top of the model, at a horizontal distance of 34 cm and a vertical height of 80 cm. The drip source commenced 24 hours after the start of the flow simulation, and lasted for 24 hours. At a simulation time of 48 hours, the vadose zone beneath the drip source is 30 to 40%

saturated in a 20-cm-wide zone (Figure 4.34). The vertical average linear velocity 20 cm beneath the point source is 136.6 cm/hr, resulting in a travel time of 0.45 hours vertically through the 60-cm-deep vadose zone. Tracer concentrations at 1 hour (Figure 4.35) and 24 hour (Figure 4.36) after the start of drip irrigation indicate a rapid rate of transport.

Estimated field-scale  $K_d s$  for tripoly-, pyro- and orthophosphate range from 0.001 to 0.037 mL g<sup>-1</sup> (Table 4.10). This results in retardation factors,

$$R = 1 + \frac{\rho_b}{s\phi} \quad (4.6)$$

where  $s$  is the water relative saturation, that range from 1.02 to 1.56, with slightly reduced travel times ranging from 0.45 to 0.69 hr.

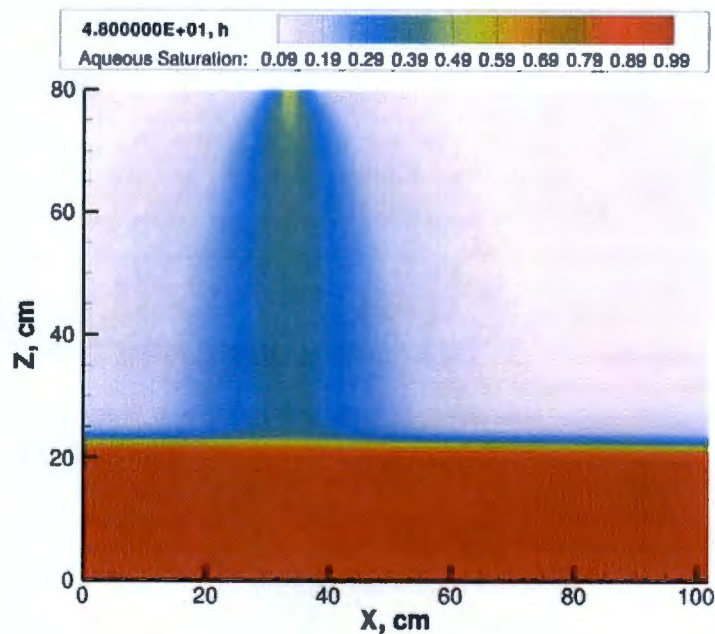


**Figure 4.34.** Simulated Water Saturations After 1 Day of 1-L/hr Drip Infiltration Applied at  $x = 34$  cm,  $z = 80$  cm

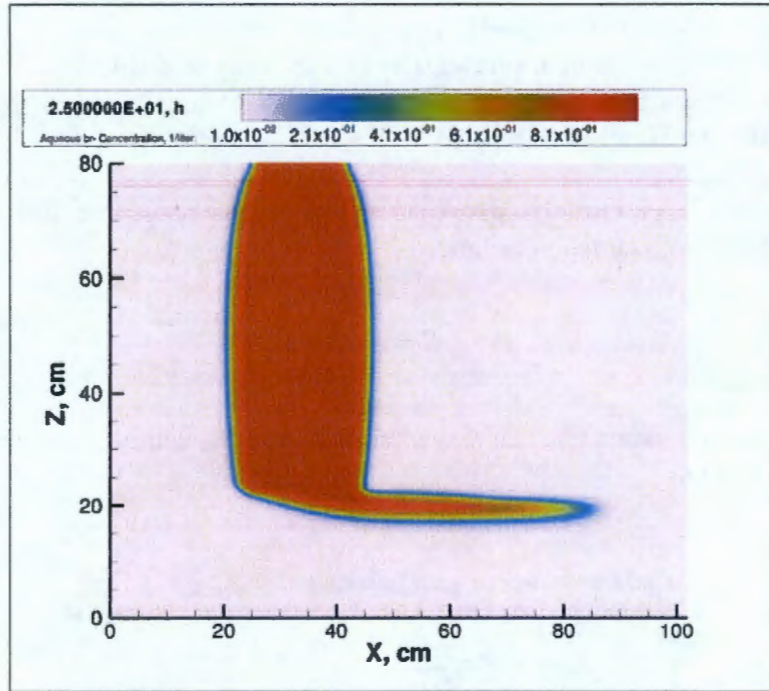


**Figure 4.35.** Simulated Tracer Aqueous Concentrations After 1 Hour of 1-L/hr Drip Infiltration Applied at  $x = 34$  cm,  $z = 80$  cm

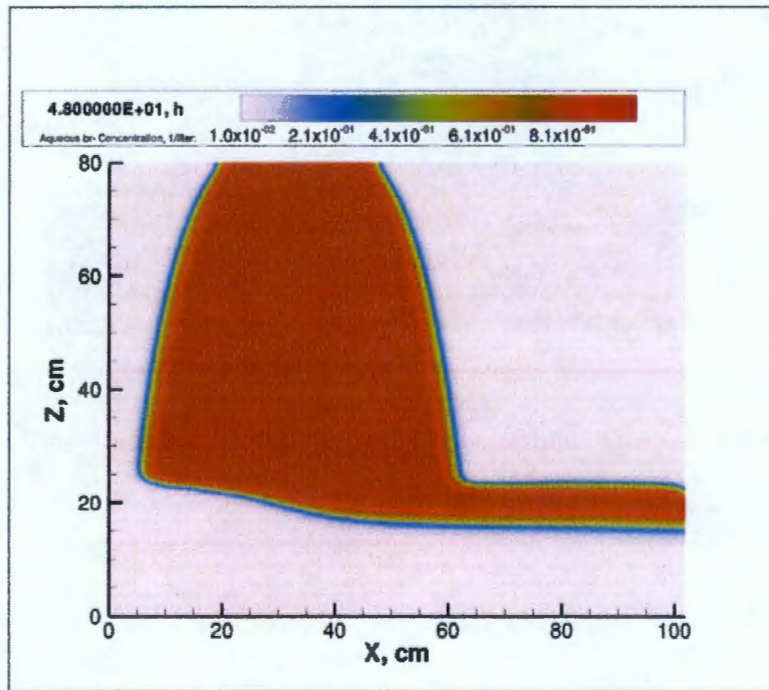


**Figure 4.36.** Simulated Tracer Aqueous Concentrations After 1 Day of 1-L/hr Drip Infiltration Applied at  $x = 34$  cm,  $z = 80$  cm

**Table 4.10.** Vertical Velocities and Saturations 20 cm Below Drip Source (model location:  $x = 34$ ,  $z = 60$ )

Source Rate, L/hr	Vertical Specific Discharge, cm/hr	Aqueous Saturation	Vertical Average Linear Velocity, cm/hr	Retardation Coefficient, $K_d = 0.001$	Retardation Coefficient, $K_d = 0.037$	Tracer Travel Time, hr	$K_d = 0.001$ , Travel Time, hr	$K_d = 0.037$ , Travel Time, hr
1	16.62	0.40	136.6	1.02	1.56	0.44	0.45	0.69
0.5	7.97	0.35	76.3	1.02	1.66	0.79	0.80	1.30
0.1	1.43	0.25	19.1	1.02	1.91	3.14	3.22	6.01
0.05	0.68	0.22	10.4	1.03	2.04	5.79	5.95	11.82

Additional simulations were conducted at lower infiltration rates over the concern that uranium may be flushed out of the vadose zone and capillary fringe at these velocities too quickly, before reacting with phosphate to form insoluble precipitates. Flow and transport parameters resulting from several drip infiltration rates are shown in Table 4.10. For a reduced application rate of 0.05 L/hr, the saturation beneath the drip source is greatly reduced (Figure 4.37) the vertical average linear velocity 20 cm beneath the point source is 10.4 cm/hr, resulting in a travel time of 5.79 hours vertically through the 60-cm-deep vadose zone. Assuming a  $K_d$  of 0.0037 for phosphate, concentrations at 1 hour (Figure 4.38) and 24 hours (Figure 4.39) after the start of drip irrigation indicate that a low water application rate will increase contact time of dissolved phosphate with U-bearing minerals in the sediment, and minimize flushing.

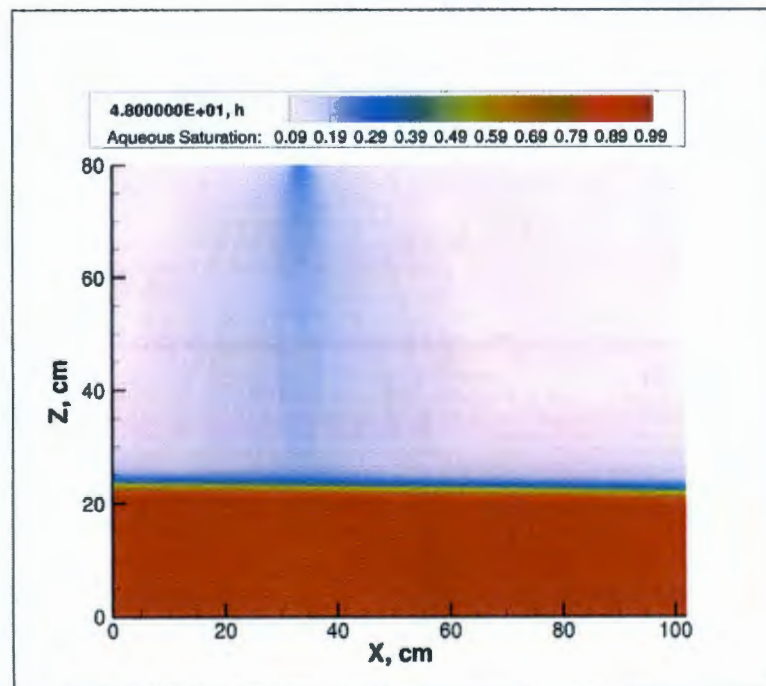


**Figure 4.37.** Simulated Water Saturations After 1 Day of 0.05-L/hr Drip Infiltration Applied at  $x = 34$  cm,  $z = 80$  cm

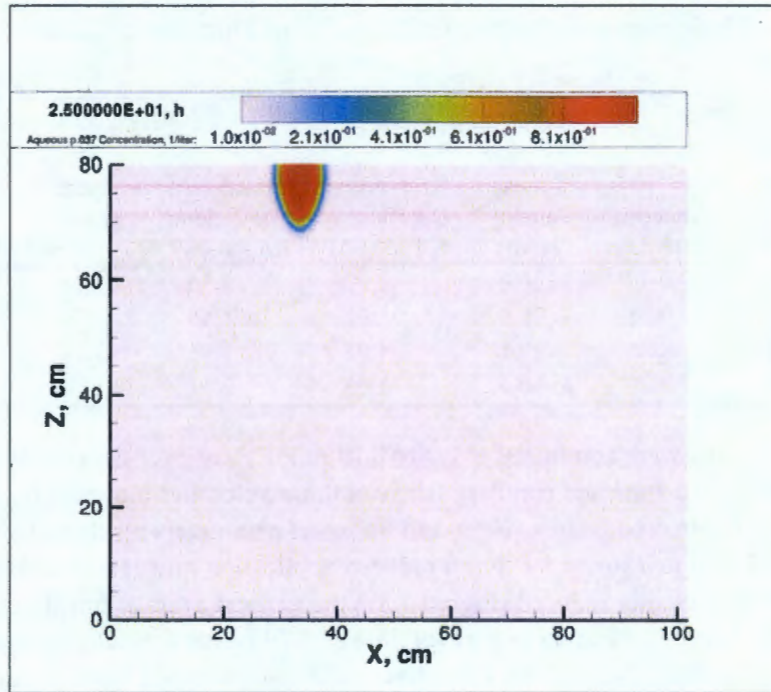


**Figure 4.38.** Simulated  $K_d = 0.037$  Phosphate Aqueous Concentrations After 1 Hour of 0.05-L/hr Drip Infiltration

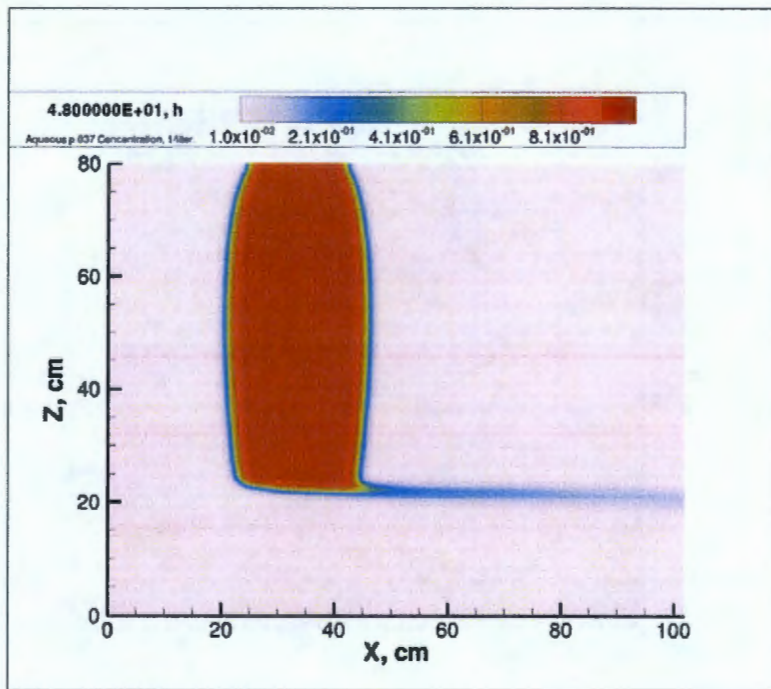


**Figure 4.39.** Simulated  $K_d = 0.037$  Phosphate Aqueous Concentrations After 1 Day of 0.05-L/hr Drip Infiltration

## 5.0 Conclusions

This report presents a large body of data from bench- and intermediate-scale treatability studies conducted under site-specific conditions to optimize polyphosphate remediation technology amendment for implementation of a field-scale technology demonstration to stabilize uranium solid phases within the 300 Area vadose zone and capillary fringe on the Hanford Site. As shown here, it is necessary to understand the geochemistry that controls uranium within this environment and evaluate the resulting effect of polyphosphate amendments on the uranium geochemistry. The general treatability testing approach consisted of conducting studies with site sediment to develop an effective chemical formulation for the polyphosphate amendments and evaluate the transport properties of these amendments under site conditions. The output from this experimental investigation is a data package that includes 1) quantification of the retardation of ortho-, pyro-, and tripolyphosphate as a function of water content, 2) quantification of the dissolution kinetics of relevant uranium solid phases including uranium-rich calcite, uranophane, and meta-torbernite, 3) development of an understanding of the mechanism of autunite formation via the reaction of solid-phase calcite-bound uranium and aqueous polyphosphate remediation technology, 4) development of an understanding of the transformation mechanism, identity of secondary phases, and the kinetics of the reaction between uranyl-carbonate and -silicate minerals with the polyphosphate remedy, 5) quantification of the extent and rate of uranium released and immobilized, based on the infiltration rate of the polyphosphate remedy and the effect of periodic wet-dry cycling on the efficacy of polyphosphate remediation for uranium in the vadose zone and capillary fringe, and 6) evaluation of stability of polyphosphate remediated uranium phases.

The results of laboratory-scale testing were used to determine a polyphosphate formulation for remediation of the vadose zone and capillary fringe via infiltration. The results suggest the following with regard to remediation of soluble uranium phases via polyphosphate infiltration:

- The apparent sorption,  $K_{d-ap}$ , for pyro-, tripol-, and the polyphosphate formulation were comparable between the compounds,  $K_{d-ap}$  0.48 – 0.51. The  $K_{d-ap}$  for ortho- was 57% less than higher-chain polyphosphate species,  $K_{d-ap} = 0.29$ .
- Exclusion from a fraction of the pore space is more important than velocity in determining the sorption of ortho- and the polyphosphate formulation during transport.
- Chemical reaction nonequilibrium may influence the migration of pyro- and tripolyphosphate compounds.
- Concentration of uranium potentially released during the infiltration of polyphosphate remedial solution is lower than that released through the dissolution of uranium-rich calcite, uranophane, or meta-torbernite in natural pore waters.
- Controlled infiltration of polyphosphate will does not increase aqueous uranium concentrations.
- Orthophosphate affords the greatest control over the aqueous concentration of uranium under the pH range of 6 to 8, maintaining aqueous uranium concentrations less than 30  $\mu\text{g/L}$  at a  $\text{g } [\text{PO}_4^{3-}]_{\text{aq}}/\text{g}$  uranium-calcite ratio of  $\leq 0.05$ . Pyrophosphate and tripolyphosphate required  $\text{g } [\text{PO}_4^{3-}]_{\text{aq}}/\text{g}$  uranium-calcite ratios of  $\sim 0.15$  to maintain aqueous uranium concentrations  $< 30 \mu\text{g/L}$ . Results presented here suggest the most rapid, complete stabilization of uranium-rich calcite would be observed through treatment with 100% orthophosphate

- A polyphosphate formulation consisting of 90% orthophosphate ( $4.74 \times 10^{-2}$  M) and 10% tripolyphosphate ( $1.75 \times 10^{-3}$  M) will provide the rapid stabilization of uranium-solid phases through transformation to uranium-phosphate phases, and mitigate the flux of uranium from the vadose zone and capillary fringe during infiltration.
- Stabilization of soluble uranium-bearing minerals occurs by the formation of a uranium-phosphate “rind” on the surface of uranium-rich calcite and uranyl-silicate minerals.

The geochemical and thermodynamic data obtained from this investigation were used to update the database for EQ3/6, version 8.0, to allow reactive transport simulation of polyphosphate infiltration at the intermediate- and field-scale using STOMP. The results of reactive transport simulations suggest that drip infiltration at an application rate of 0.05 L/hr over a scale 102 cm wide x 80 cm high x 5.5 cm deep controls the saturation beneath a drip infiltration source; the vertical average linear velocity 20 cm beneath the point source is 10.4 cm/hr. This results in a travel time of 5.79 hours vertically through the 60-cm-deep vadose zone. Assuming a  $K_d$  of 0.0037 for phosphate simulations indicates that a low water application rate will increase contact time of dissolved phosphate with U-bearing minerals in the sediment and minimize flushing. The presence of heterogeneities and the uncertainty regarding the true reactive surface area of the fine-grained materials at the field scale may have a significant effect on the efficacy and emplacement of the remedial action. Currently, additional intermediate-scale tests are being conducted to evaluate the effect of heterogeneities on the remediation of uranium minerals under conditions relevant to the vadose zone and capillary fringe. These results will be used to test and verify a site-specific, variable-saturation, reactive-transport model and to aid in the design of a pilot-scale field test of this technology. In particular, the infiltration approach and monitoring strategy of the pilot test will be based primarily on results from intermediate-scale testing.

The results of this investigation provide the necessary information for designing a field-scale remediation test to stabilize soluble uranium phases in the 300 Area vadose zone and capillary fringe on the Hanford Site, which serve as a continual source of uranium to the aquifer. Data obtained from this study will be used to develop implementation cost estimates, identify implementation challenges, and investigate the capability of the technology to meet remedial objectives. This information will be used to establish the viability of the method and determine how best to implement the technology in the field.

## 6.0 References

- Abdelouas A, W Lutze, and HE Nuttall. 1999. "Uranium Contamination in the Subsurface: Characterization and Remediation." In: *Uranium: Mineralogy, Geochemistry and the Environment*. PC Burns and RJ Finch, Eds., Mineralogical Society of America, Washington, D.C. 38:679.
- Akinremi OO and CM Cho. 1991. "Phosphate Transport in Calcium-Saturated Systems: II. Experimental Results in a Model System." *Soil Science Society of America Journal* 55:1282-1287.
- Alwan AK and PA Williams. 1980. "The Aqueous Chemistry of Uranium Minerals. Part 2. Minerals of the Liebigite Group." *Mineralogical Magazine* 43:665-667.
- Arai Y, MA Marcus, N Tamura, JA Davis, and JM Zachara. 2007. "Spectroscopic Evidence for Uranium Bearing Precipitates in Vadose Zone Sediments at the Hanford 300-Area Site." *Environmental Science and Technology* 41:4633-4639.
- Arambarri P and O Talibudeen. 1959. "Factors Influencing the Isotopically Exchangeable Phosphate in Soils." *Plant and Soil* 11(4):364-376.
- Arey JS, JC Seaman, and PM Bertsch. 1999. "Immobilization of Uranium in Contaminated Sediments by Hydroxyapatite Addition." *Environmental Science and Technology* 33:337-342.
- Arias CA, M Del Bubba, and H Brix. 2001. "Phosphorus Removal by Sands for Use as Media in Subsurface Flow Constructed Reed Beds." *Water Research* 35(5):1159-1168.
- Arvieu J and O Bouvier. 1974. "Chemical Processes in the Evolution of Phosphates in Calcareous Soils." *Science du Sol* 74:207-224.
- ASTM. 2001. *Standard Test Method for Distribution Ratios by the Short-Term Batch Method*. D 4319-93, American Society of Testing Materials International, West Conshohocken, Pennsylvania.
- Avnimelech Y. 1980. "Calcium-Carbonate-Phosphate Surface Complex in Calcareous Systems." *Nature* 288(5788):255-257.
- Baes CF Jr and JM Schreyer. 1953a. *The Chemistry of Uranium (VI) Orthophosphate Solutions: Part II, the Solubility of Uranium (VI) Orthophosphates in Phosphoric Acid Solutions*. ORNL-1578, Oak Ridge National Laboratory, Oak Ridge, Tennessee.
- Baes CF, and JM Schreyer. 1953b. *The Chemistry of Uranium (VI) Orthophosphate Solutions: Part III, the Solubility Behavior of  $UO_2HPO_4 \cdot 4H_2O$  in Perchloric Acid Solutions*. ORNL-1579, Oak Ridge National Laboratory, Oak Ridge, Tennessee.
- Baes CF, JM Schreyer, and JM Lesser. 1953. *The Chemistry of Uranium (VI) Orthophosphate Solutions: Part I, the Solubility of Uranium (VI) Orthophosphates in Acid Solutions*. ORNL-Y-12/ORNL-1577, Oak Ridge National Laboratory, Oak Ridge, Tennessee.

- Bargar JR, GEB Jr., I Evans, T Rabedeau, M Rowen, and J Rogers. 2002. "A New Hard X-Ray XAFS Spectroscopy Facility for Environmental Samples, Including Actinides, at the Stanford Synchrotron Radiation Laboratory." In Proceedings of the Euroconference and NEA Workshop on Speciation, Techniques and Facilities for Radioactive Materials at Synchrotron Light Sources. *NEA/OECD Paris*:57-68.
- Barrow NJ. 1984. "Modeling the Effects of pH on Phosphate Sorption by Soils." *Journal of Soil Science* 35:283-297.
- Bernhard G, G Geipel, T Riech, V Brendler, S Amayri, and H Nitsche. 2001. "Uranyl(VI) Carbonate Complex Formation: Validation of the  $\text{Ca}_2\text{UO}_2(\text{CO}_3)_3$  (Aq) Species." *Radiochimica Acta* 89:511-518.
- Bertrand I, RE Holloway, RD Armstrong, and MJ McLaughlin. 2003. "Chemical Characteristics of Phosphorus in Alkaline Soils from Southern Australia." *Australian Journal of Soil Research* 41:61-76.
- Bertsch PM, D Hunter, B., SR Sutton, S Bajt, and ML Rivers. 1994. "In Situ Chemical Speciation of Uranium in Soils and Sediments by Micro X-Ray Absorption Spectroscopy." *Environmental Science and Technology* 28:980-984.
- Blanchar RW and LR Hossner. 1969a. "Hydrolysis and Sorption of Ortho-, Pyro-, Tripoly-, and Trimetaphosphate in 32 Midwestern Soils." *Soil Science Society American Proceedings* 33:622-625.
- Blanchar RW and LR Hossner. 1969b. "Hydrolysis and Sorption Reactions of Orthophosphate, Pyrophosphate, Tripolyphosphate, and Trimetaphosphate Anion Added to an Elliot Soil." *Soil Science Society of America Proceedings* 33:141-144.
- Blanchar RW and LR Hossner. 1969c. "Hydrolysis and Sorption Reactions of Orthophosphate, Pyrophosphate, Tripolyphosphate, and Trimetaphosphate Anions Added to an Elliot Soil." In: *Soil Science Society of America Proceedings*.
- Bolan NS, NJ Barrow, and AM Posner. 1985. "Describing the Effect of Time on Sorption of Phosphate by Iron and Aluminum Hydroxides." *Journal of Soil Science* 36:187-197.
- Brooks SC, JK Fredrickson, SL Carroll, DW Kennedy, JM Zachara, JM Plymale, AE Kelly, KM Kemner, and S Fendorf. 2003. "Inhibition of Bacterial U(VI) Reduction by Calcium." *Environmental Science & Technology* 37:1850-1858.
- Brown CF, RJ Serne, KM Krupka, EM Pierce, and MJ Lindberg. 2005. "Uranium Contamination at the 300 Area of the Hanford Site." In: *Third International Conference on Remediation of Contaminated Sediments*, Battelle Press, Columbus, Ohio.
- Brown GE, G Calas, GA Waychunas, and J Petiau. 1988. "X-Ray Absorption Spectroscopy and Its Applications in Mineralogy and Geochemistry." In: *Spectroscopic Methods in Mineralogy and Geology*. FC Hawthorne, Ed., Mineralogy Society of America, Washington, D.C. 18:431-512.
- Brunauer S, PH Emmett, and E Teller. 1938. "Adsorption of Gases in Multimolecular Layers." *Journal of the American Chemical Society* 60:300-319.

- Bruno B, S Carroll, A Sandino, L Charlet, R Karthem, and P Wersin. 1989. "Adsorption, Precipitation and Co-precipitation of Trace Metals on Carbonate Minerals at Low Temperatures." In: *Water-Rock Interaction WRI/6 Proceedings of the 6th International Symposium*, Malvern, U.K. Publisher?
- Buck EC, NR Brown, and NL Dietz. 1996. "Contaminant Uranium Phases and Leaching at the Fernald Site in Ohio." *Environmental Science and Technology* 30:81-88.
- Buck EC, NL Dietz, JK Bates, and JC Cunnane. 1994. *Uranium-Contaminated Soils: Ultramicrotomy and Electron Beam Analysis*. ANL/CMT/PP-82412, Argonne National Laboratory, Argonne, Illinois.
- Buck EC, NL Dietz, JA Fortner, JK Bates, and NR Brown. 1995. *Characterization of Uranium- and Plutonium-Contaminated Soils by Electron Microscopy*. ANL/CMT/CP-85758; CONF-950216-65, Argonne National Laboratory, Argonne, Illinois.
- Burns PC. 1999. "The Crystal Chemistry of Uranium." In: *Uranium: Mineralogy, Geochemistry and the Environment*. PC Burns and RJ Finch, Eds., Mineralogical Society of America, Washington, D.C. 38:23-90.
- Carroll SA, J Bruno, JC Petit, and JC Dran. 1992. "Interactions of U(VI), Nd, and Th(IV) at the Calcite-Solution Interface." *Radiochimica Acta* 58/59:245-252.
- Casas I, J Bruno, E Cera, R Finch, and R Ewing. 1997a. "Characterization and Dissolution Behavior of a Becquerelite from Shinkolobwe, Zaire." *Geochemica et Cosmochimica Acta* 61(18):3879-3884.
- Casas I, J Bruno, E Cera, RJ Finch, and RC Ewing. 1994. *Kinetic and Thermodynamic Studies of Uranium Minerals. Assessment of the Long-Term Evolution of Spent Nuclear Fuel*. SKB 94-16.
- Casas I, J De Pablo, J Gimenez, ME Torrero, J Bruno, E Cera, RJ Finch, and RC Ewing. 1998. "The Role of pE, pH, and Carbonate on the Solubility of UO<sub>2</sub> and Uraninite under Nominally Reducing Conditions." *Geochimica et Cosmochimica Acta* 62(13):2223-2231.
- Casas I, I Perez, E Torrero, J Bruno, E Cera, and L Duro. 1997b. *Dissolution Studies of Synthetic Soddyite and Uranophane*. SKB-97-15, Publisher and location?
- Castro B and J Torrent. 1995. "Phosphate Availability in Calcareous Vertisols and Inceptisols in Relation to Fertilizer Type and Soil Properties." *Fertilizer Research* 40:109-119.
- Catalano J, JP Mckinley, JM Zachara, SM Heald, SC Smith, and GE Brown. 2006a. "Changes in Uranium Speciation through a Depth Sequence of Contaminated Hanford Sediments." *Environmental Science and Technology* 40(8):2517-2524.
- Catalano JG, SC Heald, JM Zachara, and GE Jr. Brown. 2004. "Spectroscopic and Diffraction Study of Uranium Speciation in Contaminated Vadose Zone Sediments from the Hanford Site, Washington State." *Environmental Science and Technology* 38:2822-2828.
- Catalano JG, and GEB Jr. 2004. "Analysis of Uranyl-Bearing Phases by EXAFS Spectroscopy: Interferences, Multiple Scattering, Accuracy of Structural Parameters, and Spectral Differences." *American Mineralogist* 89:1004-1021.

- Catalano JG, JP McKinley, JM Zachara, SC Heald, SC Smith, and GE Jr. Brown. 2006b. "Changes in Uranium Speciation through a Depth Sequence of Contaminated Hanford Sediments." *Environmental Science and Technology* 40(8):2517-2524.
- Chen F, RC Ewing, and SB Clark. 1999. "The Gibbs Free Energies and Enthalpies of Formation of U<sup>6+</sup> Phases: An Empirical Method of Prediction." *American Mineralogist* 84:650-664.
- Cho CM. 1991. "Phosphate Transport in Calcium-Saturated Systems: I. Theory." *Soil Science Society of America Journal* 55:1275-1281.
- Chukhlantsev VG and SI Stepanov. 1956. "Solubility of Uranyl and Thorium Phosphates." *Russian Journal of Inorganic Chemistry* 1(3):478-484.
- Clark JS and M Peech. 1955. "Solubility Criteria for the Existence of Calcium and Aluminum Phosphates in Soils." *Soil Science Society of America Proceedings* 19(1):171-174.
- Cole CV and SR Olsen. 1959. "Phosphorus Solubility in Calcareous Soils: I. Dicalcium Phosphate Activities in Equilibrium Solutions." *Soil Science Society of America Proceedings* 23:116-118.
- Cole CV, SR Olsen, and CO Scott. 1953. "The Nature of Phosphate Sorption by Calcium Carbonate." *Soil Science Society Proceedings*. 352-356.
- Conca JL. 1996. *Phosphate-Induced Metal Stabilization*. StARS Program, National Center for Environmental Research, Office of Research and Development, U.S. Environmental Protection Agency, Washington, D.C.
- Daly K, D Jeffrey, and H Tunney. 2001. "The Effect of Soil Type on Phosphorus Sorption Capacity and Desorption Dynamics in Irish Grassland Soils." *Soil Use and Management* 17:12-20.
- Davis JA, CC Fuller, and AD Cook. 1987. "A Model for Trace Metal Sorption Processes at the Calcite Surface: Adsorption of Cd<sup>2+</sup> and Subsequent Solid Solution Formation." *Geochim. Cosmochim. Acta* 51:1477.
- de Pablo J, I Casas, J Gimenez, M Molera, M Rovira, L Duro, and J Bruno. 1999. "The Oxidative Dissolution Mechanism of Uranium Dioxide. I. The Effect of Temperature in Hydrogen Carbonate Medium." *Geochimica et Cosmochimica Acta* 63(19/20):3097-3103.
- DeFord DH, RW Carpenter, and MW Finan. 1994. *300-FF-2 Operable Unit Technical Baseline Report*. BHI-00012, Rev. 00, Bechtel Hanford, Inc., Richland, Washington.
- Del Bubba M, CA Arias, and H Brix. 2003. "Phosphorus Adsorption Maximum of Sands for Use as Media in Subsurface Flow Constructed Reed Beds as Measured by the Langmuir Isotherm." *Water Research* 37:3390-3400.
- Delaney JM and SR Lundeen. 1990. *The LLNL Thermochemical Database*. Lawrence Livermore National Laboratory, Livermore, California.

Delgado A, JR Ruiz, M del Carmen del Campillo, S Kassem, and L Andreu. 2000. "Calcium- and Iron-Related Phosphorus in Calcareous and Calcareous Marsh Soils: Sequential Chemical Fractionation and  $^{31}\text{P}$  Nuclear Magnetic Resonance Study." *Communications in Soil Science and Plant Analysis* 31(15-16):2483-2499.

DOE. 1995. *Remedial Investigation/Feasibility Study Report for the 300-FF-5 Operable Unit*. DOE/RL-94-85, Rev. 0, U.S. Department of Energy, Richland, Washington.

Dolgaleva IV, IG Gorichev, AD Izotov, and VM Stepanoc. 2005. "Modeling of the Effect of pH on the Calcite Dissolution Kinetics." *Theoretical Foundations of Chemical Engineering* 39(6):614-621.

Dong W, WP Ball, C Liu, Z Wang, AT Stone, J Bai, and JM Zachara. 2005. "Influence of Calcite and Dissolved Calcium on Uranium (VI) Sorption to a Hanford Subsurface Sediment." *Environmental Science and Technology* 39:7949-7955.

Eching SO, and JW Hopmans, 1993. Optimization of hydraulic functions from transient outflow and soil water pressure data. *Soil Sci. Soc. Am. J.* 57:1167-1175.

Elzinga EJ, CD Tait, RJ Reeder, KD Rector, RJ Donohoe, and DE Morris. 2004. "Spectroscopic Investigation of U(VI) Sorption at the Calcite-Water Interface." *Geochemica et Cosmochimica Acta* 68(11):2437-2448.

EPA. 1996. *Record of Decision for USDOE Hanford 300-FF-1 and 300-FF-5 Operable Units Remedial Actions*. Agreement between the U.S. Department of Energy and U.S. Environmental Protection Agency, with concurrence by the Washington State Department of Ecology.

Farges F, CW Ponader, G Calas, and GE Brown. 1992. "Structural Environment of Incompatible Elements in Silicates Glass/Melt Systems: II. U(IV), U(V), and U(VI)." *Geochimica et Cosmochimica Acta* 56:4205-4220.

Freedman V, Z Zhang, S Waichler, and S Wurstner. 2005. *2005 Closure Assessments for WMA-C Tank Farms: Numerical Simulations*. Pacific Northwest National Laboratory, Richland, Washington.

Finch RJ. 1997. "Thermodynamic Stabilities of U(VI) Minerals: Estimated and Observed Relationships." *Material Research Society Symposium Proceedings* 465:1185-1192.

Finch RJ, EC Buck, PA Finn, and JK Bates. 1999. "Oxidative Corrosion of Spent  $\text{UO}_2$  Fuel in Vapor and Dripping Groundwater at  $90^\circ\text{C}$ ." In: *Proceedings of 1998 Material Research Society Fall Meeting*, Material Research Society, Boston, Massachusetts.

Finch RJ and RC Ewing. 1992. "The Corrosion of Uraninite under Oxidizing Conditions." *Journal of Nuclear Materials* 190:133-156.

Finch RJ, ML Miller, and RC Ewing. 1992. "Weathering of Natural Uranyl Oxide Hydrates: Schoepite Polytypes and Dehydration Effects." *Radiochimica Acta* 58/59:433-443.

Franklin ML and JW Morse. 1982. "The Interaction of Copper with the Surface of Calcite " *Ocean Science and Engineering* 7(2).

Freese D, SEATM Van der Zee, and WH Van Riemsdijk. 1992. "Comparison of Different Models for Phosphate Sorption as a Function of the Iron and Aluminum Oxides of Soils " *Journal of Soil Science* 43:729-738.

Frondel C. 1956. "Mineral Composition of Gummite." *American Mineralogist* 41(7/8):539-568.

Gamerding AP and DI Kaplan. 2000. "Application of a Continuous-Flow Centrifugation Method for Solute Transport in Disturbed, Unsaturated Sediments and Illustration of Mobile-Immobile Water." *Water Resources Research* 36(7):1747-1755.

Gamerding AP and DI Kaplan. 2001. "Physical and Chemical Determinants of Colloid Transport and Deposition in Water-Unsaturated Sand and Yucca Mountain Tuff." *Environmental Science and Technology* 35:2497-2504.

Gamerding AP, DI Kaplan, and CT Resch. 1998. *Uranium(VI) Sorption and Transport in Unsaturated, Subsurface Hanford Site Sediments – Effect of Moisture Content and Sediment Texture: Final Report for Subtask 2b*. PNNL-11975, Pacific Northwest National Laboratory, Richland, Washington.

Gamerding AP, DI Kaplan, DM Wellman, and RJ Serne. 2001a. "Two-Region Flow and Decreased Sorption of Uranium (VI) During Transport in Hanford Groundwater and Unsaturated Sands." *Water Resources Research* 37(12):3155-3162.

Gamerding AP, DI Kaplan, DM Wellman, and RJ Serne. 2001b. "Two-Region Flow and Rate-Limited Sorption of Uranium (VI) During Transport in an Unsaturated Silt Loam." *Water Resources Research* 37(12):3147-3153.

Garrels RM and CL Christ. 1965. *Solutions, Minerals and Equilibria*. Harper and Row Publishing Company, New York.

Gauglitz R and M Holterdorf. 1992. "Immobilization of Heavy Metals by Hydroxyapatite." *Radiochimica Acta* 58(59):253-257.

Geipel G, T Reich, V Brendler, G Bernhard, and H Nitsche. 1997. "Laser and X-Ray Spectroscopic Studies of Uranium-Calcite Interface Phenomena." *Journal of Nuclear Materials* 248:408-411.

Gerber MS. 1992. *Past Practices Technical Characterization Study – 300 Area – Hanford Site*. WHC-MR-0388, Westinghouse Hanford Company, Richland, Washington.

Gerritse RG. 1993. "Prediction of Travel Times of Phosphate in Soils at a Disposal Site for Wastewater." *Water Research* 27(2):263-267.

Giammar DE. 2001. *Geochemistry of Uranium at Mineral-Water Interfaces: Rates of Sorption-Desorption and Dissolution-Precipitation Reactions*. California Institute of Technology, Pasadena, California.

Grandstaff DE. 1976. "A Kinetic Study of the Dissolution of Uraninite." *Economic Geology* 71(8):1493-1506.

Gregory TM, EC Moreno, and WE Brown. 1970. "Solubility of  $\text{CaHPO}_4 \cdot 2\text{H}_2\text{O}$  in the System  $\text{Ca}(\text{OH})_2\text{-H}_3\text{PO}_4\text{-H}_2\text{O}$  at 5, 15, 25, and 37.5°C." *Journal of Research of the National Bureau of Standards - A. Physics and Chemistry* 74A:461-475.

Grenthe I, J Fuger, RJM Konings, RJ Lemire, AB Muller, C Nguyen-Trung, and H Wanner. 1992. *Chemical Thermodynamics of Uranium*. Organization for Economic Co-operation and Development, Nuclear Energy Agency, Amsterdam, Netherlands.

Hamad ME, DL Rimmer, and JK Syers. 1992. "Effect of Iron Oxide on Phosphate Sorption by Calcite and Calcareous Soils." *Journal of Soil Science* 43:273-281.

Hashimoto I and JR Lehr. 1973. "Mobility of Polyphosphates in Soil." *Soil Science Society of America Proceedings* 37:36-41.

Hering J and JL Schnoor. 2000. "Dissolution and Transformation Rates of Uranyl Mineral Phases." In: *American Chemical Society*, Washington, D. C.

Ho GE and S Notodarmojo. 1995. "Phosphorous Movement through Soils and Groundwater: Application of a Time-Dependent Sorption Model." *Water Science and Technology* 31(9):83-90.

Hsu PH. 1964. "Adsorption of Phosphate by Aluminum and Iron in Soils." *Soil Science Society Proceedings*. 474-478.

Hsu PH. 1965. "Fixation of Phosphate by Aluminum and Iron in Acidic Soils." *Soil Science* 99(6):398-402.

Hsu PH. 1968. "Interaction between Aluminum and Phosphate in Aqueous Solution." *Trace Inorganics in Water*. 115-127.

Hsu PH and DA Rennie. 1962. "Reactions of Phosphate in Aluminum Systems: II. Precipitation of Phosphate by Exchangeable Aluminum on a Cation Exchange Resin." *Canadian Journal of Soil Science* 42(1):210-221.

Jenkins D, JF Ferguson, and AB Menar. 1971. "Chemical Processes for Phosphate Removal." *Water Research* 5:369-389.

Jensen KA and RC Ewing. 2001. "The Okelbondo Natural Fission Reactor, Southeast Gabon: Geology, Mineralogy, and Retardation of Nuclear-Reaction Products." *Geological Society of America Bulletin* 113(1):32-62.

Johnston MA, N Miles, and GR Thibaud. 1991. "Quantities of P Fertilizer Required to Raise the Soil Test Value." *South African Journal of Plant Soil* 8:17-21.

Jurinak JJ and N Bauer. 1956. "Thermodynamics of Zinc Adsorption on Calcite, Dolomite and Magnesite-Type Minerals." *Soil Sci. Soc. Proc.* 20:466.

Kalmykov SN and GR Choppin. 2000. "Mixed  $\text{Ca}^{2+}/\text{UO}_2^{2+}/\text{CO}_3^{2-}$  Complex Formation at Different Ionic Strengths." *Radiochimica Acta* 88:603-606.

- Kaplan DI and AP Gamedainger. 1999. *Colloid Transport and Deposition in Water-Saturated and Unsaturated Sand and Yucca Mountain Tuff*. TR-110546, Pacific Northwest National Laboratory, Richland, Washington.
- Kaplan DI, TL Gervais, and KM Krupka. 1998. "Uranium (VI) Sorption to Sediments under High pH and Ionic Strength Conditions." *Radiochimica Acta* 80:201-211.
- Kaplan DI, IV Kutnyakov, AP Gamedainger, RJ Serne, and KE Parker. 2000. "Gravel-Corrected  $K_d$  Values." *Ground Water* 38:851-857.
- Kaplan DI, and RJ Serne. 1995. *Distribution Coefficient Values Describing Iodine, Neptunium, Selenium, Technetium, and Uranium Sorption to Hanford Sediments*, PNL-10379, Sup. 1, Pacific Northwest Laboratory, Richland, WA.
- Karpov VI. 1961. "The Solubility of Triuranyl Phosphate." *Russian Journal of Inorganic Chemistry* 6:271-276.
- Kartseva LN. 1969. "Effectiveness of Poly-, Pyro-, and Metaphosphates on Various Soils." *Agrokhimiya* 9:13-19.
- Kelly SD, MG Newville, L Cheng, KM Kemner, SR Sutton, P Fenter, NC Sturchio, and C Spotl. 2003a. "Uranyl Incorporation in Natural Calcite." *Environmental Science and Technology* 37:1284-1287.
- Kelly SD, MG Newville, L Cheng, M Kemner, SR Sutton, P Fenter, NC Sturchio, and C Spotl. 2003b. "Uranyl Incorporation in Natural Calcite." *Environmental Science & Technology* 37:1284-1287.
- Klute A and C Dirksen, 1986. "Hydraulic conductivity and diffusivity: Laboratory methods," In Methods of Soil Analysis, Part 1, ed A. Klute, pp. 687-734. American Society of Agronomy, Madison, Wisconsin.
- Kuo S and EG Lotse. 1972. "Kinetics of Phosphate Adsorption by Calcium Carbonate and Ca-Kaolinite." *Soil Science Society of America Proceedings* 36:725-729.
- Kuo S and EG Lotse. 1974. "Kinetics of Phosphate Adsorption and Desorption by Hematite and Gibbsite." *Soil Science* 116(6):400-406.
- Langmuir D. 1978. "Uranium Solution-Mineral Equilibria at Low Temperatures with Applications to Sedimentary Ore Deposits." *Geochimica et Cosmochimica Acta* 42:547-569.
- Langmuir D. 1997. "Aqueous Geochemistry of Uranium." In: *Aqueous Environmental Chemistry*. R McConnin, Ed., pp. 494-512. Prentice-Hall, Upper Saddle River, New Jersey.
- Leclerc ML, MC Nolin, D Cluis, and RR Simard. 2001. "Grouping Soils of the Montreal Lowlands (Quebec) According to Fertility and P Sorption and Desorption Characteristics." *Canadian Journal of Soil Science* 81:71-83.
- Lee SY, CW Francis, ME Timpson, and MP Elless. 1995. *Radionuclide Containment in Soil by Phosphate Treatment*. CONF-9503120-1, Oak Ridge National Laboratory, Oak Ridge, Tennessee.

- Lewis ET and GJ Racz. 1969. "Phosphorus Movement in Some Calcareous and Noncalcareous Manitoba Soils." *Canadian Journal of Soil Science* 49:305-312.
- Lin C and A Banin. 2005. "Effect of Long-Term Effluent Recharge on Phosphate Sorption by Soils in Wastewater Reclamation Plant." *Water, Air, and Soil Pollution* 164:257-273.
- Lindenmeier CW, RJ Serne, JL Conca, A Owen, T, and MI Wood. 1995. *Solid Waste Leach Characteristics and Contaminant-Sediment Interactions Volume 2: Contaminant Transport under Unsaturated Moisture Contents*. PNL-10722, Pacific Northwest National Laboratory, Richland, Washington.
- Lindsay WL. 1979. "Phosphates." In: *Chemical Equilibria in Soils*. John Wiley and Sons, Ed., pp. 163-209. The Blackburn Press, Caldwell, New Jersey.
- Lindsay WL and EC Moreno. 1960. "Phosphate Phase Equilibria in Soils." *Soil Science Society of America Proceedings* 24:177-182.
- Liu C, JM Zachara, O Qafoku, JP McKinley, SC Heald, and Z Wang. 2004. "Dissolution of Uranyl Microprecipitates in Subsurface Sediments at Hanford Site, USA." *Geochimica Cosmochimica Acta* 68(22):4519-4537.
- Liu C, JM Zachara, W Yantasee, PD Majors, and JP McKinley. 2006. "Microscopic Reactive Diffusion of Uranium in the Contaminated Sediments at Hanford, United States." *Water Resources Research* 42(W12420):1-15.
- Lorens RB. 1981. "Sr, Cd, Mn, and Co Distribution Coefficients in Calcite as a Function of Calcite Precipitationrate." *Geochim. Cosmochim. Acta* 45:553.
- Lucci GC. 1967. "Fixation and Degradation of Sodium Tri- and Tetrametaphosphates in Clay Soils." *Agrochimica* 11:461-474.
- Lutz JF, RA Pinto, R Garcia-Lagos, and HG Hilton. 1966. "Effect of Phosphorus on Some Physical Properties of Soils: Ii. Water Retention." *Soil Science Society of America Journal* 30:433-437.
- Lytle FW, RB Greeger, DR Sandstrom, EC Marques, J Wong, CL Spiro, GP Huffman, and FE Huggins. 1984. "Measurement of Soft X-Ray Absorption Spectra with a Fluorescent Ion Chamber Detector." *Nuclear Instruments & Methods in Physics Research, Section A: Accelerators, Spectrometers, Detectors, and Associated Equipment* 226:542-548.
- MacIntire WH, LJ Hardin, and FD Oldham. 1937. "Fertilizers." *Industrial Engineering and Chemistry* 29:224-234.
- Madrid L and P de Arambarri. 1985. "Adsorption of Phosphate by Two Iron Oxides in Relation to Their Porosity." *Journal of Soil Science* 36:523-530.
- Malquori A and L Radaelli. 1967. "Reaction between Soil and Condensed Phosphates: I. Comparative Insolubility of Mono- and Polyphosphate Ions Induced by Al, Fe, and Ca Compounds." *Agrochimica* 10:354-370.

- McBride MB. 1979. "Chemisorption and Precipitation of  $Mn^{2+}$  at  $CaCO_3$  Surfaces." *Soil Science Society of America Journal* 43:693.
- McGrail BP, PFC Martin, and CW Lindenmeier. 1997a. "Accelerated Testing of Waste Forms Using a Novel Pressurized Unsaturated Flow (PUF) Method." In: *Materials Research Society Symposium Proceedings*, Publisher, Location.
- McGrail BP, PFC Martin, and CW Lindenmeier. 1999. "Method and Apparatus for Measuring Coupled Flow, Transport, and Reaction Processes under Liquid Unsaturated Flow Conditions." In: *Battelle Memorial Institute*. Complete what is was in and add Publisher, Location.
- McGrail PB, WL Ebert, AJ Bakel, and DK Peeler. 1997b. "Measurement of Kinetic Rate Law Parameters on a Na-Ca-Al Borosilicate Glass for Low-Activity Waste." *Journal of Nuclear Materials* 249:175-189.
- McGraw MA. 1996. *Effect of Colloid Size, Colloid Hydrophobicity, and Volumetric Water Content on the Transport of Colloids through Porous Media*. University of California, Berkeley, California.
- McGraw MA and DI Kaplan. 1997. *Colloid Suspension Stability and Transport through Unsaturated Porous Media*. PNNL-11565, Pacific Northwest National Laboratory, Richland, Washington.
- McKinley JP, JM Zachara, C Liu, SC Heald, BI Prenitzer, and BW Kempshall. 2006. "Microscale Controls on the Fate of Contaminant Uranium in the Vadose Zone, Hanford Site, Washington." *Geochimica Cosmochimica Acta* 70:1873-1887.
- McKinley JP, JM Zachara, J Wan, DE McCready, and SM Heald. 2007. "Geochemical Controls on Contaminant Uranium in Vadose Hanford Formation Sediments at the 200 Area and 300 Area, Hanford Site, Washington." *Vadose Zone Journal* 6(4):1004-1017.
- Meece DE and LK Benninger. 1993. "The Co-precipitation of Pu and Other Radionuclides with  $CaCO_3$ ." *Geochimica et Cosmochimica Acta* 57:1447-1458.
- Milton GM and RM Brown. 1987. "Adsorption of Uranium from Groundwater by Common Fracture Secondary Minerals." *Canadian Journal of Earth Sciences* 24:1321.
- Moore RC, C Sanchez, J Schelling, J Jones, DR Anderson, F Salas, D Lucero, and K Holt. 2001. *Bench-Scale Testing of In-Situ Formation of Apatite in Hanford Soils for Sorption of Uranium and Technetium*. SAND2001-3001, Sandia National Laboratories, Albuquerque, New Mexico.
- Morris DE, PG Allen, JM Berg, CJ Chisholm-Brause, SD Conradson, RJ Donohoe, NJ Hess, JA Musgrave, and CD Tait. 1996. "Speciation of Uranium in Fernald Soils by Molecular Spectroscopic Methods: Characterization of Untreated Soils." *Environmental Science and Technology* 30(7):2322-2331.
- Morse JW. 1983. "The Kinetics of Calcium Carbonate Dissolution and Precipitation." In: *Carbonates: Mineralogy and Chemistry*. RJ Reeder, Ed., 11:227-264. Mineralogical Society of America, Blacksburg, Virginia.

- Morse JW, PM Shanbhag, A Saito, and GR Choppin. 1984. "Interaction of Uranyl Ions in Carbonate Media." *Chemical Geology* 42:85-99.
- Moskvin AI, AM Shelyakina, and PS Perminov. 1967. "Solubility Product of Uranyl Phosphate and the Composition and Dissociation Constants of Uranyl Phosphato-Complexes." *Russian Journal of Inorganic Chemistry* 12(12):1756-1760.
- Mucci A and JW Morse. 1983. "The Incorporation of  $Mg^{2+}$  and  $Sr^{2+}$  into Calcite Overgrowths: Influences of Growth Rate and Solution Composition." *Geochim. Cosmochim. Acta* 47:217.
- Muljadi D, AM Posner, and JP Quirk. 1966. "The Mechanism of Phosphate Adsorption by Kaolinite, Gibbsite, and Pseudoboehmite." *Journal of Soil Science* 17(2):230-237.
- Murakami T, T Ohnuki, H Isobe, and T Sato. 1997. "Mobility of Uranium During Weathering." *American Mineralogist* 82:888-899.
- Nagpal NK. 1985. "Long-Term Phosphorus Sorption in a Brunisol in Response to Dosed-Effluent Loading." *Journal of Environ. Qual.* 14(2):280-285.
- Nagpal NK. 1986. "Effect of Soil and Effluent Characteristics on Phosphorus Sorption in Dosed Columns." *Journal of Environ. Qual.* 15(1):73-78.
- Nash K. 1993. "Stability and Stoichiometry of Uranyl Phosphonate Coordination Compounds in Acid Aqueous Solutions." *Radiochimica Acta* 61:147-154.
- Nash K. 1994. "Actinide Phosphonate Complexes in Aqueous Solutions." *Journal of Alloys and Compounds* 213/214:300-304.
- Nash K. 2000. *Organophosphorous Reagents in Actinide Separations: Unique Tools for Production, Cleanup and Disposal*. ANL/CHM/CP-100858, Argonne National Laboratory, Argonne, Illinois.
- Nash K, EJ Jensen, and MA Schmidt. 1998a. "In-Situ Actinide Immobilization of Actinides for Groundwater Cleanup: Laboratory Demonstration with Soil from the Fernald Environmental Management Project." In: *Science and Technology for Disposal of Radioactive Tank Wastes*. WW Schultz and NJ Lombardo, Eds., pp. 507-518. Plenum Press, New York.
- Nash K, MP Jensen, and MA Schmidt. 1997. "Actinide Immobilization in the Subsurface Environment by In-Situ Treatment with a Hydrolytically Unstable Organophosphorous Complexant: Uranyl Uptake by Calcium Phytate." In: *Proceedings of International Conference on Actinides*, Publisher?, Baden-Baden, Germany.
- Nash K, MP Jensen, and MA Schmidt. 1998b. "Actinide Immobilization in the Subsurface Environment by In-Situ Treatment with a Hydrolytically Unstable Organophosphorous Complexant: Uranyl Uptake by Calcium Phytate." *Journal of Alloys and Compounds* 271-273:257-261.
- Nash K, LR Morse, MP Jensen, EH Appelman, MA Schmidt, S Friedrich, M Redko, and JJ Hines. 1999. *Water-Soluble Organophosphorous Reagents for Mineralization of Heavy Metals*. ANL/CHM/CP-98479, Argonne National Laboratory, Argonne, Illinois.

- Newville M. 2001. "IFEFFIT: Interactive XAFS Analysis and FEFF Fitting." *Journal of Synchrotron Radiation* 8:322-324.
- Nguyen SN, RJ Silva, HC Weed, and J Andrews, John E. 1992. "Standard Gibbs Free Energies of Formation at the Temperature 303.15K of Four Uranyl Silicates: Soddyite, Uranophane, Sodium Boltwoodite, and Sodium Weeksite." *Journal of Chemical Thermodynamics* 25:359-376.
- Noubactep C, J Sonnefeld, D Merten, T Heinrichs, and M Sauter. 2006. "Effects of the Presence of Pyrite and Carbonate Minerals on the Kinetics of the Uranium Release from a Natural Rock." *Journal of Radioanalytical and Nuclear Chemistry* 270(2):325-333.
- O'Hare PAG, J Boerio, and HR Hoekstra. 1976. "Thermochemistry of Uranium Compounds: Vii. Solution Calorimetry of Alpha and Beta- $\text{Na}_2\text{UO}_4$ , Standard Enthalpy of Formation of Beta- $\text{Na}_2\text{UO}_4$  and the Enthalpy of the Alpha to Beta Transition at 298.15 K." *Journal of Chemical Thermodynamics* 8:845-855.
- O'Hare PAG, BM Lewis, and SN Nguyen. 1988. "Thermochemistry of Uranium Compounds Xvii. Standard Molar Enthalpy of Formation at 298.15 K of Dehydrated Schoepite  $\text{UO}_3 \cdot 0.9\text{H}_2\text{O}$ . Thermodynamics of (Schoepite+Dehydrated Scheopite+Water)." *Journal of Chemical Thermodynamics* 20:1287-1296.
- Olsen R and FS Watanabe. 1957. "A Method to Determine a Phosphorus Adsorption Maximum of Soils as Measured by the Langmuir Isotherm." *Soil Science Society Proceedings Vol#?:144-149*.
- Onaka T, T Miyajima, and S Ohashi. 1981. "On the Binding of Magnesium to Long-Chain Polyphosphate Ions." *Journal of Inorganic and Nuclear Chemistry* 43(12):3323-3327.
- Oostrom M, C Hofstee, RJ Lenhard, and TW Wietsma. 2003. "Flow Behavior and Residual Saturation Formation of Injected Carbon Tetrachloride in Unsaturated Heterogeneous Porous Media." *Journal of Contaminant Hydrology* 64:93-112.
- Oostrom M and RJ Lenhard. 2003. "Carbon Tetrachloride Flow Behavior in Unsaturated Hanford Caliche Material: An Investigation of Residual NAPL." *Vadose Zone Journal* 2:25-33.
- Parfitt RL, RJ Atkinson, and RSC Smart. 1975. "The Mechanism of Phosphate Fixation by Iron Oxides." *Soil Science Society of America Proceedings* 39:837-841.
- Payne TE, JA Davis, and TD Waite. 1996. "Uranium Adsorption on Ferrihydrite - Effects of Phosphate and Humic Acid." *Radiochimica Acta* 74:239-243.
- Pekarek V and V Vesely. 1965. "A Study on Uranyl Phosphates - II. Sorption Properties of Some 1- to 4-Valent Cations on Uranyl Hydrogen Phosphate Heated to Various Temperatures." *Journal of Inorganic and Nuclear Chemistry* 27:1151-1158.
- Pena F and J Torrent. 1984. "Relationship between Phosphate Sorption and Iron Oxides in Alfisols from a River Terrace Sequence of Mediterranean Spain." *Geoderma* 33:283-296.

- Perez I, I Casas, M Martin, and J Bruno. 2000. "The Thermodynamics and Kinetics of Uranophane Dissolution in Bicarbonate Test Solutions." *Geochimica et Cosmochimica Acta* 64(4):603-608.
- Perez I, C I., ME Torrero, E Cera, L Duro, and J Bruno. 1997. "Dissolution Studies of Soddyite as a Long-Term Analogue of the Oxidative Alteration of the Spent Nuclear Fuel Matrix." *Mat. Res. Soc. Symp. Proc.* 465:565-572.
- Philen ODJ and JR Lehr. 1967. "Reactions of Ammonium Polyphosphates with Soil Minerals." In: *Soil Science Society of America Proceedings*
- Pierce EM, JP Icenhower, RJ Serne, and JG Catalano. 2005. "Experimental Determination of UO<sub>2</sub> (Cr) Dissolution Kinetics: Effects of Solution Saturation State and pH." *Journal of Nuclear Materials* 345:206-218.
- Pierce EM, BP McGrail, MM Valenta, and DM Strachan. 2006. "The Accelerated Weathering of a Radioactive Low-Activity Waste Glass under Hydraulically Unsaturated Conditions: Experimental Results from a Pressurized Unsaturated Flow (PUF) Test." *Nuclear Technology* 155(2):149-155.
- Pingitore NEJ. 1986. "Modes of Co-precipitation of Ba<sup>2+</sup> and Sr<sup>2+</sup> with Calcite." In: *Geochemical Processes at Mineral Surfaces*. JA Davis and KF Hayes, Eds., p. 574. American Chemical Society, Washington D.C.
- Pingitore NEJ and MP Eastman. 1984. "The Experimental Partitioning of Ba<sup>2+</sup> into Calcite." *Chemical Geology* 45:113.
- Pingitore NEJ, MP Eastman, M Sandidge, K Oden, and B Freiha. 1988. "The Co-precipitation of Manganese (II) with Calcite: An Experimental Study." *Marine Chemistry* 25:107.
- Pokrovsky OS, JA Mielczarski, O Barres, and J Schott. 2000. "Surface Speciation Models of Calcite and Dolomite/Aqueous Solution Interfaces and Their Spectroscopic Evaluation." *Langmuir* 16:2677-2688.
- Qafoku N, JM Zachara, C Liu, PL Gassman, OS Qafoku, and SC Smith. 2005. "Kinetic Desorption and Sorption of U(VI) During Reactive Transport in a Contaminated Hanford Sediment." *Environmental Science and Technology* 39(9):3157-3165.
- Racz GJ and RJ Soper. 1967. "Reaction Products of Orthophosphates in Soils Containing Varying Amounts of Calcium and Magnesium." *Canadian Journal of Soil Science* 47:223-230.
- Rajan SSS and RL Fox. 1972. "Phosphate Adsorption by Soils 1. Influence of Time and Ionic Environment on Phosphate Adsorption." *Communications in Soil Science and Plant Analysis* 3(6):493-504.
- Reeder R, J., EJ Elzinga, CD Tait, KD Rector, RJ Donohoe, and DE Moris. 2004. "Site-Specific Incorporation of Uranyl Carbonate Species at the Calcite Surface." *Geochimica et Cosmochimica Acta* 68(23):4799-4808.
- Reeder RJ, M Nugent, GM Lamble, CD Tait, and DE Morris. 2000. "Uranyl Incorporation into Calcite and Aragonite: XAFS and Luminescence Studies." *Environmental Science and Technology* 34:638-644.

- Reeder RJ, M Nugent, CD Tait, DE Morris, SM Heald, KM Beck, WP Hess, and A Lanzirotti. 2001. "Co-precipitation of Uranium(VI) with Calcite: XAFS, Micro-XAS, and Luminescence Characterization." *Geochimica et Cosmochimica Acta* 65(20):3491-3503.
- Riley RG, JM Zachara, and FJ Wobber. 1992. *Chemical Contaminant on DOE Lands and Selection of Contaminant Mixtures for Subsurface Science Research*. DOE/ER-0547T, U.S. Department of Energy, Office of Energy Research, Washington, D.C.
- Robertson WD and J Harman. 1999. "Phosphate Plume Persistence at Two Decommissioned Septic System Sites." *Ground Water* 37(2):228-236.
- Roh Y, SR Lee, S-K Choi, MP Elless, and SY Lee. 2000. "Physicochemical and Mineralogical Characterization of Uranium-Contaminated Soils." *Soil and Sediment Contamination* 9(5):463-486.
- Sakadevan K and HJ Bavor. 1998. "Phosphate Adsorption Characteristics of Soils, Slags and Zeolite to Be Used as Substrates in Constructed Wetland Systems." *Water Research* 32(2):393-399.
- Samadi A and RJ Gilkes. 1999. "Phosphorus Transformations and Their Relationships with Calcareous Soil Properties of Southern Western Australia." *Soil Science Society of America Journal* 63:809-815.
- Sandino A and J Bruno. 1992. "The Solubility of  $(\text{UO}_2)_3(\text{PO}_4)_2 \cdot 4\text{H}_2\text{O}(\text{S})$  and the Formation of U (VI) Phosphate Complexes: Their Influence Speciation in Natural Waters." *Geochimica et Cosmochimica Acta* 56:4135-4145.
- Savenko AV. 2001. "Sorption of  $\text{UO}_2^{2+}$  on Calcium Carbonate." *Radiochemistry* 43(2):174-177.
- Sawhney BL and DE Hill. 1975. "Phosphate Sorption Characteristics of Soils Treated with Domestic Waste Water." *Journal of Environ. Qual.* 4(3):342-346.
- Scheyer JM and CF Baes. 1954. "The Solubility of Uranium (VI) Orthophosphates in Phosphoric Acid Solutions." *American Chemical Society Journal* 76:354-357.
- Schmid LA and RR McKinney. 1969. "Phosphate Removal by a Lime-Biological Treatment Scheme." *Water Pollution Control Federation* 41(7):1258-1276.
- Schreyer JM and CF Baes. 1954. "The Solubility of Uranium (VI) Orthophosphates in Phosphoric Acid Solutions." *Journal of the American Chemical Society* 76:354-357.
- Scott CO. 1958. *Sorption of Orthophosphate and Non-Orthophosphate Phosphorus by Soils*. Iowa State College, Ames, Iowa..
- Seaman JC, JS Arey, and PM Bertsch. 2001. "Immobilization of Nickel and Other Metals in Contaminated Sediments by Hydroxyapatite Addition." *Journal of Environmental Quality* 30:460-469.
- Sergeyeva EI, AA Nikitin, IL Khodakovkiy, and GB Naumov. 1972. "Experimental Investigation of Equilibria in the System  $\text{UO}_3\text{-Co}_2\text{H}_2\text{O}$  in 25 - 200°C Temperature Interval." *Geochemistry International* 9:900-910.

- Serne RJ, CF Brown, HT Schaeff, EM Pierce, MJ Lindberg, and J Catalano. 2002a. *FY02 Progress Report: 300 Area Uranium Leach and Adsorption Project*.
- Serne RJ, CF Brown, HT Schaeff, EM Pierce, MJ Lindberg, Z Wang, PL Gassman, and JG Catalano. 2002b. *300 Area Uranium Leach and Adsorption Project*. PNNL-14022, Pacific Northwest National Laboratory, Richland, Washington.
- Shanbhag PM and JW Morse. 1982. "Americium Interaction with Calcite and Aragonite Surfaces in Seawater." *Geochim. Cosmochim. Acta* 46:241.
- Shen CY and FW Morgan. 1973. "Hydrolysis of Phosphorous Compounds." In: *Environmental Phosphorous Handbook*. EJ Griffith, A Beeton, JM Spencer and DT Mitchell, Eds., p. 241. John Wiley & Sons, New York.
- Smith JDK. 1984. *Uranium Geochemistry, Mineralogy, Geology, Exploration, and Resources*. Institute of Mining and Metallurgy, London, England.
- Sowder AG, SB Clark, and RA Fjeld. 1999. "The Transformation of Uranyl Oxide Hydrates: The Effects of Dehydration on Synthetic Metaschoepite and Its Alteration to Becquerelite." *Environmental Science and Technology* 33:3552-3557.
- Sowder AG, SB Clark, and RA Fjeld. 2000a. "Dehydration of Synthetic Autunite Hydrates." *Radiochimica Acta* 88:533-538.
- Sowder AG, SB Clark, and RA Fjeld. 2000b. "The Impact of Mineralogy in the U(VI)-Ca-Po<sub>4</sub> System on the Environmental Availability of Uranium." *Journal of Radioanalytical and Nuclear Chemistry* 248(3):517-524.
- Stipp SL and MF Hochella Jr. 1991. "Structure and Bonding Environments at the Calcite Surface as Observed with X-Ray Photoelectron Spectroscopy (XPS) and Low Energy Electron Diffraction (LEED)." *Geochimica et Cosmochimica Acta* 55(6):1723-1736.
- Stipp SLS. 1999. "Toward a Conceptual Model of the Calcite Surface: Hydration, Hydrolysis, and Surface Potential." *Geochimica et Cosmochimica Acta* 63(19/20):3121-3131.
- Stumm W and J Leckie. 1970. "Phosphate Exchange with Sediments: Its Role in the Productivity of Surface Water." In: *Proceedings of the 5th International Pollution Research Conference*, Pergamon Press, San Francisco, California,.
- Sutton CD and S Larsen. 1964. "Pyrophosphate as a Source of Phosphorus for Plants." *Soil Science* 97:196-201.
- Sutton M, P Warwick, and A Hall. 2003. "Uranium (VI) Interactions with OPC/PFA Grout." *Royal Society of Chemistry* 5:922-928.
- Takefuji K. 1967. "Properties of Potassium Tripolyphosphate Salts." *Nippon Dojo-Hiryogaku Zasshi* 28:497-502.

- Tesoriero AJ and JF Pankow. 1996. "Solid Solution Partitioning of  $Sr^{2+}$ ,  $Ba^{2+}$ ,  $Cd^{2+}$  to Calcite." *Geochimica et Cosmochimica Acta* 60:1053-1063.
- Tessier A, PGC Campbell, and M Blsson. 1979. "Sequential Extraction Procedure for the Speciation of Particulate Trace Metals." *Analytical Chemistry* 51(7):844-851.
- Thompson HA, GA Parks, and GE Brown Jr. 1998. "Structure and Composition of Uranium (VI) Sorption Complexes at the Kaolinite - Water Interface." In: *Adsorption of Metals by Geomedia*. EA Jenne, Ed., pp. 349 - 370. Academic Press, San Diego, California.
- Tidwell VC, DE Morris, JC Cunnane, and SY Lee. 1996. "Characterizing Soils Contaminated with Heavy Metals: A Uranium Contamination Case Study." *Remediation Journal*. 81-96.
- Tofflemire TJ and M Chen. 1977. "Phosphate Removal by Sands and Soils." *Ground Water* 15(5). Groundwater?
- Toor GS, GS Bahl, and AC Vig. 1997. "Pattern of P Availability in Different Soils as Assessed by the Adsorption Equations." *Journal of the Indian Society of Soil Science* 45:719-723.
- Tsuge T and T Yoshida. 1958. "Study of Polyphosphate Salts." *Nippon Dojo-Hiryogaku Zasshi* 28:497-502.
- Tuli A, MA Denton, JW Hopmans, T Harter, and JL MacIntyre. 2001. Multi-step outflow experiment: From soil preparation to parameter estimation. Land, Air and Water Resources Rep. 100037. University of California, Davis.
- van Cappellen P, L Charlet, W Stumm, and P Wersin. 1993. "A Surface Complexation Model of the Carbonate Mineral-Aqueous Solution Interface." *Geochimica et Cosmochimica Acta* 57:3505-3518.
- van Der Zee SEATM, F Leus, and M Louer. 1989. "Prediction of Phosphate Transport in Small Columns with an Approximate Sorption Kinetics Model." *Water Resources Research* 25(6):1353-1365.
- van Der Zee SEATM, and WH van Riemsdijk. 1986. "Sorption Kinetics and Transport of Phosphate in Sandy Soil." *Geoderma* 38:293-309.
- Van Genuchten M. 1980. A closed-form equation for predicting the hydraulic conductivity of unsaturated soil. *Soil Sci. Soc. Am. J.* 44:892-898.
- van Riemsdijk WH, LJM Boumans, and FAM De Haan. 1984. "Phosphate Sorption by Soils: I. A Model for Phosphate Reaction with Metal-Oxides in Soil." *Soil Science Society of America Journal* 48(3):537-541.
- van Wazer JR. 1950. "Structure and Properties of the Condensed Phosphates: I. Some General Considerations About Phosphoric Acids." *Journal of the American Chemical Society* 72:639-644.
- van Wazer JR, and CF Callis. 1958. "Metal Complexing by Phosphates." 1011-1046.

- van Wazer JR, EJ Griffith, and JF McCullough. 1955. "Structure and Properties of the Condensed Phosphates: VII. Hydrolytic Degradation of Pyro- and Tripolyphosphate." 1955:287-291.
- van Wazer JR, EJ Griffith, and JH McCullough. 1952. "Hydrolysis of Condensed Phosphates." *Journal of the American Chemical Society* 74:4977.
- Vdovic N. 2001. "Electrokinetic Behaviour of Calcite - the Relationship with Other Calcite Properties." *Chemical Geology* 177:241-248.
- Vermeul VR, JS Fruchter, BG Fritz, R Mackley, DM Wellman, and MD Williams. 2008. "In-Situ Uranium Stabilization through Polyphosphate Injection: Pilot-Scale Treatability Test at the Hanford Site 300 Area." In: *Waste Management 2008*, Waste Management, Phoenix, Arizona.
- Vermuel VR, JS Fruchter, DM Wellman, BA Williams, and MD Williams. 2006. *Site Characterization Plan: Uranium Stabilization through Polyphosphate Injection – 300 Area Uranium Plume Treatability Demonstration Project*. PNNL-16008, Pacific Northwest National Laboratory, Richland, Washington.
- Vesely V, V Pekarek, and M Abbrent. 1965. "A Study on Uranyl Phosphates: Iii. Solubility Products of Uranyl Hydrogen Phosphate, Uranyl Orthophosphates and Some Alkali Uranyl Phosphates." *Journal of Inorganic and Nuclear Chemistry* 27:1159-1166.
- Violante A, C Colombo, and A Buondonno. 1991. "Competitive Adsorption of Phosphate and Oxalate by Aluminum Oxides." *Soil Science Society of America Proceedings* 55:65-70.
- Vochten R. 1990. "Transformation of Cherkovite and Sodium Autunite into Lehnerite." *American Mineralogist* 75:221-225.
- Wang Z, JM Zachara, PL Gassman, C Liu, O Qafoku, W Yantasee, and JG Catalano. 2005a. "Fluorescence Spectroscopy of U(VI)-Silicates and U(VI)-Contaminated Hanford Sediment." *Geochimica Cosmochimica Acta* 69(6):1391-1403.
- Wang Z, JM Zachara, JP McKinley, SC Smith, and SM Heald. 2005b. *Cryogenic Laser Induced U(VI) Fluorescence Studies of a U(VI) Substituted Calcite: Implications to U(VI) Speciation in Contaminated Hanford Sediments*. Pacific Northwest National Laboratory, Richland, Washington.
- Webb SM. 2004. "Sixpack: A Graphical User Interface for XAS Analysis Using IFEFFIT." *Physica Scripta*:in press.
- Wellman DM, AP Gamedainger, DI Kaplan, and RJ Serne. 2008a. "Effect of Particle Scale Heterogeneity on Uranium (VI) Retardation During Transport in Unsaturated Porous Media." *Vadose Zone Journal* 7(1):67-78.
- Wellman DM, KM Gunderson, JI Icenhower, and SW Forrester. 2007a. "Dissolution Kinetics of Synthetic and Natural Meta-Autunite Minerals,  $X_{3-N}^{n+}[(UO_2)(PO_4)]_2 \cdot XH_2O$ , under Acidic Conditions." *Geochemistry Geophysics Geosystems* 8(Q11001):1-16.

Wellman DM, JP Icenhower, AP Gamedinger, and SW Forrester. 2006a. "Effects of pH, Temperature, and Aqueous Organic Material on the Dissolution Kinetics of Meta-Autunite Minerals,  $(\text{Na, Ca})_2\text{-}_1[(\text{UO}_2)(\text{PO}_4)]_2 \cdot 3\text{H}_2\text{O}$ ." *American Mineralogist* 91:143-158.

Wellman DM, JP Icenhower, and AT Owen. 2006b. "Comparative Analysis of Soluble Phosphate Amendments for the Remediation of Heavy Metal Contaminants: Effect on Sediment Hydraulic Conductivity." *Environmental Chemistry* 3:219-224.

Wellman DM, JP Icenhower, and WJ Weber. 2005. "Elemental Dissolution Study of Pu-Bearing Borosilicate." *Journal of Nuclear Materials* 340:149-162.

Wellman DM, EM Pierce, M Oostrom, and JS Fruchter. 2007b. *Experimental Plan: 300 Area Treatability Test: In Situ Treatment of the Vadose Zone and Smear Zone Uranium Contamination by Polyphosphate Infiltration*. PNNL-16823, Pacific Northwest National Laboratory, Richland, Washington.

Wellman DM, EM Pierce, EL Richards, BC Butler, KE Parker, JN Glovack, SD Burton, SR Baum, ET Clayton, and EA Rodriguez. 2007c. *Interim Report: Uranium Stabilization through Polyphosphate Injection - 300 Area Uranium Plume Treatability Demonstration Project*. PNNL-16683, Pacific Northwest National Laboratory, Richland, Washington.

Wellman DM, EM Pierce, VR Vermeul, SV Mattigod, EL Richards, MD Williams, JS Fruchter, and JP Icenhower. 2008b. "In Situ Uranium Stabilization through Polyphosphate Remediation: Development and Demonstration at the Hanford Site 300 Area, Washington State." In: *Waste Management Research Trends*, ed. F Columbus, Nova Science Publishers, Inc., Hauppauge, New York.

Wellman DM, JM Zachara, NP Qafoku, C Liu, SC Smith, and SW Forrester. (In press.) "Advective Desorption of Uranium (VI) from Contaminated Hanford Vadose Zone Sediments under Saturated and Unsaturated Conditions." *Vadose Zone Journal*.

White MD and M Oostrom. 2006. *STOMP Subsurface Transport over Multiple Phases, Version 4.0, User's Guide*. PNNL-15782, Pacific Northwest National Laboratory, Richland, Washington.

Wierenga PJ and MT Van Genuchten. 1989. "Solute Transport through Small and Large Unsaturated Soil Columns." *Ground Water* 27(1):35-42.

Wietsma, TW, M Oostrom, M, MA Covert, TW Queen, and MJ Fayer. 2008. An automated apparatus for constant flux, constant head, and falling head hydraulic conductivity measurements. Soil Science Society of America J. In Press.

Willett IR, CJ Chartres, and TT Nguyen. 1988. "Migration of Phosphate into Aggregated Particles of Ferrihydrite." *Journal of Soil Science* 39:275-282.

Williams BA, CF Brown, W Um, MJ Nimmons, RE Peterson, BN Bjornstad, RJ Serne, FA Spane, and ML Rockhold. 2007. *Limited Field Investigation Report for Uranium Contamination in the 300 Area, 300-FF-5 Operable Unit, Hanford Site, Washington*. PNNL-16435, Pacific Northwest National Laboratory, Richland, Washington.

Wolery TJ. 1992. *Eq3nr, a Computer Program for Geochemical Aqueous Speciation-Solubility Calculations: Theoretical Manual, User's Guide, and Related Documentation (Version 7.0)*. UCRL-MA-110662, Lawrence Livermore National Laboratory, Livermore, California.

Wolery TW and RL Jarek. 2003. *EQ3/6, Theoretical Manual, User's Guide, and Related Documentation (Version 8.0)*. Sandia National Laboratory, Albuquerque, New Mexico.

Wright J, LM Peurrung, TE Moody, JL Conca, X Chen, PP Didzerekis, and E Wyse. 1995. *In Situ Immobilization of Heavy Metals in Apatite Mineral Formulations*. Pacific Northwest Laboratory, Richland, Washington.

Young JS and JS Fruchter. 1991. *Addendum to Data Compilation Task Report for the Source Investigation of the 300-FF-1 Operable Unit Phase I Remedial Investigations*. EMO-1026, Environmental Management Operations for the U.S. Department of Energy, Richland, Washington.

Yuan TL and DE Lucas. 1982. "Retention of Phosphorus by Sandy Soils as Evaluated by Adsorption Isotherms." In: *Soil and Crop Science Society of Florida*, Florida. Verify complete reference.

Zachara JM, CF Brown, J Christensen, E Dresel, C Kelly, J McKinley, RJ Serne, and W Um. 2007. *A Site Wide Perspective on Uranium Geochemistry at the Hanford Site*. CH2M Hill Hanford Group, Richland, Washington.

Zachara JM, J Davis, C Liu, J McKinley, N Qafoku, DM Wellman, and S Yabusaki. 2005. *Uranium Geochemistry in the Vadose Zone and Aquifer Sediments from the 300 Area Uranium Plume*. PNNL-15121, Pacific Northwest National Laboratory, Richland, Washington.

Zachara JM, JA Kittrick, LS Dake, and JB Harsh. 1989. "Solubility and Surface Spectroscopy of Zinc Precipitates on Calcite." *Geochim. Cosmochim. Acta* 53:9.

Zachara JM, JA Kittrick, and JB Harsh. 1988. "The Mechanism of  $Zn^{2+}$  Adsorption on Calcite." *Geochim. Cosmochim. Acta* 52:2284.

Zhang Z, V Freedman, S Waichler, and M White. 2004. *2004 Initial Assessments of Closure for the S-SX Tank Farm: Numerical Simulations*. Pacific Northwest National Laboratory, Richland, Washington.

Zhang Z, V Freedman, and M White. 2003. *2003 Initial Assessments of Closure for the C Tank Farm Field Investigation Report (FIR): Numerical Simulations*. Pacific Northwest National Laboratory, Richland, Washington.

## Distribution

<u>No. of Copies</u>		<u>No. of Copies</u>	
<b><u>ONSITE</u></b>		<b><u>ONSITE</u></b>	
<b>4 DOE-Richland Operations Office</b>		<b>30 Pacific Northwest National Laboratory</b>	
J.V. Borghese	E6-44	JS Fruchter	K6-96
KM Thompson	A6-38	DM Wellman (20)	K3-62
Public Reading Room (2)	H2-53	CC Bovaird	K3-62
		M Oostrom	K6-33
		TW Wietsma	K8-96
		DH Bacon	K9-33
		VR Vermeul	K6-96
		Hanford Technical Library (2)	P8-55



**Pacific Northwest**  
NATIONAL LABORATORY

902 Battelle Boulevard  
P.O. Box 999  
Richland, WA 99352  
1-888-375-PNNL (7665)  
[www.pnl.gov](http://www.pnl.gov)



U.S. DEPARTMENT OF  
**ENERGY**